PALLADIUM-REDUCED GRAPHENE OXIDE/METAL ORGANIC FRAMEWORK AS AN EFFICIENT ELECTRODE MATERIAL FOR BATTERY-TYPE SUPERCAPACITOR APPLICATIONS

By

DANIEL MALESELA TEFFU

DISSERTATION

Submitted in fulfilment of the requirements for the degree of

MASTER OF SCIENCE

in

CHEMISTRY

in the

FACULTY OF SCIENCE AND AGRICULTURE

(School of Physical and Mineral Sciences)

at the

UNIVERSITY OF LIMPOPO

SUPERVISOR: PROF K.D MODIBANE (UL)

CO-SUPERVISORS: PROF M.J HATO (UL)

: DR K MAKGOPA (TUT)

2021

DEDICATION

To my beautiful daughter

Mmasefako Pholomo Mashitisho

DECLARATION

I **Daniel Malesela Teffu** declare the work titled **PALLADIUM-REDUCED GRAPHENE OXIDE/METAL ORGANIC FRAMEWORK AS AN EFFICIENT ELECTRODE MATERIAL FOR BATTERY-TYPE SUPERCAPACITOR APPLICATIONS** as my own study and that all the sources that I have used or quoted in this work have been specified and acknowledged by means of complete references and that this work has not been submitted before for any other degree at any other institution.

Name of student **: Daniel Malesela Teffu**

Student number **:** [redacted]

Student signature **:**

Date **:**

AKNOWLEDGEMENTS

I would like to thank the almighty God for giving me the strength and courage to persure this work until the end. I would also like to extend my gratitude to my supervisor Prof KD Modibane for the courage, support and patience he has shown to me throughout my master's degree. Thanks for believing in me and pushing me to the level that I am research wise. You are indeed a great supervisor. To my co-supervisors Prof MJ Hato and Dr K Makgopa, thank you for the support and the knowledge you have instilled in me throughout my masters' work. I would also like to thank Prof E Iwuoha for allowing me to do part of my studies at the SensorLab, University of the Western Cape (UWC), I really appreciate working with one of the greatest scientists in South Africa and Africa as a whole. I send my gratitudes to NanoRG@UL (2018-2020) for the courage and support in the lab and all the scientific contributions. To Thabang Somo, thanks for being a great friend and collegue and for contributing greatly towards my study especially correcting and designing of my dissertation. I would also like to thank the UWC SensorLab crew, especially Dr Miranda Ndipingwi and Dr Chinwe for helping me through my electrochemical studies in their lab. I really appreciate your efforts and contributions. To my family especially my mother Anna, father Lesibana, sisters (Mumsy, Mankoko and Paulinah) and my brothers Daniel and Isaac, thanks for the support you have shown to me throughout my studies, ***"Kea leboga Bathokwa".*** I would also like to thank all my friends for the support and courage. Last but not least, I thank the mother of my beautiful daughter (Pauli Mashitisho) for the support, love and courage you have given me since we met. I really appreciate you.

To National Reseaerch Foundation (NRF) and Sasol Foundation, South Africa, a great thank you for the financial support thoughout my studies.

ABSTRACT

Recently, the use of electrochemical supercapacitors as energy storage devices has drawn great attention due to their high charge/discharge rate, long life span, high power and energy densities. However, the choice of electrode materials used is vital for the performance of supercapacitors. This study focused on the development of a low cost hybrid electrode based on reduced graphene oxide/metal organic framework composite (rGO/MOF) and a novel palladium (Pd) nanoparticles loaded on rGO/MOF termed Pd-rGO/MOF nanocomposite. The prepared nanocomposites were used for high performance electrochemical double layer capacitor-(EDLC) and battery-type supercapacitors known as supercabattery.

The rGO material reported in this work was chemically derived through the oxidation-reduction method using a hydrazine as a reducing agent. Furthermore, palladium nanoparticles were loaded on the rGO using the electroless plating method. The rGO/MOF and novel Pd-rGO/MOF nanocomposites were prepared using an impregnation method in dimethylformamide. The physical and morphological properties of the synthesised materials were investigated using scanning electron microscopy (SEM), transmission electron microscopy (TEM), X-ray diffraction (XRD), Fourier transform infrared spectroscopy (FTIR), energy dispersive X-ray spectroscopy (EDX), differential scanning calorimetry (DSC) and thermogravimetric analysis (TGA). The XRD and FTIR analyses showed crystalline phases and vibrational bands for both parent materials, respectively. The TGA/DSC results showed enhancement of the thermal stability of the composite as compared to MOF material. The SEM/EDS and TEM/EDX confirmed the presence of octahedral structure of MOF in the rGO sheet-like structure and elemental composition of the synthesised composite. The resultant of Pd-rGO/MOF nanocomposite showed a morphology in which a thin layer of rGO coating existed over MOF with unique bright spots indicating the presence of Pd nanoparticles. This observation agreed well with the structural properties revealed by both XRD and FTIR with the reduction of MOF intensities upon Pd-rGO loading as well as enhancement of thermal stability of the nanocomposites. The electrochemical properties of the prepared electrodes were determined using cyclic voltammetry (CV), galvanostatic charge-discharge (GCD) and electrochemical impedance spectroscopy (EIS). To evaluate the electrochemical performance of the prepared electrode materials, both two and three electrode cells were assembled. From the CV and GCD

results, the nanocomposites demonstrated a battery-type behaviour and therefore asymmetric supercabattery cells were assembled using the composites as positive electrodes, and activated carbon as a negative electrode. The specific capacity of rGO/MOF in three electrode cell was found to be 459.0 C/g at a current density of 1.5 A/g in 3M potassium hydroxide. Furthermore, the asymmetric supercapacitor based on the rGO/MOF nanocomposite and activated carbon (AC) as a negative electrode exhibited a maximum energy density of 11.0 Wh/kg and the maximum power density of 640.45 W/kg. The loading of palladium nanoparticles on the nanocomposite was to improve the electrochemical active sites and the performance of the supercapacitor electrode. After incorporation of Pd nanoparticles, the specific capacitance in three electrode cell improved to 712 C/g at a higher current density of 2 A/g with the same electrolyte. The assembled supercabattery has shown improved maximum energy and energy density of 26.44 Wh/kg and 1599.99 W/kg, respectively. Based on these findings, the synthesised rGO/MOF and Pd-rGO/MOF nanocomposites are promising electrode materials for future supercabattery applications.

LIST OF PUBLICATIONS AND CONFERENCES

This study resulted in three full research articles, one published and one submitted that form part of this dissertation:

1. **Daniel M. Teffu**, Mogwasha D. Makhafola, Katlego Makgopa, Mpitloane J Hato, Emmanuel I. Iwuoha, Kwena D. Modibane. Comprehending the contemporary state of art in supercapacitors using metal organic framework composites: A Review. **Under review**.
2. **Daniel M. Teffu**, Mogwasha D. Makhafola, Miranda M. Ndipingwi, Edwin Makhado, Mpitloane J. Hato, Emmanuel I. Iwuoha, Kwena D. Modibane, Katlego Makgopa. Interrogation of electrochemical performance of reduced graphene oxide/metal-organic framework hybrid for asymmetric supercapacitor application. *Electroanalysis (2020)*, doi.org/10.1002/elan.202060303
3. **Daniel M. Teffu**, Emmanuel M. Ramoroka, Mogwasha D. Makhafola, Katlego Makgopa, Emmanuel I. Iwuoha, Mpitloane J. Hato, Kwena D. Modibane. High performance asymmetric supercabattery based on reduced graphene oxide/metal organic framework nanocomposite decorated with palladium nanoparticles. **In preparation**.

Conference contributions

1. **Teffu D.M**, Makhafola M.D, Hato M.J. and Modibane K.D, Reduced graphene oxide/metal organic framework hybrid composite for supercapacitor application. Oral Presentation. Faculty Research Day, Faculty of Science and Agriculture, Fusion Boutique Hotel, Polokwane, South Africa, 20th September 2018.
2. **Teffu D.M**, Makhafola M.D, Hato M.J. and Modibane K.D, Reduced graphene oxide/metal organic framework hybrid composite for supercapacitor application. Oral Presentation. SACI-North Section, University of Venda, Thohoyandou, South Africa, 31st October 2019.

TABLE OF CONTENTS

TABLE OF CONTENTS

LIST OF FIGURES

LIST OF SCHEMES

LIST OF TABLES

LIST OF ABBREVIATIONS AND SYMBOLS

MOF	Metal organic framework
CPM	Crystalline porous material
EDLC	Electrochemical/electric double layer capacitor
IHP	Inner Helmholtz Plane
OHP	Outer Helmholtz Plane
GO	Graphene oxide
RC	Resistor capacitor
ESR	Equivalence series resistance
CV	Cyclic voltammetry
GCD	Galvanostatic charge discharge
EIS	Electrochemical impedance spectroscopy
OCV	Open circuit voltage
CPE	Constant phase element
AC	Activated carbon
CNTs	Carbon nanotubes
MWCNTs	Multiwalled carbon nanotubes
CVD	Chemical vapour deposition
CPs	Conducting polymers
DMSO	Dimethylsulfoxide
SCs	Supercapacitors
rGO	Reduced graphene oxide
SEM	Scanning electron microscopy
TEM	Transmission electron microscopy
SAED	Selected area electron diffraction
XRD	X-ray diffraction
FTIR	Fourier transform infrared
TGA	Thermogravimetric analysis
PSD	Pore size distribution
Pd	Palladium nanoparicles
Ag/AgCl	Silver/silver chloride
A	Ampere
IL	Ionic liquid

ZIF	Zeolitic imidazole framework
BTC	1, 2, 5-benzenetricarboxylate imidazole
BDC	1, 4-benzenedicarboxylate
KOH	Potassium hydroxide
LIBs	Lithium ion batteries
ES	Electrochemical supercapacitor
EDX	Energy dispersive X-ray spectroscopy
NF	Nickel foam

CHAPTER ONE
INTRODUCTION

1.1. Background

Energy is fundamental to any country's economy, because, it makes a huge input into the economy and without it there would be less or no developments resulting in a poor economic growth [1, 2]. Over population also contributes to the increased energy demand. After the introduction of Industrial Revolutions, the social and industrial developments of almost all countries have depended greatly on the burning of non-renewable energy sources especially coal, gas, and oil as they accessible easily [3]. The burning of fossil fuels for energy production has resulted in accumulations of excess carbon dioxide in the atmosphere. The carbon dioxide emission from the energy production industries is the main contributor of greenhouse effect resulting in harmful living conditions for humans and animals [4]. Strategies used to resolve the global-carbon emissions issue includes the development of renewable, non-harmful energy sources such as solar energy, wind energy, biofuels, and hydro energy [5, 6]. Most of the renewable energy is obtained directly as electricity, so the improvement of reliable electrochemical energy storage devices such as fuel cells, batteries and supercapacitors is very important [7].

1.2. Problem statement

The commonly used energy storage devices includes batteries and supercapacitors. However, supercapacitors are expected to replace batteries completely due to their fast charging/discharging rate, high energy density and very long cycling stability [8]. Furthermore, this device can be used either by itself as the primary power source or in combination with batteries or fuel cells. Supercapacitors are classified into electrochemical double-layer capacitors (EDLC), pseudocapacitors and supercabattery. The performance of an electrochemical supercapacitor (ES) is primarily dependent on the quality and the type of electrode material used. So far, there are various electrode materials that have been studied in supercapacitor applications including graphene materials (carbons), metal oxides/hydroxides and conducting polymers. Carbon materials especially graphene materials have been studied intensively for supercapacitors and they exhibited an electrochemical double

layer behaviour. This is due to their high electric conductivity, high thermal and chemical stability, and outstanding mechanical properties among other carbon based materials [9, 10]. These materials show more of electrostatic (non-faradaic) behaviour rather than pseudocapacitive nature (faradaic), resulting in longer cycling stability of the electrode. Reduced graphene oxide (rGO) amongst other carbon materials has shown better performances in supercapacitors due to its high conductivity and excellent mechanical stability of the materials. However, rGO has a drawback of restacking of the graphene sheets as a result of the strong van der Waals forces which lead to agglomeration [11]. This phenomenon of restacking results in the decrease in the conductivity and the surface area of the rGO and therefore compromising the performance of the supercapacitor electrode material.

1.3. Motivation of the study

The prevention of the agglomeration and restacking is the key challenge in processing graphene based materials, as its unique properties are associated particularly with the individual graphene sheets. There are various methods for preparing graphene materials in prevention of restacking including chemical vapour deposition (CVD), chemical exfoliation and chemical derivation of graphene. However, CVD and chemical exfoliation suffers from drawbacks such as small scale production and high temperature production. Chemically derived graphene is more researched due to simple manufacturing, low cost and a straight forward up-scaling method [12]. Furthermore, the restacking can be overcome by introduction of fillers such as pseudocapacitive materials, porous materials and transition metals which separates the graphene sheets, and simultaneously contributing to the total capacitance of the system.

Crystalline porous materials (CPMs) have been massively researched and used in different fields owing to their appealing features such as high surface area, crystalline structure and extremely well-ordered porours structure [13]. Metal organic frameworks (MOFs) are class of CPM materials composed of a metal ions and organic linkers and these materials are investigated for several uses including as fuel cells [14], batteries and supercapacitors [15]. This is due to their diverse structure, adjustable pore sizes,

high specific surface area, abundant active sites and easy to manufacture. The introduction of MOFs in graphene sheets can reduce resctacking and contribute to the performance of the supercapacitor particularly in supercabattery which is a combination of high-power EDLC and high-energy density battery-type electrode. The large specific surface area of MOFs can also increase the contact area between MOFs electrode and electrolyte, which further improves the specific capacitance. Furthermore, the adjustable pore size can ensure the fast transport of electrons and electrolyte ions while the abundant active sites can promote the pseudocapacitance [16].] Srimuk *et al.* [17] prepared a composite material based on rGO and MOF which was coated on flexible carbon paper and applied as a supercapacitor electrode material and showed a high specific capacitance of 385 F/g at a current density of 1 A/g. Therefore, this work focuses on the development of a hybrid composite based on chemically derived reduced graphene oxide and MOF materials prepared by impregnation method of 1:1 ration for supercabattery applications. Furthermore, the introduction of Pd nanoparticles to the on reduced graphene nanosheet composite electrode material was reported to increase more active sites, dissociation ability and thus results in high performances [18]. Their synthesised Pd-rGO electrode material exhibited high specific capacitance of 637 F/g, exceptional cyclic performance and extreme energy density of 56 Wh/ kg and power density of 1166 W/ kg at a current density of 1.25 A/g. Hence in this work, the electrochemical performance of a novel Pd-rGO/MOF nanocomposite was synthesised by electroless deposition of Pd followed by impregnation method.

1.4. Aims and Objectives

1.4.1. Aims

The main aim of this work is to develop a reduced graphene oxide/metal organic framework composite doped with palladium nanoparticles for advanced supercapacitor applications in an aqueous electrolyte.

1.4.2. Objectives

The objectives of this work are to:

1. synthesise Cu based MOF, rGO and their composite.
2. load palladium nanoparticles to the rGO and incorporate MOF to produce Pd-rGO/MOF composite.
3. characterise the prepared materials using different analytical instruments.
4. study the electrochemical properties and apply each material as a supercapacitor electrode.

1.5. Dissertation outline

This dissertation attempts to investigate the performance of Pd-rGO/MOF composite as an electrode material for supercapacitor applications.

- **Chapter one** summarises the need for enhanced supercapacitors, research problem statement and motivation followed by aim and objectives of the study.
- **Chapter two** presents a literature review on types of supercapacitors, MOFs as electrode materials, carbon materials as SC electrode materials and MOF/carbon hybrid electrodes as electrode materials.
- **Chapter three** gives the review of the analytical instruments used in this study.
- **Chapter four** focuses on the synthesis of rGO/MOF hybrid composite and its application as an electrochemical supercapacitor electrode.
- **Chapter five** focuses on the synthesis of Pd-rGO/MOF hybrid composite and its application as an electrochemical supercapacitor electrode.
- **Chapter six** gives overall conclusions drawn from the study and the recommendations for future research.

References

1. Koohi-Fayegh S, Rosen MA, (2020). A review of energy storage types, applications and recent developments. Journal of Energy Storage, 27, 101047.
2. Guo H, Xu Y, Zhang X, Zhou X, Chen H, (2020). Transmission characteristics of exergy for novel compressed air energy storage systems-from compression and expansion sections to the whole system. Energy, 116798.
3. Wu S, Zhou C, Doroodchi E, Moghtaderi B, (2020). Techno-economic analysis of an integrated liquid air and thermochemical energy storage system. Energy Conversion and Management, 205, 112341.
4. Jovanovic M, Pezo M, Turanjanin V, Bakic V, (2009). Fossil fuels substitution by the solar energy utilization for the hot water production in the heating plant ‘“ Cerak ”’ in Belgrade. International Journal of Hydrogen Energy, *34*(16), 7075–7080.
5. Yao X, Zhang X, Guo Z, (2020). Science of the Total Environment The tug of war between local government and enterprises in reducing China’s carbon dioxide emissions intensity. Science of the Total Environment, *710*, 136140.
6. Noghreian E, Koofigar HR, (2020). Sustainable Energy , Grids and Networks Power control of hybrid energy systems with renewable sources (wind-photovoltaic) using switched systems strategy. Sustainable Energy, Grids and Networks, 21, 100280.
7. Zhan C, Zeng X, Ren X, Shen Y, Lv R, Kang F, (2020). Dual-ion hybrid supercapacitor : Integration of Li-ion hybrid supercapacitor and dual-ion battery realized by porous graphitic carbon. Journal of Energy Chemistry, *42*, 180–184.

8. Hashemi M, Rahmanifar MS, El-kady MF, Noori A, (2018). Nano Energy The use of an electrocatalytic redox electrolyte for pushing the energy density boundary of a flexible polyaniline electrode to a new limit. Nano Energy, 44, 489–498.
9. Choi H, Yoon H, (2015). Nanostructured Electrode Materials for Electrochemical Capacitor Applications, 906–936.
10. Torad NL, Salunkhe RR, Li Y, Hamoudi H, Imura M, (2014). Electric Double-Layer Capacitors Based on Highly Graphitized Nanoporous Carbons Derived from ZIF-67. Chemistry - A European Journal, 20, 7895 – 7900.
11. Bello A, Makgopa K, Fabiane M, Dodoo-Ahrin D, Ozoemena KI, Manyala N, (2013). Chemical adsorption of NiO nanostructures on nickel foam-graphene for supercapacitor applications. Journal of Materials Science, 48(19), 6707–6712.
12. Lemine AS, Zagho MM, Altahtamouni TM, Bensalah N, (2018). Graphene a promising electrode material for supercapacitors — A review. International Journal of Energy Research, 1–17.
13. Gao X, Dong Y, Li S, Zhou J, Wang L, Wang B, et al. (2020). MOFs and COFs for Batteries and Supercapacitors. Electrochemical Energy Reviews, 3, 81–126.
14. Ramohlola KE, Masikini M, Mdluli SB, Monama GR, Hato MJ, et al. (2017). Electrocatalytic Hydrogen Production Properties of Poly (3- aminobenzoic acid) doped with Metal Organic Frameworks. International Journal of Electrochemical Science, 12, 4392–4405.
15. Yap MH, Fow KL, Chen GZ, (2017). Synthesis and applications of MOF-derived porous nanostructures. Green Energy & Environment, 2(3), 218–245.

16. Sundriyal S, Kaur H, Kumar S, Mishra S, Kim K, Deep A, (2018). Metal-organic frameworks and their composites as efficient electrodes for supercapacitor applications. Coordination Chemistry Reviews, 369, 15–38.

17. Srimuk P, Luanwuthi S, Krittayavathananon A, (2015). Electrochimica Acta Solid-type supercapacitor of reduced graphene oxide-metal organic framework composite coated on carbon fi ber paper. Electrochimica Acta, 157, 69–77.

18. Dar RA, Giri L, Karna SP, Srivastava AK, (2016). Performance of palladium nanoparticle-graphene composite as an efficient electrode material for electrochemical double layer capacitors. Electrochimica Acta, 196, 547–557.

CHAPTER TWO

COMPREHENDING THE CONTEMPORARY STATE OF ART IN SUPERCAPACITORS USING METAL ORGANIC FRAMEWORK COMPOSITES: A REVIEW

Summary

Nowadays, generation, storage, and utilisation of clean energy are the challenging problems faced by the world at large, due to depletion and non-reliable energy sources. These energy setbacks have made scientists to put more focus on developing electrochemical energy storage devices comprised of fuel cells, supercapacitors or batteries. Fuel cells as well as batteries possess higher energy density when compared to supercapacitors but low power density, unnecessary installation cost, bulkiness, and short life time are major draw backs for fuel cells and batteries up to date. Nevertheless, supercapacitors exhibit some energy qualities including light-weight; easy portability, making it much convenient for transportation and excellent cyclability. Moreover, supercapacitors have the potential of possessing high specific and energy densities through surface modifications of electrode materials and composites formation. For instant, metal organic framework (MOF) composites are reported to exhibit enhanced energy density, forming hybrid supercabattery, which is a combination of supercapacitors and batteries. Hence, this review discusses developments and recent findings on supercapacitor technologies with much attention focused on MOFs and their composites as electrode materials together with other important parameters that are capable of enhancing the overall electrochemical device performances.

Keyworks: Metal organic frameworks, electrode material, supercabattery, supercapacitor, pseudocapacitor.

2.1. Introduction

Over the last decade, a drastic rising of energy demand has forced researchers and scientists to overlook and develop clean, maintainable and sufficient energy storage and conversion techniques that are much more reliable and renewable [1]. There are

various energy sources such as wind, solar, hydrothermal being developed to produce renewable and clean energy but the problem evolves when it comes to the storage of the produced energy [1-8].Hence, there is a need to come up with new mechanisms to improve the storage devices. It has been reported that the energy produced by wind and solar is not always available for use so it is very important for it to be stored for future times when there is no wind or light [3]. Several energy storage devices, including capapcitors, batteries and fuel cells, are currently being studied [4, 5]. Batteries and electrochemical capacitors have been recognized as the future for energy storage technologies [9-11]. Researchers shifted their focus to capacitors due to their ability to charge and discharge very fast as well as their longer life cycles [10]. Within a capacitor, two electrically conductive plates, which serve as electrodes, are kept apart by dielectric material such as glass, plastic or ceramic. There are two types of capacitors which include conventional capacitors and supercapacitors. Conventional capacitors are usually used as condensers due to their low energy densities as well as power densities whereassupercapacitors have high energy density even after hundreds or thousands of can charge and discharge cycles [11]. The main difference is the presence of a dielectric material in the conventional whereas supercapacitors use a membrane for free mobility of ions [10]. The ragone plot in Figure 1(a) shows that supercapacitors can close the gap between conventional capacitors which has higher power and lower energy densities and batteries which have lower power and higher energy densities [12-16]. It is shown that supercapacitors based on the conventional and electric double-layer capacitor (EDLC) possess higher power density, however, lower energy density compared to other candidates. In addition, lithium ion batteries (LIBs) showed to have higher energy density than any other candidate [17, 18], but their power density is lower [12, 19]. Remarkably, several types of asymmetric supercapacitors [19] demonstrated average energy and power densities, which is better than the one of the produced by LIBs. Hence, asymmetric supercapacitors have been given much consideration in the energy storage applications owing to their comparable performance with LIBs as well as safer [20] and ecofriendly nature [21]. A supercapacitor is made up of two electrodes, separating membrane, an electrolyte and current collector. They are categorised into EDLC, pseudocapacitors and supercabattery [12] according to their constituents and the electrodes materials.

Electrochemical double layer capacitors consist of a similar capacitance mechanism as the normal conventional capacitors but instead of storing energy in the dielectric layer, EDLC utilises a permeable membrane and electrode/electrolyte interfaces for their energy storage. The capacitance in these supercapacitors is dependent on the distance between the electrodes, the type of electrolyte being used, and the separating membrane between the cathode and anode electrodes [22]. These types of supercapacitors are made up of carbon based electrode materials [23]. In pseudocapacitors the process is more of faradaic redox process rather than just a physical process. Metal oxides and polymers are dominantly utilized as electrode materials [22]. Their oxidation-reduction processes are reliant on electrode potential and alter with charging and discharging [21, 22]. This mechanism facilitates enhanced capacitance and energy density than EDLCs [16]. However, the cyclability of these two materials is poor [24-26].The two electrode materials can be combined to form a hybrid supercapacitor and when the two electrodes are similar, it's called a symmetric supercapacitor but for different electrodes an asymmetric supercapacitor [22]. There are several requirements for suitable material for supercapacitors such as large surface area, adjustable porosity, high electrical conductivity, good cyclability (>105 cycles) and modifiable morphology [25, 26]. As a result, various materials have been used as electrode material such as graphene [23], activated carbon [27], carbon nanotubes [28], transition metal oxide [22, 29], conducting polymers [30] and MOFs [31, 32]. Of the electrode materials, MOFs have emerged as favourable electrode candidates of supercapacitors [32]. These materials consist of sufficcient pores and networks to transfer electrons and give rise to evenly distributed reactive sites that are important for improved supercapacitive properties [31]. Hence this review focuses on the recent advancements of MOFs for supercapacitor applications. The review further discusses many aspects related to reactions involving supercapacitors and their related mechanisms along with the summary of parameters responsible for monitoring the activity of electrocatalyst. We then present the classification of supercapacitors with much attention given to the structural properties and synthetic pathways of MOFs and their composites. Moreover, the counterparts related to MOF composites approaches are discussed and several literature findings that address drawbacks faced by MOFs are defined. Lastly, we summarise and provide a future perception for realisation of MOF as electrochemical storage material.

2.2. Supercapacitors

2.2.1. Electrochemical double layer capacitor

Electrochemical double layer capacitors (EDLCs) use non-faradaic processes for energy storage. They do not involve any chemical reactions, meaning no forming or breaking of bonds. In EDLC, charges are attached to the surface of the electrode materials when potential is applied. It was shown that the capacitance in EDLC is controlled by the size of the double layer in the electrode interface [24, 33]. For example, Figure 2.1(b) below represents a schematic charged electrochemical double layer capacitor [33] in which ions are physisorbed the electrode materials as a result of difference in potential. The figure presents an exceptional power density, which is attributed to fast ad/desorption kinetics of ions in the electrolyte at the electrode surface which results into the electric double layer when the device is being charged or discharged [24]. Anions are adsorbed by the positive electrode while negative electrode attracts cations. Hence a double of charged is formed to avoid recombination of ions at electrodes. It was seen that the parameters such as double layer, increase in specific surface area and distance between electrodes decreased, allow EDLC to attain higher energy density [33]. Moreover, it was mentioned above that the energy storage mechanism in EDLC does not involve any chemical reactions and only physical charge processes takes pace. The first EDL capacitance model was reported in 1853 [25] as shown in Figure 2.1c. In the illustration, the electrode is immersed in an electrolyte in the presence of electric field to form the electric double layer at electrode-electrolyte interface through electrostatic force to form a Helmholtz layer model. In addition, Gouy and Chapman prolonged this model by the addition of a diffusion layer (Figure 2.1c), which forms as a result of the thermal motion of ions [25]. Moreover, Stern reported a new model based on combining Helmholtz model, Gouy-Chapman model and the model is given in Figure 2.1c [25], where Stern and diffuse layers are taken in to consideration for the capacitance in EDLC. Additionally, two planes are used to divide Stern and compact layer. The first plane is the inner Helmholtz plane (IHP) which forms closer to the electrode surface and it moves through the center of the specifically adsorbed ions [34]. The second plane is the outer Helmholtz plane (OHP) which forms at the distance from the electrode surface and it passes through the center of solvated ions [34].

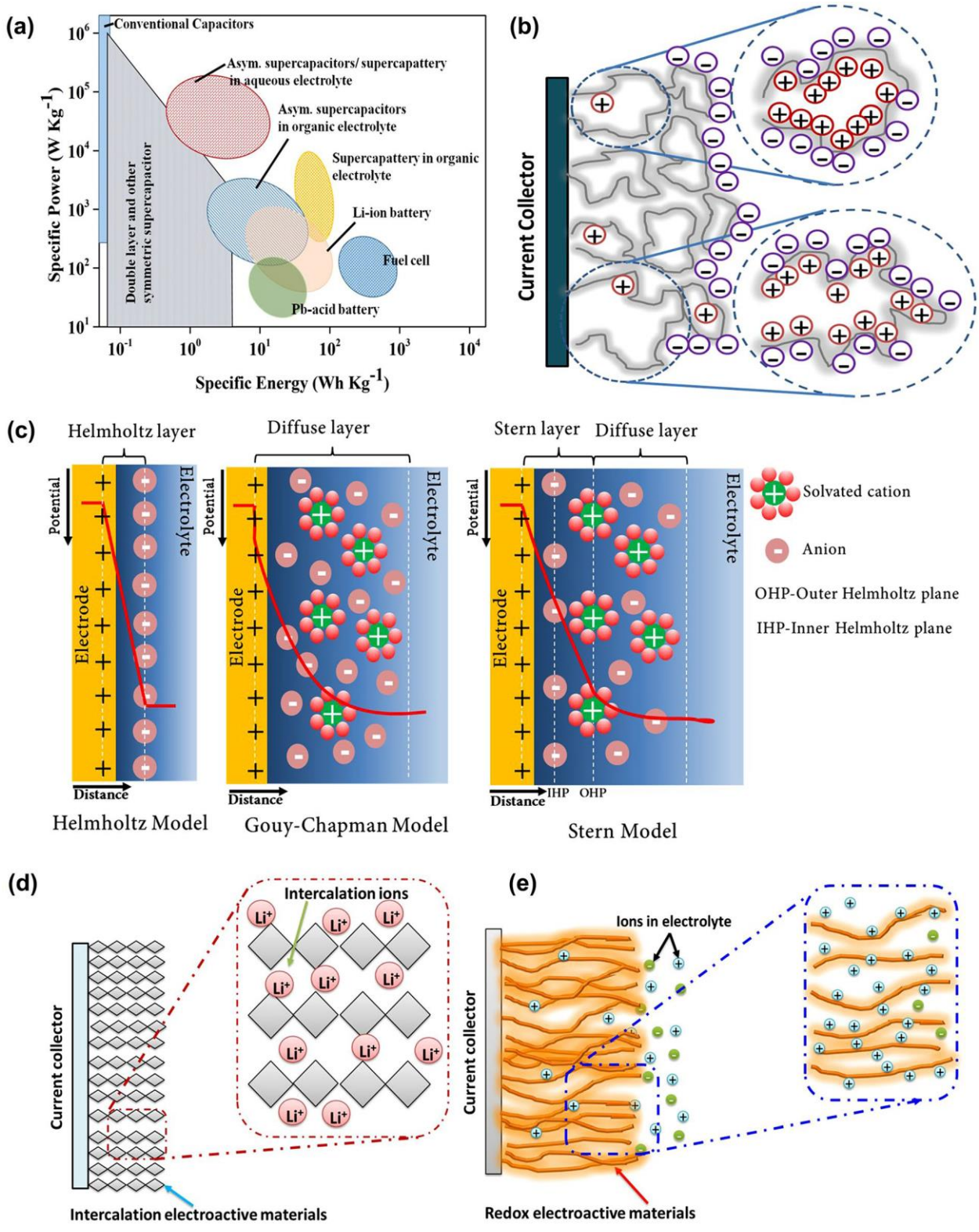

Figure 2.1: (a) Ragone plot of several energy storage devices, (b) Charge storage mechanism of EDL capacitor, (c) EDLC structures, (d) Intercalation and (e) surface redox [34].

It was seen that carbon materials are the widely used materials for electrochemical double layer capacitors [35]. This is due to their low manufacturing cost, high surface area, electrical conductivity, high mechanical and chemical stability as well as controllable morphology [35]. Recently, the electrodes of electrical double layer supercapacitors are fabricated of based on the carbon nanotubes (CNTs), graphite nanoparticles (GNPs) and graphene electrodes due to light-weight, electrochemical stability, and excellent conductivity [24, 30, 35].

2.2.2. Pseudocapacitor

The redox reactions in pseudocapacitors are electrode potential dependent and change with charging and discharging. There are three pseudomechanisms that are featured in this type of capacitance such as underpotential deposition, redox, and intercalation pseudocapacitance. The underpotential deposition is usually observed when the metal ions results in an adsorbed monolayer on the metal surface above their redox potential [36, 37]. Redox pseudocapacitance occurs when ions are physisorbed on the surface of a material with a faradaic charge –transfer [36]. The intercalation pseudocapacitance takes place if ions intercalate into channels of a redox-active material accompanied by a faradaic charge-transfer [36-38]. The ions intercalate within the electrode materials during redox faradaic transfer while preserving its original crystal structure in intercalation [38]. Battery-type electrode materials usually follow the intercalation-decalaction redox reaction [63]. Moreover, Figure 2.1(d-e) shows a schematic charge storage mechanism of a typical pseudocapacitor [34]. This behavior has better advantages in energy storage aspects due the involvement of chemical reactions within the bulk material [37, 39, 40]. The mechanisms are a result of different electrochemical physical processes depending on the type of materials used. The most frequently chosen electrode materials for pseudocapacitors are metal oxides and polymers [22, 41]. Metal oxides have high conductivity, high specific capacitance coupled with very low resistance resulting in high specific power, which make them very appealing in commercial applications [41]. Conducting polymers and are currently used as pseudocapacitor electrode materials because they show high capacitance and conductivity, another advantage over carbon based materials is their low equivalent series resistance and low cost [42].

2.2.3. Supercabattery

It was shown that charge adsorption and the physical processes on the electrode/electrolyte interface are observed in EDLC's whereas the redox and faradaic processes are seen in pseudocapacitors are the two mechanisms of storing energy in supercapacitors [34]. These two storage mechanisms may be combined to form a hybrid supercapacitor [30]. EDLC's gives higher power densities while pseudocapacitors provide higher energy densities, hence, the combination of the two mechanisms can give a supercapacitor with both high power and energy densities, therefore higher performances are observed [10]. This is termed supercabattery due to this combination of an EDLC electrode material with high power densities and a battery-type electrode which exhibits high energy densities. It is also known as asymmetric supercapacitor or battery–supercapacitor hybrid device. The asymmetric supercapacitor hybrid device defines an alignment of two types of electrode materials within positive and negative ends of an electrode [39]. These terms were well known and utilized prior to the currently used terms including supercabattery, hybrid capacitor or battery–supercapacitor hybrid device [34]. In addition, the alkaline-ion hybrid supercapacitors or battery–supercapacitor hybrid device are also used and referred to as hybrid supercapacitor, where the alkaline ions are utilized in de/intercalation procedure. In supercabattery devices, the battery type materias serve as positive electrode. It was seen that the supercabattery amalgamates the gap between supercapacitor and battery with enhanced performance [42]. Generally, this device is a hybrid mechanism of capacitive and faradaic charge storage combined in a single device to provide an optimum energy and power density. It was reported that there are four possibilities in assembling a supercabattery device [34]:

i. Capacitive redox system (pseudocapacitance) + capacitive non-redox system (Double layer capacitance).

ii. Capacitive redox system (pseudocapacitance) + capacitive redox system (pseudocapacitive).

iii. Capacitive non-redox system (double layer capacitance) + Non-capacitive redox system (battery type).

iv. Capacitive redox system (pseudocapacitive) + Non-capacitive redox system (battery type).

The energy storage performance of several materials for supercapacitors or battery are clearly differentiated by their electrochemical behavior using cyclic voltammetry (CV, Figure 2.2(b)), galvanostatic charge–discharge (GCD, Figure 2.2(c)) and electrochemical impedance spectroscopy (EIS, Figure 2(d)) in electrochemical cell (Figure 2.2(a)) made of electrolyte, reference, counter and working electrode system [42, 44]. It was shown that a rectangular curve shown in Figure 2.2(b) resembles an ideal supercapacitor but EDLC materials do not show ideally, and it results in a deformed rectangular shape as shown in Figure 2.2(b) [43]. The Galvanostatic charge-discharge curves of pseudocapacitance using which materials where different shapes were observed as compared to those of EDLC (Figure 2.2(c). It was demonstrated that EDLC materials charge and discharge in straight lines whereas pseudocapacitive materials charge and discharge nonlinearly as a result of the faradaic interactions [43]. The different capacitance can be due to the electrode materials, however in other cases, the electrolyte also plays an important role in the behaviour of a certain material.

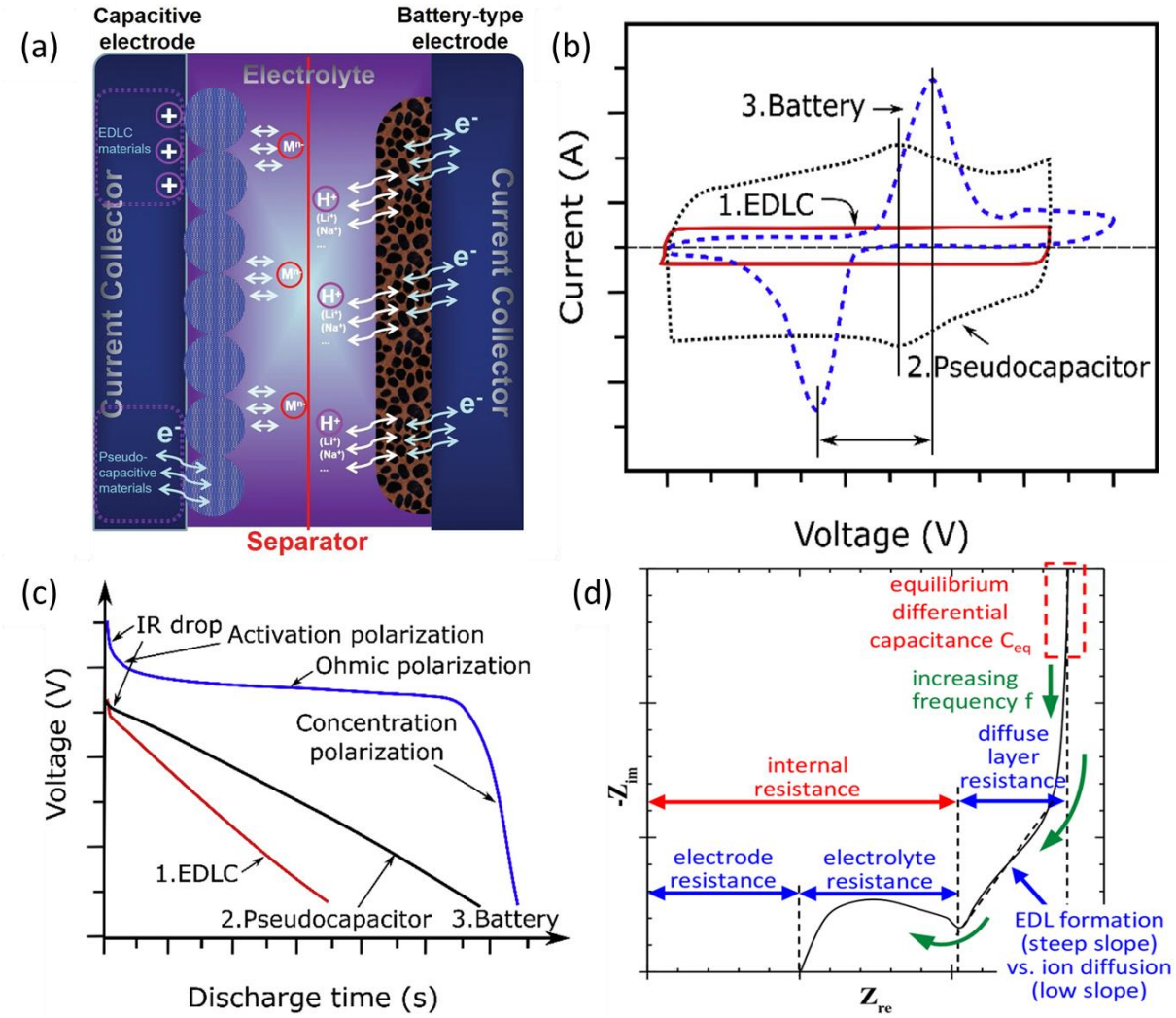

Figure 2.2: (a) Three electrode system for supercabattery measurement, copyright [42], (b) CV and (c) GCD curves of battery, EDLC and pseudocapacitor electrode material, copyright [43], and (d) EIS curves of electrode materials [44].

For example, Figure 2.3(a) shows that CV profile for graphene film functionalised with ionic liquid (IL-CMG) has a rectangular-like shape whereas RuO_2/ IL-CMG film exhibits quasi-rectangular shapes. The GCD curves of such materials (EDLC) reveal an almost linear voltage discharge curve at a constant current. It was seen that most carbon materials falls under the EDLC category [43]. On the other hand, MnO_2, RuO_2 and polyaniline (PANI) are considered as good pseudocapacitive electrode materials for application in energy storage devices. Moreover, CV profiles of such materials appear to be almost similar to EDLC materials as illustrated by the CV of IL-CMG film in Figure 2.3(a). However, the energy storage mechanism in pseudocapacitive materials is

dominated by the reversible surface redox reactions which are a result of peaks shown on the CV profile of RuO2/IL-CMG film. The peaks are due to the activities that take place on the surface of the electrode such as the insertion/de-insertion in metal oxides or doping/de-doping in conducting polymers performed in neutral or acidic electrolyte without tempering with the structure of the electrode material [34, 44]. In contrast, battery-type electrode materials demonstrates a different CV and GCD profiles, in which a high current response observed at potentials with more inherent redox activities advocates that the storage mechanism is based on reversible faradaic reactions through crystal phase transition. The GCD curve forms a voltage plateau which is a result of the presence of bulk redox reactions. For example, Figure 2.3(d) shows battery-type electrodes based on Co_3O_4. The CV curve of Co_3O_4 (Figure 2.3(d)) and Ni foam-Co_3O_4 nanowire arrays in Figure 3(b)) clearly displays the perfect oxidation and reduction peaks in alkaline electrolyte confirming the reversible faradaic reactions [34, 45]. Similarly, the composites based on EDLC electrode materials combined with battery-type electrode material and pseudocapacitive electrode materials display both non faradaic and faradaic behaviors in their CV and GCD profiles. Therefore, the functionalised graphene is one of best examples for composite electrode based on EDLC and pseudocapacitive materials and the CV (black color CV plot of rGO in Figure 2.3(d)) curves exhibits both EDLC and pseudocapacitor properties [46].

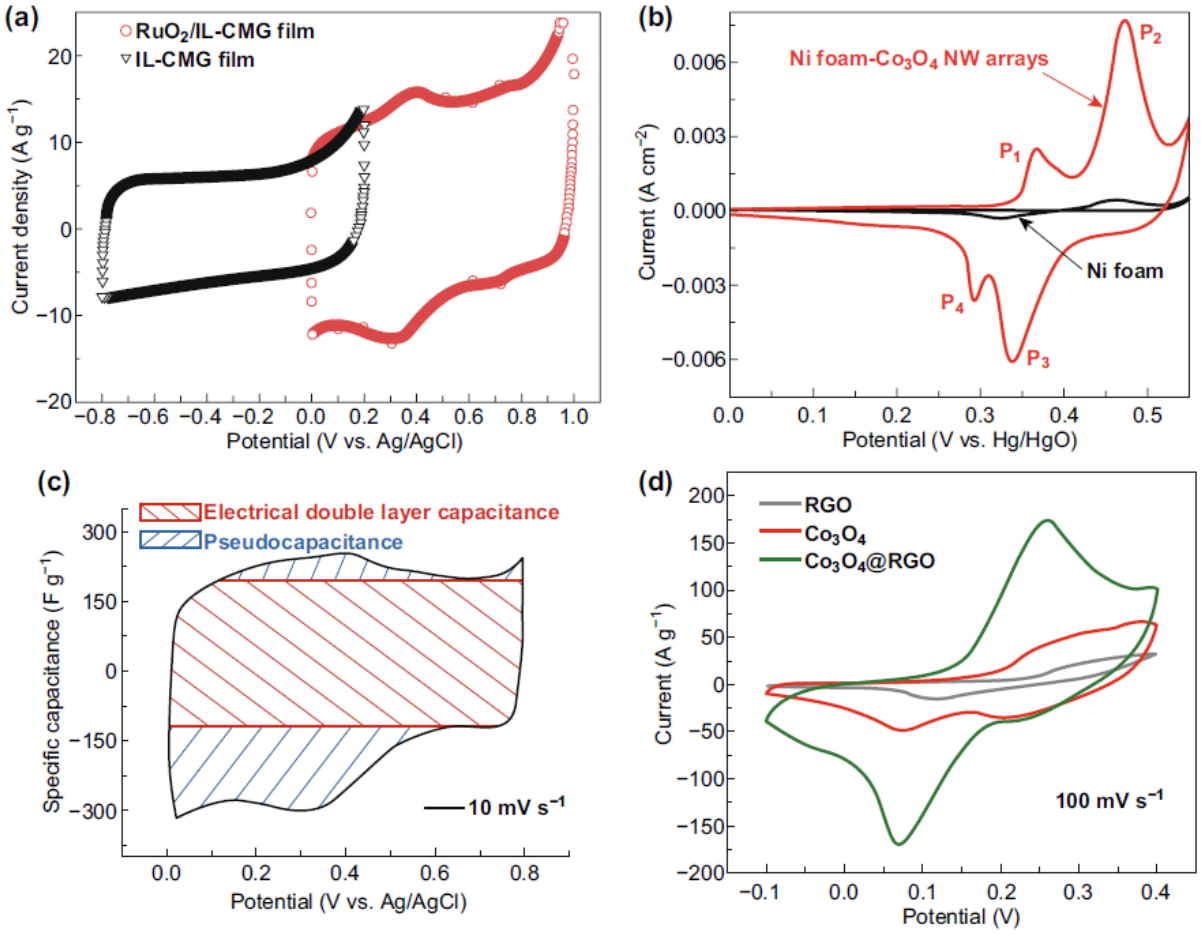

Figure 2.3: CV profiles of (a) capacitor electrode [EDLC (IL-CMG film) and pseudocapacitance (RuO_2/IL-CMG film)], (b) Battery-type electrode, (c) Composite electrode and (d) composite electrode (supercapattery [Co_3O_4@rGO]: EDLC [rGO] + battery [Co_3O_4] composite electrode) [34].

2.3. Factors affecting the performance of supercabattery

Electrochemical evaluation of supercapacitors deals with the determination of specific capacitance, power density and energy density at a specific current density. These parameters determine the performance of every supercapacitor. The main objective of the supercapattery is to get a highly enhanced performance by merging the high-power of supercapacitor with the high energy density from a battery [47].

The capacitance of a supercapacitor can be determined from both the CV and EIS, from the CV the capacitance is defined by:

$$C = \frac{\int IdV}{\Delta V \times v} \qquad (2.1)$$

Where C is the capacitance, $\int IdV$ is the integrated area under the CV, ΔV is the potential range and v is the potential scan rate. The capacitance can also be calculated from the GCD as;

$$C = \frac{I \times \Delta t}{\Delta V} \quad (2.2)$$

where Δt = discharge time while ΔV = potential range used. The specific capacitance can be calculated as;

$$Cs = \frac{C}{m} \quad (2.3)$$

where Cs = specific capacitance, C = capacitance and m = mass. Energy density of a supercapacitor can be determined from the obtained specific capacitance using the formula:

$$E = \frac{1}{2} Cs \times (\Delta V)^2 \quad (2.4)$$

Where E is the specific energy, Cs is the specific capacitance and ΔV is the potential range used.

Large Cs and broader potential window are the key parameters in attaining higher energy and power supercapacitors. The power density which determines how fast a supercapacitor can deliver energy is obtained using the equation;

$$P = \frac{E}{\Delta t} \quad (2.5)$$

Where P is the power density, E is the specific energy and ΔV is the potential range used. The columbic efficiency of a supercapacitor can also be obtained from the charge-discharge curves using the equation;

$$\eta = \frac{td}{tc} \times 100 \quad (2.6)$$

Where η is the coulumbic efficiency, td is the discharge time and tc is the charging time. In most instances the coulumbic efficiency is used for the determination of cyclic stability of the electrode material.

In supercabattery, specific capacities of the battery-type material in three electrode and two electrode systems are obtained from the galvanostatic charge-discharge curves using Equation 2.7:

$$Q_s = \frac{I*\Delta t}{m} \quad (2.7)$$

In the above equation Qs is the specific capacity, I is the average applied current, Δt is the discharging time and m is the active mass. The energy density (ED) and power density(PD) are calculated using Equations 2.8 and 2.9, respectively:

$$ED(Wh\ kg^{-1}) = \frac{1}{2*3.6} Qs\Delta V \quad (2.8)$$

$$PD(Wkg^{-1}) = \frac{ED*3600}{\Delta t} \quad (2.9)$$

where ΔV is the change in potential window.

In two electrode system, the mass ratio between the two electrodes are determined using Equation 2.10:

$$\frac{m^+}{m^-} = \frac{Q^-}{Q^+}\left(\frac{\Delta V^-}{\Delta V^+}\right) \quad (2.10)$$

Where Q = potential window and ΔV. The + sign denotes the positive electrode while the – sign denotes negative electrode.

2.4. Supercabattery electrode materials

In supercabattery, a cathode electrode is normally a battery-type or pseudocapacitive materials. The energy density of the electrode is influenced by the capacitance, so use of its full theoretical capacitance of the materials is important. Hence, it is necessary to understand the different parameters that are linked with the capacitance of the material. The battery-type electrodes mainly store the charges using redox faradaic reactions, and the performance also depends on surface area, diffusion of electron and ions into the electrode, electrical conductivity with multivalent oxidation states of the materials. The redox/faradaic reactions takes place in both pseudocapacitive and battery-type electrode materials, however, their electrochemical behaviors such as

CV, and GCD vary due to the phase change in battery-type material. It was seen that transition metal hydroxide/oxide and conducting polymer based electrode materials belong to the category of pseudocapacitance; whereas some of the multivalent oxidation states, transition metal oxides, are used as battery-type electrodes for charge storage. Figure 2.4 gives overview of the operational potential range of various pseudocapacitive and battery- type electrode materials including their application in the positive and negative potentials in water-based aqueous electrolyte [48, 49]. It was well documented that key properties like porous structure, high surface area and tunable chemical functionalities of MOFs make them potential candidate materials in the application of supercapacitors [31], hence, the focus in this work is on MOFs and their composites for supercabattery applications.

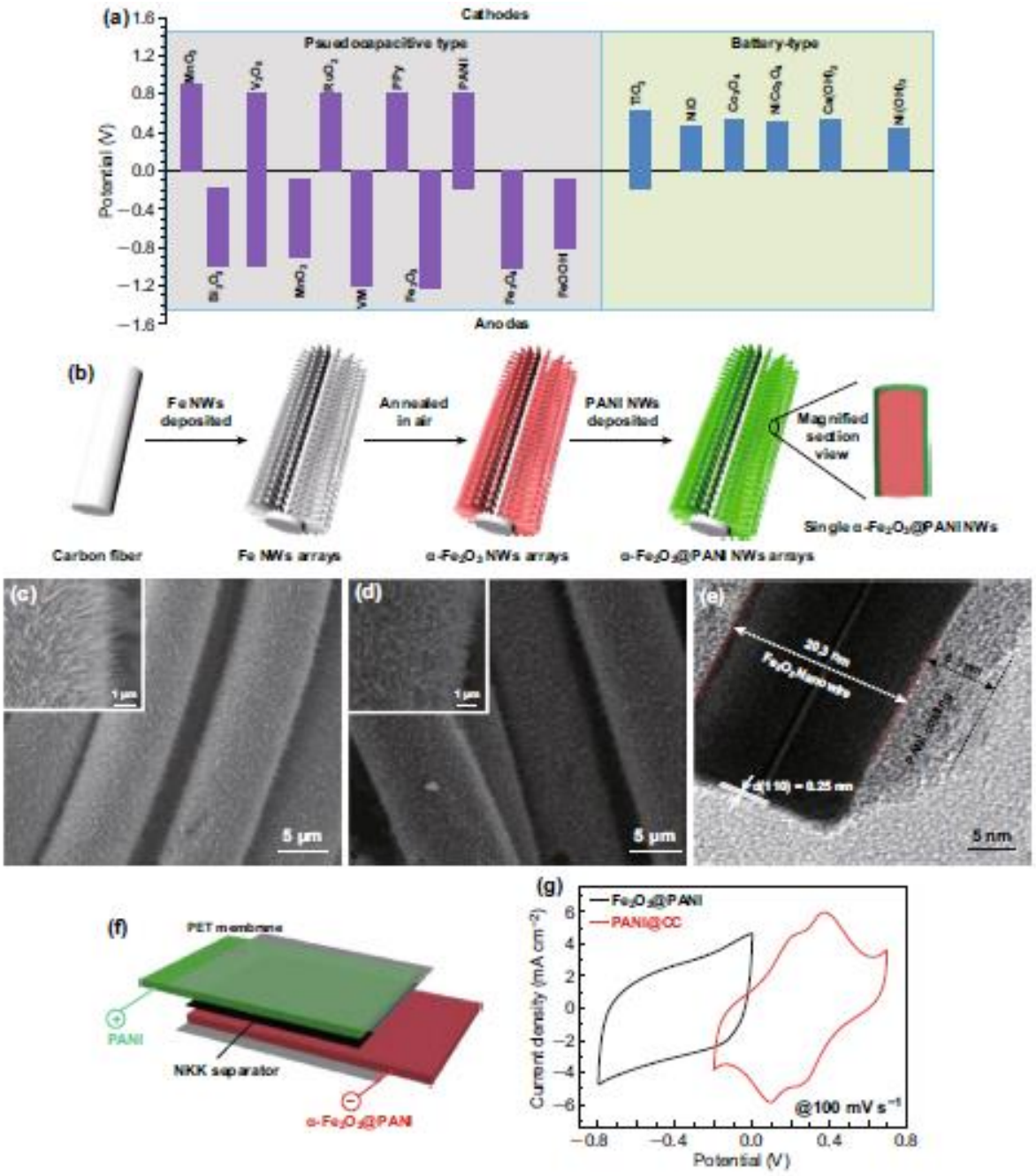

Figure 2.4: (a) Illustration of the potential range of the various redox active electrode materials, (b) The design and fabrication of an electrode based on ofα-Fe_2O_3@PANI nanowires. SEM images of (c) α-Fe_2O_3 and (d) α-Fe_2O_3@PANI, (e) TEM image of α-Fe_2O_3@PANI. (f) Fabrication of asymmetric supercapacitor and (g) CV comparison of PANI@CC and α-Fe_2O_3@PANI electrodes at 100 mV/s [49].

2.4.1. Pure metal organic frameworks

Metal organic frameworks (MOFs) are new porous materials with high surface area, tunable structures and high crystalinity, these materials are a combination of metal ions (Cu. Mn, Zn, Co) and organic linkers such as 1,2,5-benzenetricarboxylate (BTC), Imidazole and 1,4-benzenedicarboxylate (BDC). There are several synthetic routes for preparation of MOFs where metal salts were combined with organic linkers to produce the high crystalline structures [50-62] as shown in Figure 2.5(a-c). This techniques depicts synthetic routes through which they give rise to accurate control and tuneable structural shape and pore size [56]. Microwave-assisted technique as shown in the figure has shown to be an attractive technique for quick preparation of nano-porous materials [56, 57]. Apart from excellent crystallinity and high effectiveness, other advantages of Microwave-assisted method are good structural selectivity, and narrow particle size distribution [56]. This method involves applying heat to solution mixture of the substrates with microwave within 60 minutes to yield nano-sized structures. This method produces excellence of the crystals which are normally similar to the ones synthesised through solvothermal processes [57]. Mechanochemical method is used to prepare MOF in a solvent-free environment. The method involves molecular bonds breakage though mechanical process and chemical alterations [58]. With regard to mechanochemical method, it takes a less period of time (normally, 10 to 120 minutes) to achieve qualitative yields [56]. Occasionally, metal oxides are selected as starting materials in mechanochemical method over metal salts due to the former producing H_2O as a by-product [56, 58]. Currently, mechanochemical synthesis method is rapidly used in the preparation of MOFs through the use of liquid-assisted grinding (LAG), in which a portion of solvent is added into a solid reaction mixture [56, 59]. The liquid can function as phase directing agent and LAG can accurately act as selective agent for pillared-layered frameworks [60]. The electrochemical preparation of MOFs uses metal ions acting as anodes within electrochemical cell with methanol assisting to dissolve the organic linker. In case of HKUST-1, trimesic acid dissolved in alcohol and copper cathode were used in electrochemical synthesis for period of 150 min at a voltage of 12-19 V and a current of 1.3 A, to attain a greenish blue precipitate [56]. After activation by heat, a dark blue colored powder of octahedral crystals structure in nature with 0.5 to 5 μm size) possessing surface area of 1820 m^2/g was obtained [61]. The experimental

parameters such as solvent, electrolyte, voltage-current density, and temperature on the preparation of MOF are vital in obtaining a desired structure [62].

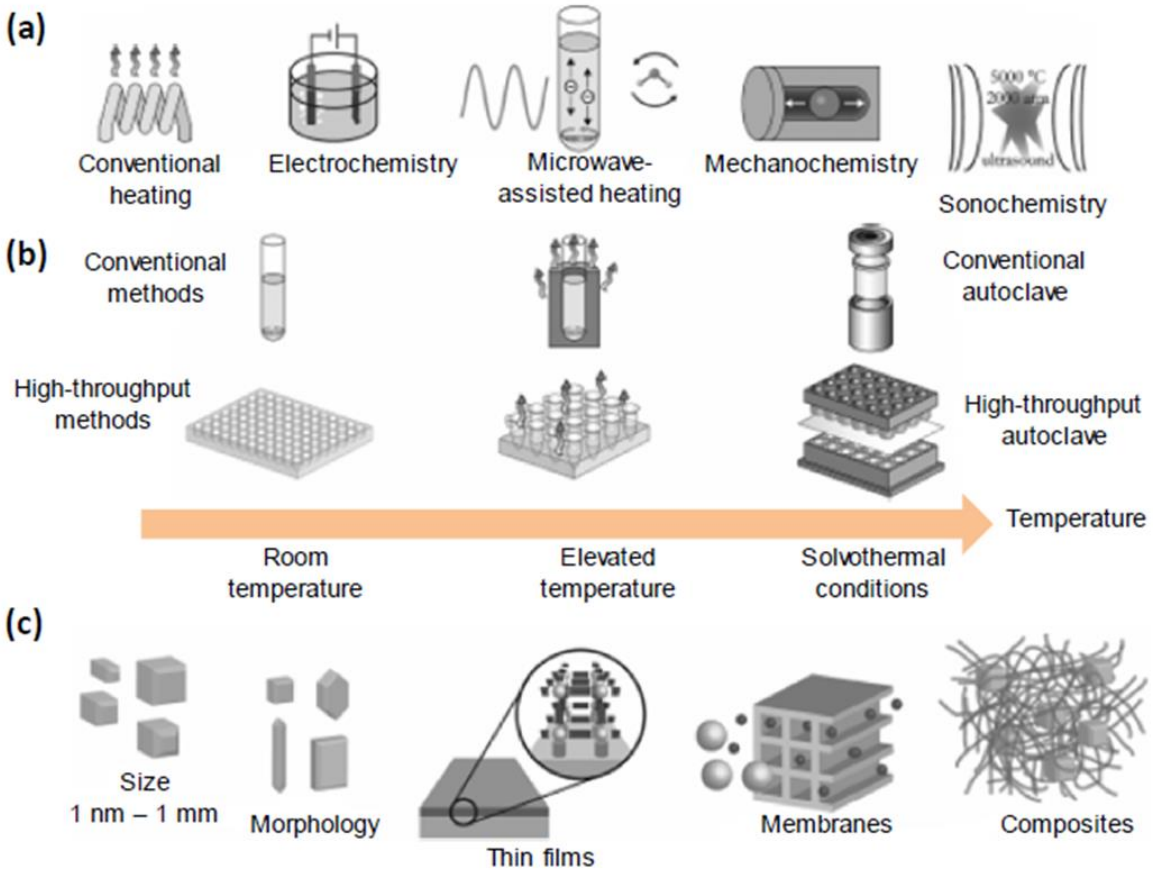

Figure 2.5: Different synthetic routes of MOF structures, operational temperatures related to each method and their final reaction products [58].

Metal organic frameworks as electrode materials are currently being studied for supercapacitors applications [50, 51], this is because of the ability to allow penetration of an electrolyte into the electrode material pores [50]. The fast diffusion process is vital for the supercapacitor performance and is one of the requirements for supercapacitor applications. MOFs usually show pseudocapacitance due to the high faradaic redox reactions between the electrode/electrolyte interactions and such faradaic reactions results in higher specific capacitances and better performance [51]. However, the stability of the metal organic frameworks is compromised by the chemical reactions and the MOF electrodes degrade after sometime of charging and discharging [50]. Diaz et al. [52] demonstrated the use of Co8-MOF-5 for supercapacitor applications, where the cyclic voltammetry of the material is observed

to be rectangular in shape which is characteristic of electrochemical double layer capacitors in Tetrabutylammonium hexafluorophosphate (TBAPF6) solution. As a result, the supercapacitor exhibits poor specific capacitance of 3.27 and 1.98 F/g calculated from cyclic voltammetry and charge-discharge at a current density of 0.01 A/g, respectively. This was because of the electrodes were dominated by carbon black than Co8-MOF-5 and the lower conductivities of the MOF [53, 54]. It was also reported that the stability of the electrodes determined at a current density of 0.01 A/g possessed capacitance 8% reduction after cycling 1000 times [52]. Considering the higher specific surface area of Co8-MOF-5 which was found to be 2900 m^2/g according to Langmuir, Diaz et al. [52] could not collaborate the low capacitance values with the electrode-electrolyte interaction but concluded that the low values were due to the poor conductivity of the metal organic framework. Lee et al. [55] also made use of Co-MOF electrode where the capacitance was calculated from charge-discharge at 0.6 A/g in 1M LIOH solution was found to be 206.76 F/g as presented in Figure 6(a) The stability of the material was found to be 98.5 % after 1000 cycles but the performance was also not good in the electrolytes used and the energy of the electrodes was found to be 7.18 wh/kg as shown by inset in Figure 2.6(a).

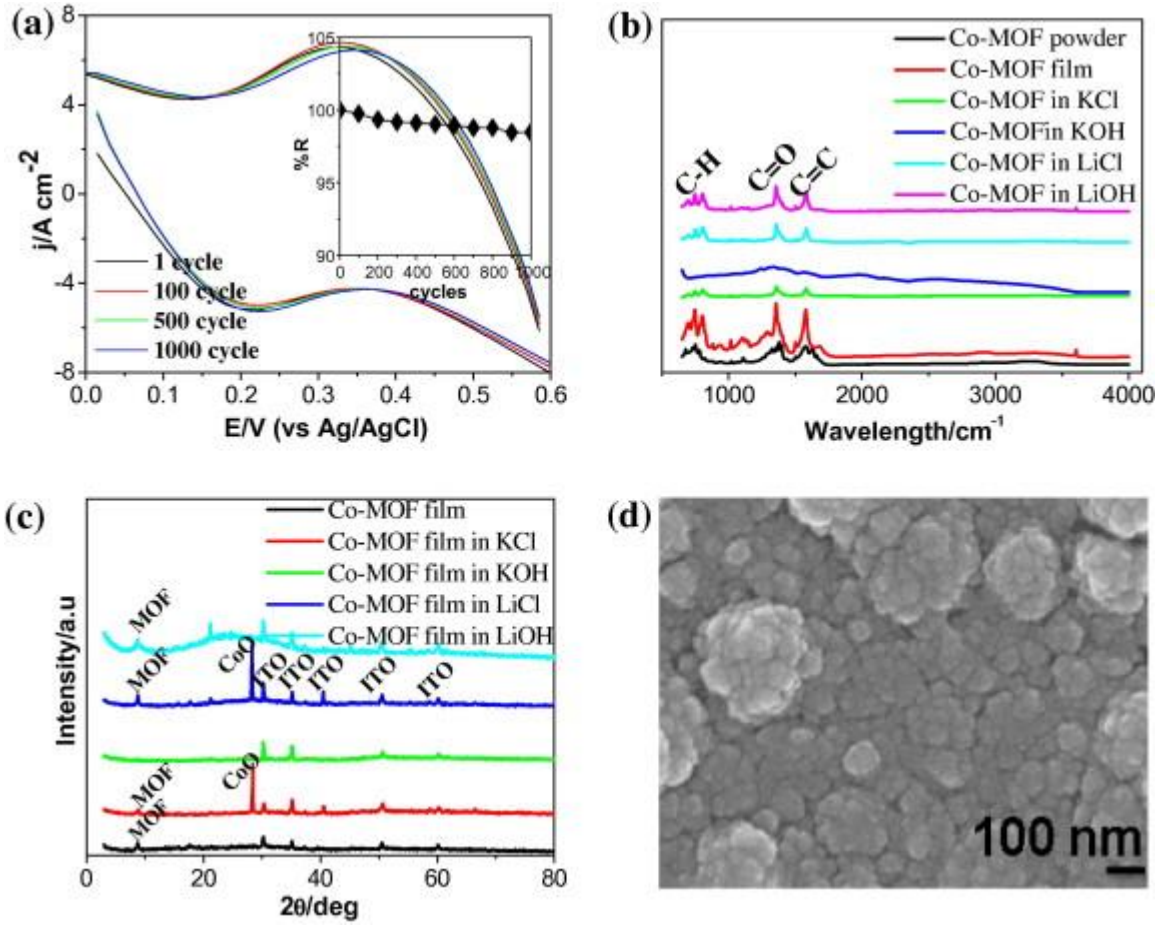

Figure 2.6 :(a) Cycling stability of Co-MOF film for 1000 cycles, (b) FTIR spectra of Co-MOF in different electrolytes, (c) XRD patterns, and (d) SEM image of Co-MOF in LiOH after 1000 cycles [55].

Lee's work has demonstrated the importance of electrolytes in supercapacitor applications as the performance decreased when utilising KOH, KCl and LiCl [55]. Lee and co-works [55] used fourier-transform infrared spectroscope (FTIR), X-ray power diffractometer (XRD) and scanning electron microscope (SEM) to verify the structural stability and crystallinity of MOF films upon 1000 CV cycles in several electrolytes. In Figure 2.6 (b), they observed the MOF characteristic peaks in FTIR spectrum, showing that the inherent framework and structure of the MOFs was retained in LiOH, LiCl and KCl electrolytes whereas KOH electrolyte damaged the strcutures as a result of more basic character of this particular electrode. In addition, the XRD patterns after 1000 CV cycles (Figure 2.6 (c) in LiOH electrolyte displayed a broad XRD peaks as an indicative of the transformation of MOF structure into fine crystalline structure and a new phase of cobalt oxide emerged when LiCl and KCl electrolytes were employed. Figure 2.6 (d) presents a SEM image of Co-MOF after 1000 cycles in LiOH. The image

reveals that after 1000 cycles, the material contained nanocrystalline granules, which resulted as a result of constant de/formation of framework forcing reordering of MOF crystals structure [55]. Furthermore, Tan and co-workers [63] prepared a Zirconium-based MOF, which showed a specific capacitance of 134 F/g at a scan rate of 5 mV/s. However, it was seen that the poor conductivity of MOFs hampers the charge transfer between the MOFs-based electrode and the current collectors, subsequently obstructing the utilization of MOFs as electrode candidates [65]. Furthermore, Yang *et al.* [65] synthesized Ni-MOF-24 material and observed a capacitance of 1127 F/g for this material in 6 M KOH electrolyte at the current density of 0.5 A/g.

2.4.2. Metal organic framework composites

It was shown that carbon materials are mostly utilised in double layer supercapacitors due to their abundance, high electrical conductivity, unable morphology and lower production cost. They can also be further modified to tailor their structural and chemical properties for different applications including supercapacitor applications. The commonly used categories of carbon materials include transition metal oxide, carbon-nanotubes (CNT), graphene, and activated carbons (AC). Activated carbon has been applied in supercapacitors because of its electrochemical double layer behaviour, however the readily available activated carbons have low surface areas limiting their application in supercapacitors. These materials were incorporated in metal organic frameworks to give nano-porous carbons with much better performances. For example, Liu et al. [65] reported a nano-porous carbon (NPC) derived from MOF-5 structures for suprecapacitor applications. In their work, a vacuum preteated and heat treatment processes were used to prepare the PFA/MOF-5 composite. Furthermore, the composite was carbonised to prepare the final NPC. The NPC exhibited a specific capacitance of 204 F/g at a scan rate 5 mV/s which performed better than the ordered mesoporous silica material SBA-15.

2.4.3. Metal organic framework and metal composites

The transition metal oxides have been incorporated with MOF due to their ability to transition into various oxidation states allowing rich redox reactions and high specific capacitance [66]. Meng et al. [67] attained Co_3O_4 from Co-MOF through a solvo-thermal method, followed annealing at low temperatures, resulting in a specific capacitance of 150 F/g using 2 M KOH electrolyte at 1 A/g. Furthermore, Yang et al.

[68] synthesised a series of Zn/Ni-MOF materials, and amongst the samples, MOF-2 exhibited a maximum specific capacitance of 1620 F/g at a current density 0.25 A/g with only 8% loss of the capacitance after 3000 cycles. In other studies, Xu et al. [69] prepared nanrods derived from 1D Ni-MOF which has shown high performances with specific capacitance of 1698 F/g at 1 A/g and 94.8% retention after 1000 cycles. Ramasubbu et al. [70] reported on practical applicability of synthesised MOF composite material made of TiO_2 aerogel/Co-MOF as a hybrid device for supercapattery. Their device was prepared through the combination of a battery-type electrode (for energy improvement) with a capacitive electrode (to improve the power) for increased operating potential window to give a large specific capacity of 111.2 C/g. They presented an asymmetry supercabattery where the battery side of the device was made up of TiO_2/Co-MOF material while the capacitive side was made up of activated carbon (AC) as shown in Figure 2.7 (a). The AC was chosen to act as capacitive electrode since it has high conductivity and large pore sizes that are responsible for absorption of electrolyte ions [71]. The electrochemical evaluation of AC electrode and TiO_2/Co-MOF electrode (Figure 2.7 (b)) were measured separately in a three-electrode cell for estimation of a potential window for supercapattery [70]. Steady potential windows were reported for activated carbons and TiO_2/Co-MOF materials which were determined to be −0.9 to 0 V and 0 to 0.6 V vs Ag/AgCl, respectively. This showed that AC electrode performs better at lower potentials rather than positive potentials. Furthermore, the two electrodes were placed in 2M KOH electrolyte to evaluate their supercapattery studies [70]. Based on three electrode system, it is anticipated that the potential window for the prepared supercapattery device is the addition of the potential window of TiO_2 aerogel/Co-MOF composite and AC electrodes which was seen to operate up to 1.5 V [70]. Figure 2.7 (c) shows the CV curves of the supercapattery at a potential ranging between 0 and 1.5 V at multiple scan rates [70], displaying nearly quadrangular shaped CV curves with an further wide redox peak due to the non-faradaic and faradaic activities [72]. In addition, Figure 7(d) displays the GCD curves of the TiO_2 aerogel/Co-MOF//AC cell at a current density range of of 0.5 – 2.5 A/g [70]. The GCD curves showed a non-linear profile owing to the presence of the faradic activities of TiO_2 aerogel/Co-MOF and nearly symmetric at all current densities which indicate the better kinetic competency of the device [73].

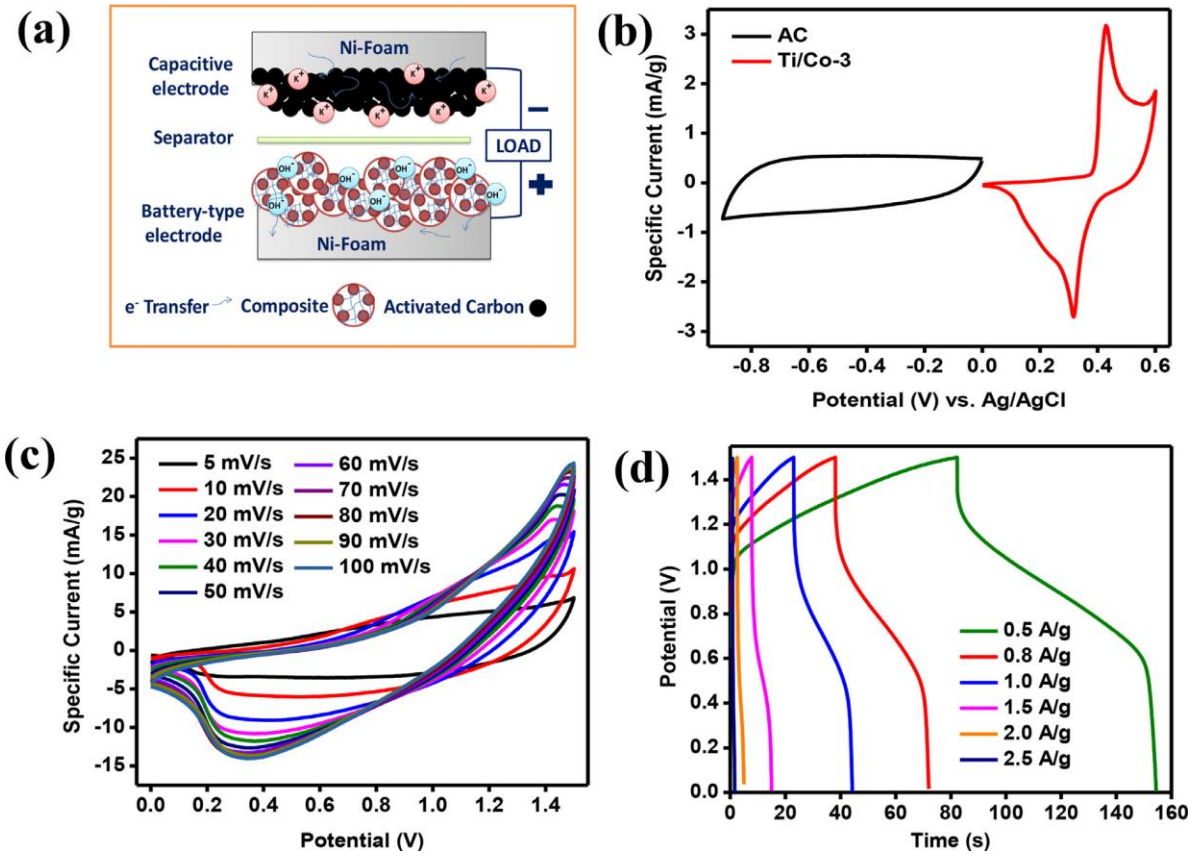

Figure 2.7: (a) Schematic illustration of an asymmetric supercapattery, b) Comparison of CV curves for AC and TiO_2/Co-MOF electrodes, (c) CV and (d) GCD of battery-type electrode [70].

In addition to metal oxide, Ye et al. [74] fabricated as asymmetric supercapattery device from NiCo-MOF as positive electrode and AC as negative electrodes. The assembled NiCo-MOF//AC supercapattery device demonstrated a specific capacitance of 172.7 F/g at a current density of 0.5 A/g with very good cyclic stability retention of 92.7% after 4000 cycles. The high electron transfer of carbon-based materials can be well expressed by adding bimetallic MOFs to their structures. Furthermore, Liu et al. [75] prepared NiCo-MOF hybrid composite with acetylene black (AB) to form NiCo-MOF/AB composite (Figure 2.8 (a) and (b)). The assembled NiCo-MOF/AB//AC asymmetric supercapattery (Figure 2.8 (c) and (d)) resulted in a specific capacitance of 115.05 F/g at a current density of 0.5 A/g with a maximum energy density of 33.84 Wh/kg and power density of 15.1 kW/kg.

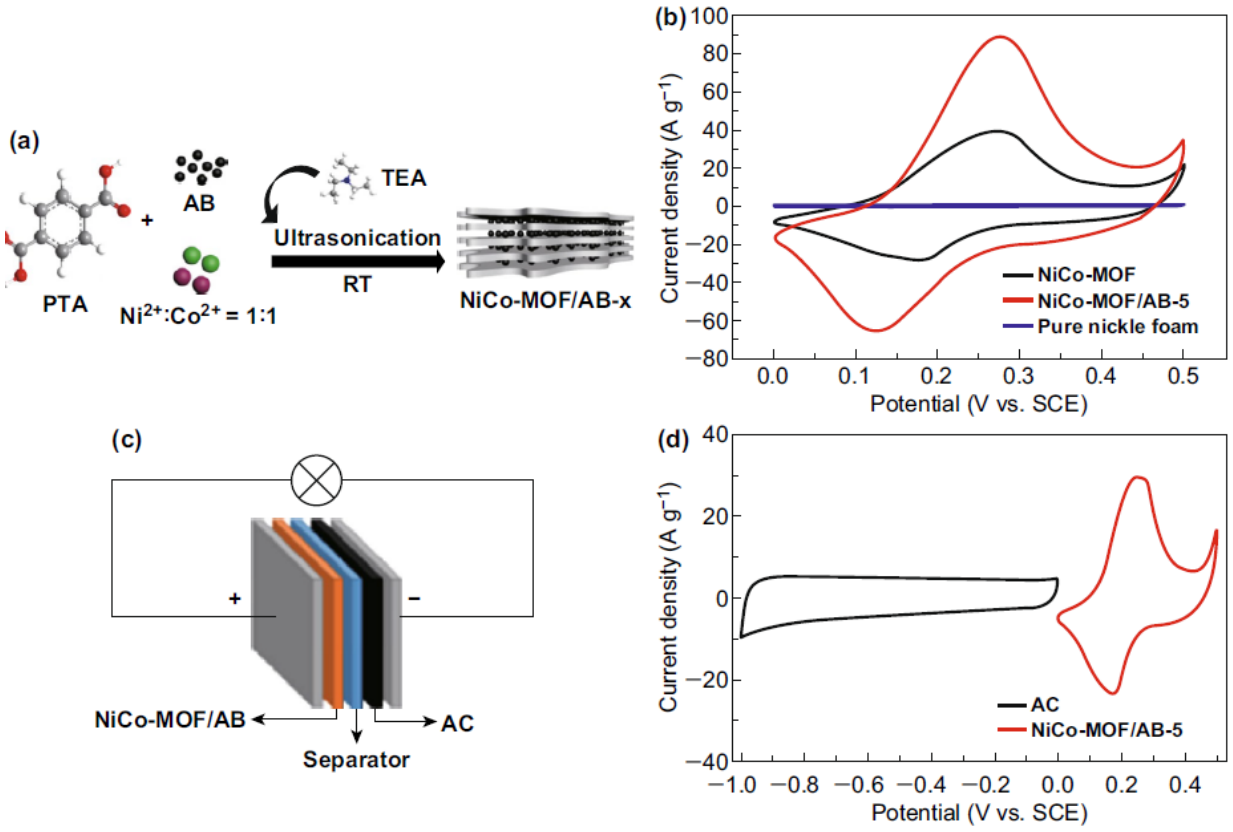

Figure 2.8: (a) Schematic diagram of NiCo-MOF/AB composite preparation. (b) CV profiles of nickel foam, NiCo-MOF and NiCo-MOF/AB composite at a scan rate 50 mV/s. (c) Scheme showing the assembling of asymmetric supercapattery (NiCo-MOF/AB//AC). (d) CV curves of NiCo-MOF/AB composite and AC [75].

2.4.4. Metal organic framework and conducting polymer composites

The combination of MOFs with conducting polymers has shown good conductive properties [76].Conducting polymers are usually synthesised via the chemical oxidation as well as the electrochemical deposition. There are two states of these polymers that usually occur during their charge and discharge which are p-doping and n-doping where the ions from the electrolyte are extracted or inserted on the polymer backbone. Polymer structures are usually in straight chains which expose the whole polymer chains to the electrolyte ions. The disadvantage of using conducting polymers is that the polymer chain is being damaged during fast charge/discharge periods. Patterson and co-workers [76] have synthesised polypyrrole (PPy)–Co-MOF, PPy–Ni-MOF and PPy–HKUST-1 composites. The structural and electrochemical properties

of these composites consisting of three differing MOF types for use in supercapacitive applications were compared. The SEM images (Figure 2.9 (a-f)) of the resulted composites have shown PPy particles linked on the surface of large MOF crystals, which promotes the electron transfer between MOF particles. The enhancement of electron transfer was attributed to high conductivities of PPy with one-dimensional structure. With regard to electrochemical analyses (Figure 2.9 (g-j)), the authors reported a massive boost in terms of specific capacitance from 0.2 F/g in unmodified MOFs to more than 185 F/g upon composite formation at a current density of 0.8 mA/cm^2. Furthermore, the synthesised PPy-MOF composites displayed not so good cyclability, with only 70% of capacitance retained after 2500 cycles. They concluded that higher amount of PPy and balanced modification of particle surface hydrophobicity/hydrophilicity are recommended so that the MOF/electrolyte interface is limited, resulting in more stable electrode materials.

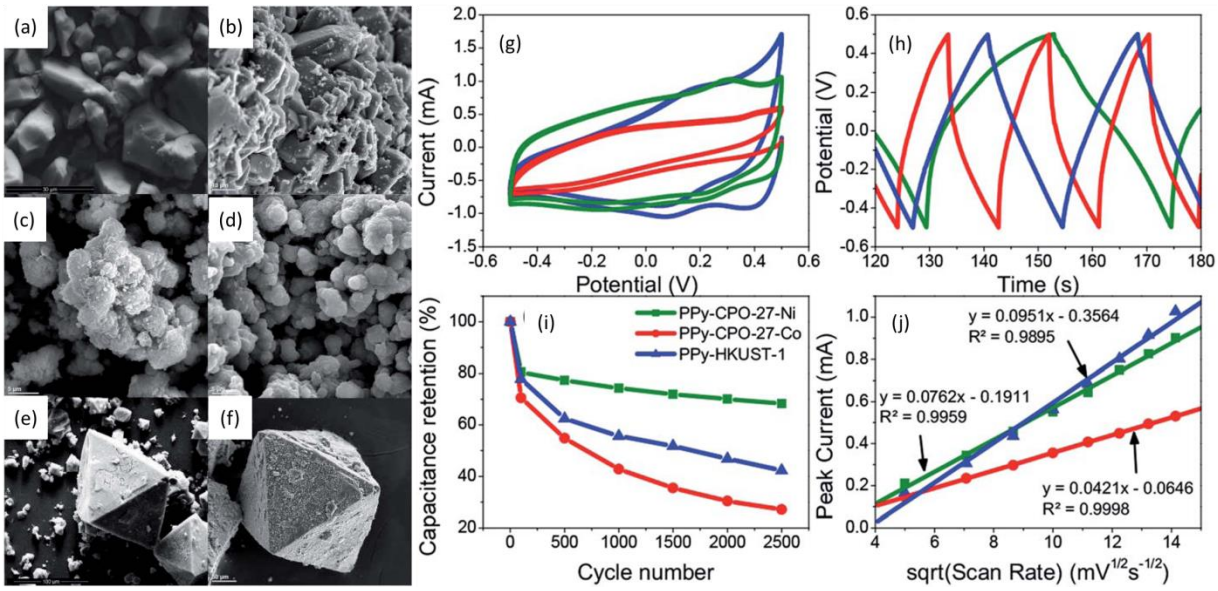

Figure 2.9: SEM images of (a) Co-based, (c) Ni-based and (e) HKUST-1 MOFs and of (b) PPy–Co-MOF, (d) PPy–Ni-MOF and (f) PPy–HKUST-1 composites. (g) CV, (h) GCD, (i) long term charge retention, (j) diffusion coefficient results for all the composites [76].

2.4.5. Metal organic frameworks and carbon-based material composites

The applications of most pure MOFs and its composite with conducting polymers, metal oxides and metal hydroxides have shown a pseudocapacitive-type and battery-type of charge storage mechanism [77-101], as shown in Table 2.1. The fast faradaic

reactions included in the electrodes results in the electrode are deteriorated after certain number of cycles [77]. Furthermore, MOFs in ES applications have been reported to possess relatively easy decomposition, thermal stability and chemical stability as result of their skeleton structure [38]. Therefore, such factors limit the use of MOFs in ES applications. It was seen that carbon materials have been reviewed and shown to exhibits an EDLC in most supercapacitor applications. This section describes strategies that can be followed for the modification of MOFs with carbon materials recognised for their good electrical properties, surface area, and good physical stabilities. Therefore, the composites based on MOF materials with carbon materials can theoretically meet the important requirements of a high performance electrode material for supercapacitor applications. Hybridisation of carbon material with MOFs and forming a double shell structure are the common ways to avoid the irreversible capacity/capacitance loss caused in charge-discharge processes and therefore improving the stability and performance. This is due to higher chemical and thermal stability of the graphene materials and the MOF-carbon composites are theoretically good candidates for supercapacitor materials [78].

Both single and multi-wall carbon nanotubes have been explored as electrode materials in energy storage and they have shown excellent pore structure, good thermal and chemical stability [79, 80]. However, individually these materials do not show sufficient electrochemical performance [79]. Nevertheless, MOF/CNT composites exhibits higher surface area, good physical properties and excellent pore size distribution characteristics due to the presence MOFs, good scale of electrical conductivity is observed due to the presence of highly conducting CNT component. Wen et al. [80] reported a composite of Ni-MOF and CNTs in 6M KOH electrolyte used as a positive electrode in an asymmetric hybrid supercapacitor. This Ni-MOF/CNT composite delivered specific capacitance of 1765 F/g at a current density of 0.5 A/g. The CV curves of the composite were tested at a potential range of -0.1 to 0.6V at a scan rate of 10mV/s. A pair of redox peaks is observed resulting from the reversible redox reaction of Ni^{2+}/Ni^{3+} (Figure 2.10 (a)). The composite material displays both enhanced currents and depressed peak separation, demonstrating the improved utilisation of the electro active species. The capacitance performance was measured using GCD as shown in Figure 2.10(b***)***. The specific capacitance of Ni-MOF/CNT composite was found to be 1765 F/g at a current density of 0.5 A/g. Figure 2.10 (c)

shows the orientation of CNTs and the Ni-MOF in the composite as well as the exchange of ions between the two materials. The hybrid asymmetric SC based on Ni-MOF/CNT and rGO/C_3N_4 as positive and negative electrodes respectively exhibited a high energy density of 36.6 Wh/kg at a power density of 480 W/kg. Moreover, this asymmetric supercapacitor demonstrated an excellent life cycle with almost 95% capacitance retention after 5000 consecutive charge–discharge cycles [80].

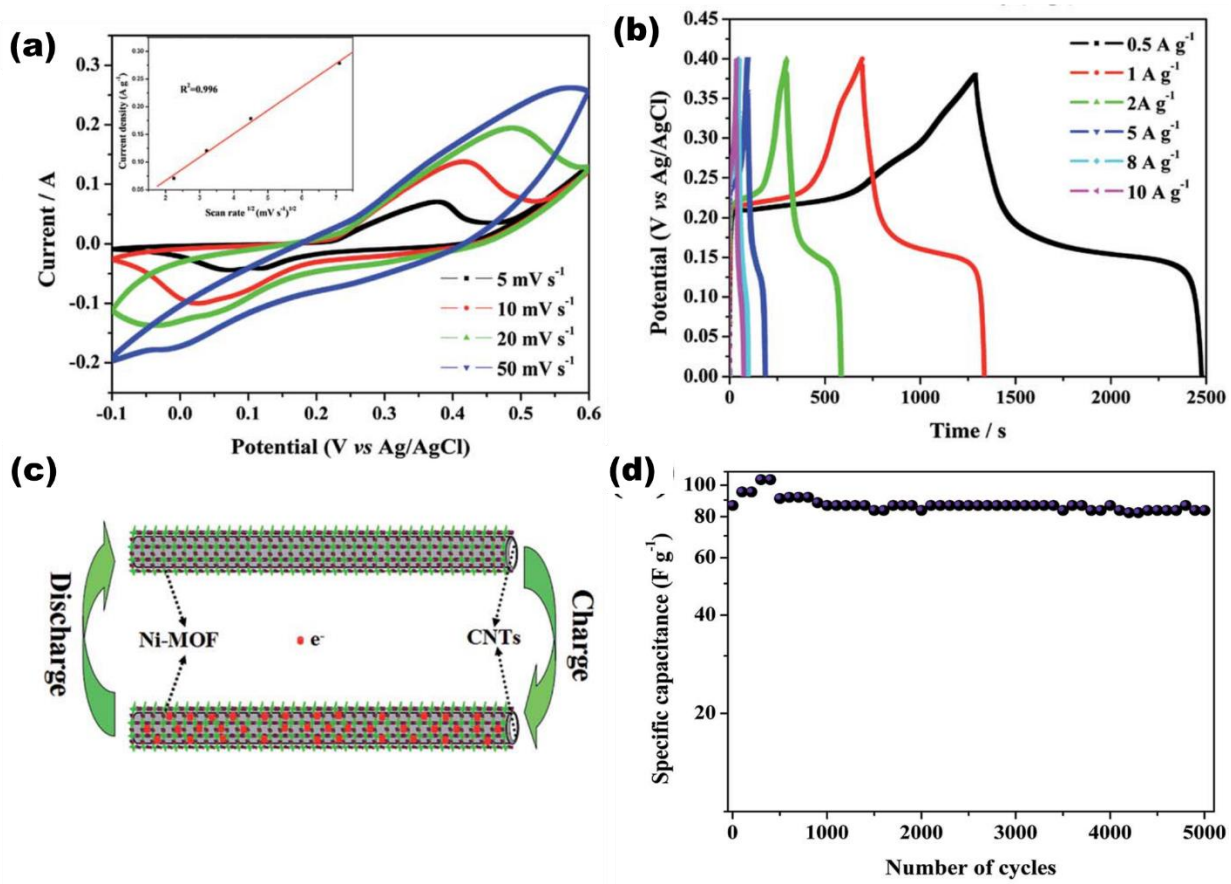

Figure 2.10: (a) CV curves of Ni-MOF/CNT-5 hybrid composite at different scan rates (inset; peak current as a function of the square root of scan rates). (b) GCD curves of Ni-MOF/CNT-5 at different current densities. (c) An illustration showing the transfer of electrons in the Ni-MOF/CNT composite. (d) Stability testing at a current density of 2 A/g for 5000 cycles [80].

On the other hand, Zhou et al. [81] developed an in-situ preparation of GO and Ni-MOF hybrid composite as an electrode material for ES application. This synthesis method for the hybrid composite resulted in flower-like structures (SEM-image) with improved surface area (74.02 m^2/g) as shown in Figure 2.11.

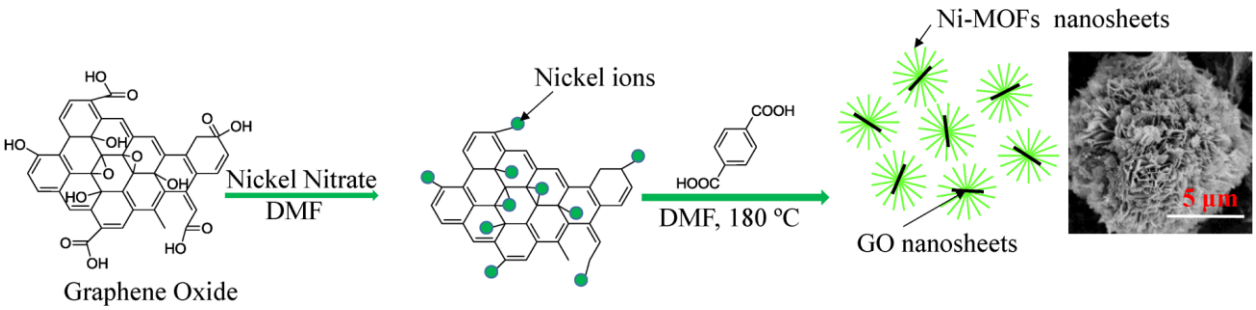

Figure 2.11: Scheme showing the in-Situ hybridisation of Ni−MOF with GO nano-sheets, copied with permission from [81].

The Ni-MOF@GO composite was tested for electrochemical performance in a three electrode system and the CV curves of the composite exhibited a pseudocapacitive behaviour which was due to the reversible intercalation-deintercalation of OH^- ions (Figure 2.12 (a)). The GCD shows an increase in discharge time as the current density decreases with non-linear shapes as shown in Figure 2.12 (b).The maximum specific capacitance of the MOF/GO composite was 2192.4 F/g obtained at a specific current of 1 A/g (Figure 2.12 (c)) and 85.1% of its capacitance was preserved after 3000 cycles at a specific current of 10 A/g (Figure 2.12 (d)). According to Zhou [81], the outstanding capacitive behaviour of the composite are due to the unique flower-like structure and the synergetic effects shown by the Ni−MOF and the GO nano-sheets, which improves the electroactive sites with fast paths to allow ion movements as well as allowing excellent electron movement between the Ni−MOF and the GO nano-sheets [81].

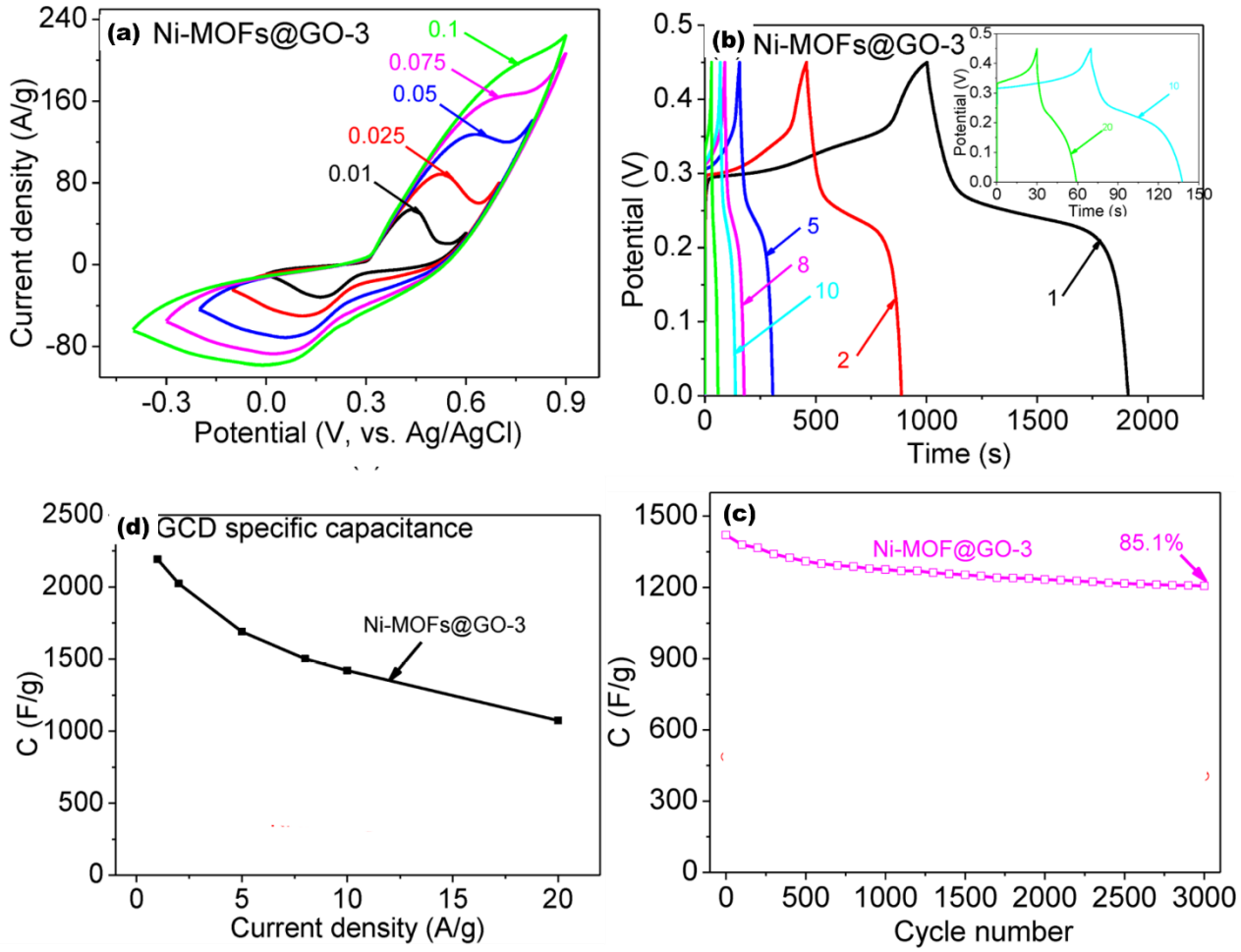

Figure 2.12: (a) CV curves of Ni-MOF@GO-3 at different scan rate. (b) GCD curves of Ni-MOF@GO-3 at different current densities. (d) Stability test of Ni-MOF@GO-3 for 3000 cycles [81].

Amongst the graphene materials, rGO has emerged as the most cited material for EDLC SCs due to high electrical conductivity, excellent chemical and physical stabilities, and high surface area. The incorporation of rGO nanosheets on MOF structures is believed to produce a supercapacitor electrode material with high power and energy density as well as improved capacitances. For example, Srimuk et al. [82] developed MOF/rGO composite for supercapacitor applications. During the synthesis, 10%wt of rGO was incorporated to MOF and a composite with high specific surface area of 1241 m^2/g and pore volume of 0.78 cm^3/g was produced. Figure 2.13 (a) shows SEM image of MOF/rGO composite where highly crystalline MOF structured are observed in the presence of partially agglomerated rGO nanosheets. The three electrode system was used to determine the electrochemical performance of the composite performed in 0.5M Na_2SO_4 electrolyte. The CV curve of the composite in

Figure 2.13 (b) was performed at a scan rate of 100mV/s and they show rectangular shapes which are characteristic of good EDLC electrode materials. The GCD results were in good correspondence with the CV results were a high discharge time is observed for the composite than rGO and MOF separately (Figure 2.13(c)). The electrode material exhibited a maximum specific capacitance of 385 F/g at a current density of 0.5 A/g as indicated in Figure 13(d). A solid-type hybrid full cell resulted in an energy density of 42 Wh/kg and power density of 3100 W/kg using a polymer gel electrolyte.

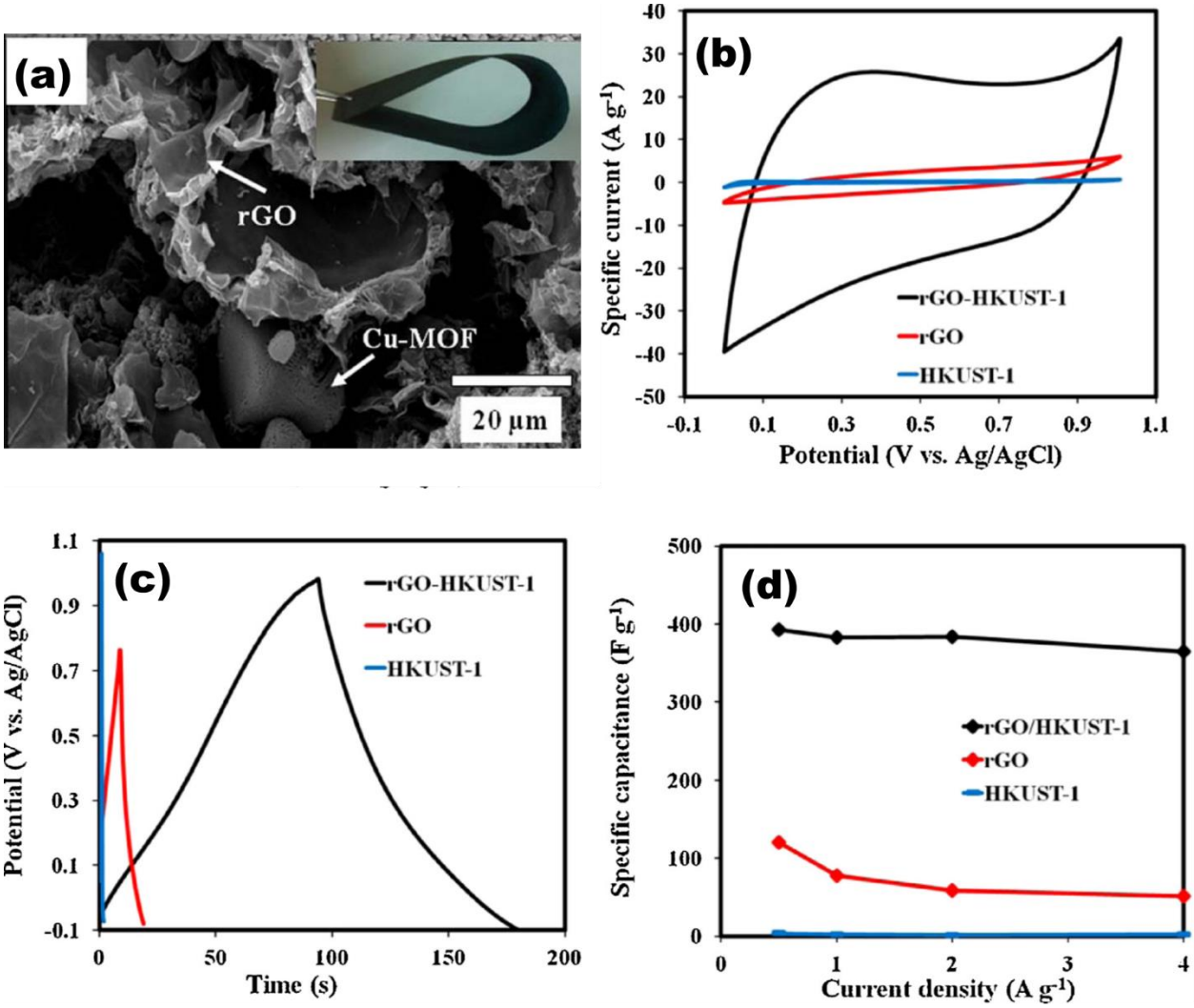

Figure 2.13: (a) SEM image of rGO-HKUST-1 composite. (b) CV curves of the as-prepared supercapacitor electrodes at a scan rate of 100mV/s, (c) GCD curves, and (d) the specific capacitances vs. applied current densities [82].

The presence of a redox additive electrolyte (RAE) is important for the enhancement of ES as it improves the redox activity of the electrolyte and therefore improves the

performance of the SC. Sundriyal et al. [83] developed a MOF/rGO composite for ES applications in a 1.0M Na2SO4 electrolyte with 0.2M K_3 [$Fe(CN)_6$] as a RAE. The ZIF/rGO hybrid electrode in the three-electrode cell shows a highly improved specific capacitance of 1453 F/g at a high specific current of 4.5 A/g performed at a potential window of −0.1 V to 0.5 V. Furthermore, the composite electrode was investigated in a symmetrical supercapacitor. The operation of the device included the presence of the RAE which has delivered high values of specific capacitance (326 F/g at a current density of 3 A/g) with maximum energy and power density of 25.5 Wh/kg and 2.7 kW/kg respectively. The device retained about 88% of the initial specific capacitance after 1000 charge and discharge cycles. Their results has shown the importance of carbon material as a support for MOF materials and that the MOF/carbon composite materials are promising electrode materials for future SC with high energy and power density.

Table 2.1: Summary of the electrochemical energy storage parameters of different types of MOFs for supercapacitors in three and two electrode systems.

Active Material	**Components**	**Electrolyte**	**Current density**	**Specific capacity/ cance**	**Energy density ($WhKg^{-1}$)**	**Power density (WKg^{-1})**	**Ref.**
MOF-5	MAC-A	6M KOH	0.25 A/g	271 F/g	A	A	[84]
	IMCSs-4-8-6	6M KOH	0.05 A/g	242 F/g	A	A	[85]
	carbon	1M NEt_4BF_4/PC	0.6 A/g	175 F/g	A	A	[86]
ZIF-8	PCPs	1M KOH	1 A/g	245 F/g	A	a	[87]
	NPCF	1MH2SO4	1 A/g	332 F/g	A	a	[88]

	ZIF-8/PANI	6.0M	1 A/g	236 F/g	A	a	[89]
ZIF-8 + ZIF-67	NC@GC	1MH2SO4	2 A/g	270 F/g	A	a	[90]
	Nanoporous Co3O4	6M KOH	*5 mV/s	272 F/g	A	a	[91]
UiO-66	HP-UiO-66	6M KOH	0.2 A/g	849 F/g	A	a	[92]
MOF-74	MOF-74–NiCo1	6M KOH	1 A/g	797 F/g	A	a	[93]
Ni-MOF	Pure Ni-MOF	6M KOH	1 A/g	1698 F/g	A	a	[69]
Co-MOF	PureCo-MOF	5M KOH	1 A/g	2564 F/g	A	a	[70]
Ni-MOF	Ni-MOF/CNT	6.0M KOH	0.5 A/g	1765 F/g	A	a	[80]
	$NiCo_2O_4$@Ni-MOF	2.0M	2mA/cm^2	209 mA/g	A	a	[94]
	Mo/Ni-MOF	KOH	1 A/g	802 C/g	A	a	[95]
	Ni-MOF/rGO	3.0M KOH	1 A/g	1154 F/g	A	a	[96]
	RGO/HKUST-1	KOH	1 A/g	385 F/g	A	a	[82]
	CNT/Mn-MOF//CNT/Mn-MOF	1.0 M Na_2SO_4	0.25 A/g	B	6.9	2240	[97]
	AC// Ni@Cu-MOF	6.0 M KOH	1 A/g	B	17.3	798.5	[98]

	ZIF-67/rGO//ZIF-67/rGO	1.0 M Na_2SO_4	3 Ag^{-1}	B	25.5	2700	[99]
	AC// NiCo-MOF	2.0 M KOH	0.5 Ag^{-1}	B	49.4	562.5	[100]
	Ni-MOF/CNT//rGO/C3N4	6.0M KOH	0.5 Ag^{-1}	B	36.6	480	[101]

a=three electrode system and b= two electrode system

2.4.6. Metallic nanoparticle loaded MOF-carbon composites.

Metallic nanoparticles are believed to enhance the activity in MOF and carbon electrode materials. These materials provide larger active sites for the electrode/electrolyte interactions and thus improving the performance of an electrode. Previously Hu et al. [102] developed an electrode material based on Pd-rGO/MWCMT for electrochemical applications. SEM images (Figure 2.14 (a)) of Pd-rGO-MWCNT shows plenty of nanoparticles distributed on the composite surface, indicating successful synthesis of the palladium loaded hybrid composite. The CV curves in Figure 2.14 (b) compares materials that are palladium loaded with those without it. It is observed that there is an improved electrochemical performance and redox activity in palladium containing materials. Pd-rGO/MWCNT exhibited high catalytic activity and therefore confirms the importance of Pd nanoparticles in electrochemical performance.

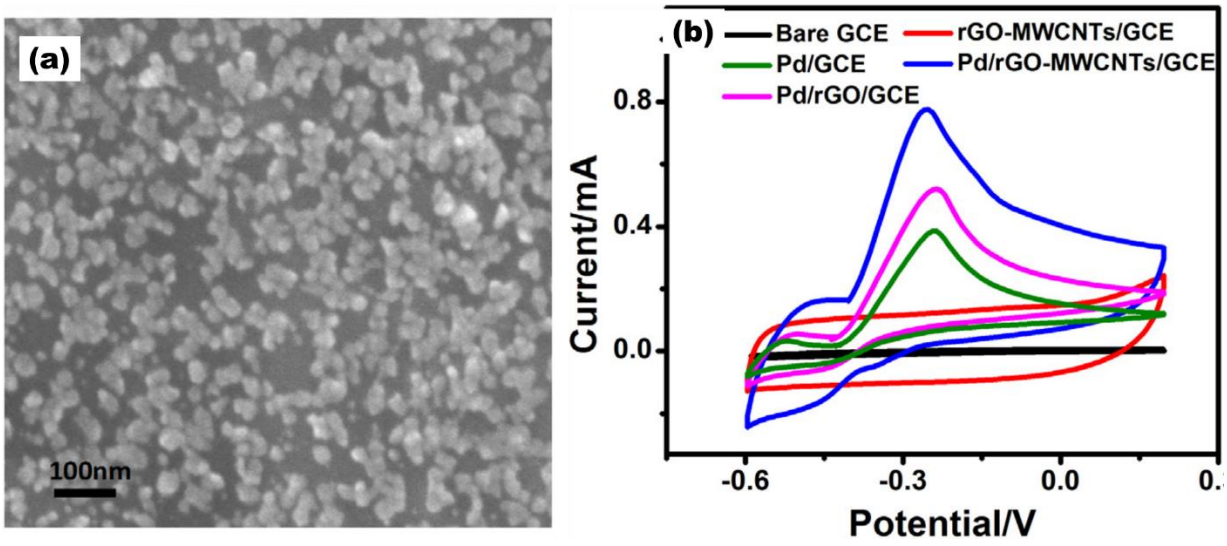

Figure 2.14: (a) The SEM image of the prepared Pd/rGO-MWCNTs. (b) CV curves of bare GCE, rGO-MWCNTs/GCE, Pd/rGO-MWCNTs/GCE, Pd/rGO/GCE and Pd/GCE with hydrazine in 0.1 M PBS [102].

On the other hand, Gupta et al [103] developed a PdO nanoparticle loaded RGO for ES applications. Gold particles were later loaded on the composite for enhancement in the SC applications. The CV curves of rGO, PdO-RGO and Au-PdO-RGO composites in Figure 15 (b) has shown an EDL-capacitance, this is evidence that metallic nanoparticles could be involved in the improvement of electrochemical performance without showing any pseudocapacitive activity. RGO and PdO-RGO electrodes exhibited a specific capacitance of 135.0 F/g and 158.9 F/g at a current density of 0.2 A/g respectively (Figure 2.15 (a)). There palladium and gold nanoparticles exhibited an increase in the electrochemical performance of the electrode materials without tempering with the nature of the electrodes.

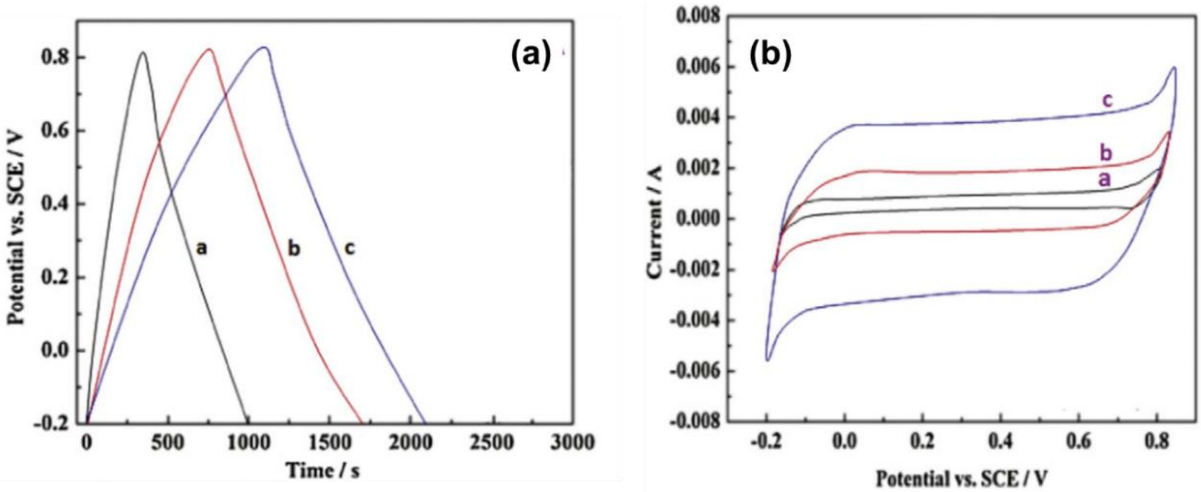

Figure 2.15: (A) GCD curves of rGO (a), PdO-RGO (b) and Au-PdO-RGO at a current density of 0.2 A/g. (B) CV curves of RGO (a), PdO-RGO (b) and Au-PdO-RGO at a scan rate of 5 mV/s [103].

Furthermore, the electrochemical performance of Pd-RGO composite and its precursors were determined using a three electrode system in 5.0 mM $K_3[Fe(CN)_6]$ containing 1.0 M KCl electrolyte. The CV curves of the composite produced a high current response which is due to reduced kinetic transfer resulting from the presence of palladium nanoparticles (Figure 2.16 (A)). The increase in palladium loading to the RGO shows a direct relationship to the current response in 1.0M KCl electrolyte (Figure 2.16 (B)). The GCD curves of RGO and Pd-RGO on glassy carbon electrode (GCE) were compared at a current density of 1.75 A/g and it is observed that Pd containing RGO shows high discharge performance as indicated in Figure 2.16 (C). Finally Figure 2.16 (D) shows the specific capacitance vs current density of Pd-rGO and it exhibited a high specific capacitane of 637 F/g at a current density of 1.25 A/g with high power and energy density of 56 Wh/kg and 1166 W/kg respectively [104].

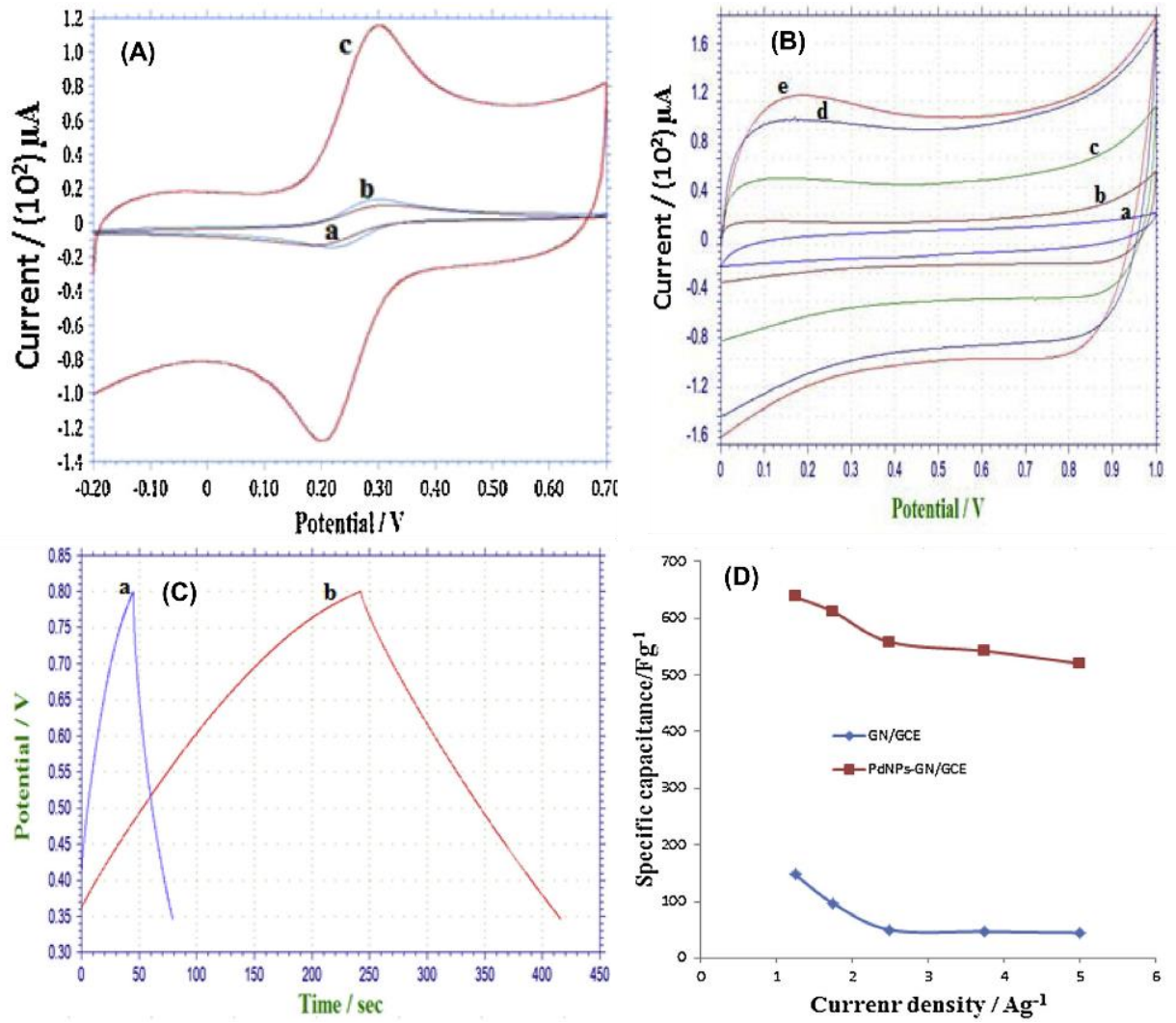

Figure 2.16: (A) CV of (a) GO (b) GO and (c) PdNPs-GO in 5.0 mM $K_3[Fe(CN)_6]$ containing 1.0 M KCl at a scan rate of 100 mV/s. (B) CV of (a) GO, (b) PdNPs-GO (7.3% $PdCl_2$), (c) (14.6% $PdCl_2$), (d) (29.3% $PdCl_2$) and (e)(58.6% $PdCl_2$)) in 1 M KCl at a scan rate of 100 mV/s. (C) GCD curves of (a) GO, (b) PdNPs-GO at current density of 1.75 A/g. (D) Specific capacitance of GN/GCE and PdNPs-GO vs current density [104].

These results have shown the importance of incorporating nanoparticles, especially palladium nanoparticles in ES electrodes for enhanced performances. However, the selection of a suitable electrolyte in the electrochemical testing and applications of this electrode is also important. Therefore, in the next topic a brief review on the present types and examples of certain electrolytes is discussed.

2.5. Electrolytes

Electrolytes are conducting solutions with positive and negative ions used in SC analysis. They are classified into aqueous and non–aqueous as shown in figure 17(a) [105]. Aqueous electrolytes include Na_2SO_4, H_2SO_4, KOH, and KCl which are commonly used due to their high conductivity, abundance and low cost. Aqueous electrolytes are good in lowering the ESR which provides high power densities, however they are limited to narrow potential windows which therefore produces low values of energy densities. Aqueous electrolytes can further be subdivided into acid electrolyte (H_2SO_4), basic electrolyte (KOH) and neutral electrolyte (Na_2SO_4). Organic electrolytes used in SC are prepared by dissolving salts in organic solvents such as acetonitrile. This type of electrolytes exhibits high operating potential range which boots the energy density to higher values. However, these electrolytes suffer some drawbacks such as higher cost, low specific capacitance, a lower conductivity, and they are flammable, volatile and toxic. For high performances in electrochemical SC, a relevant, low cost and more conductive electrode has to be selected. Figure 17(b) summarizes the effects of electrolyte on the performance of an electrochemical supercapacitor. An ideal electrolyte for supercapacitors comprises of a wide potential range, good electrochemical stability, low internal resistance, low cost and high abundance [21].

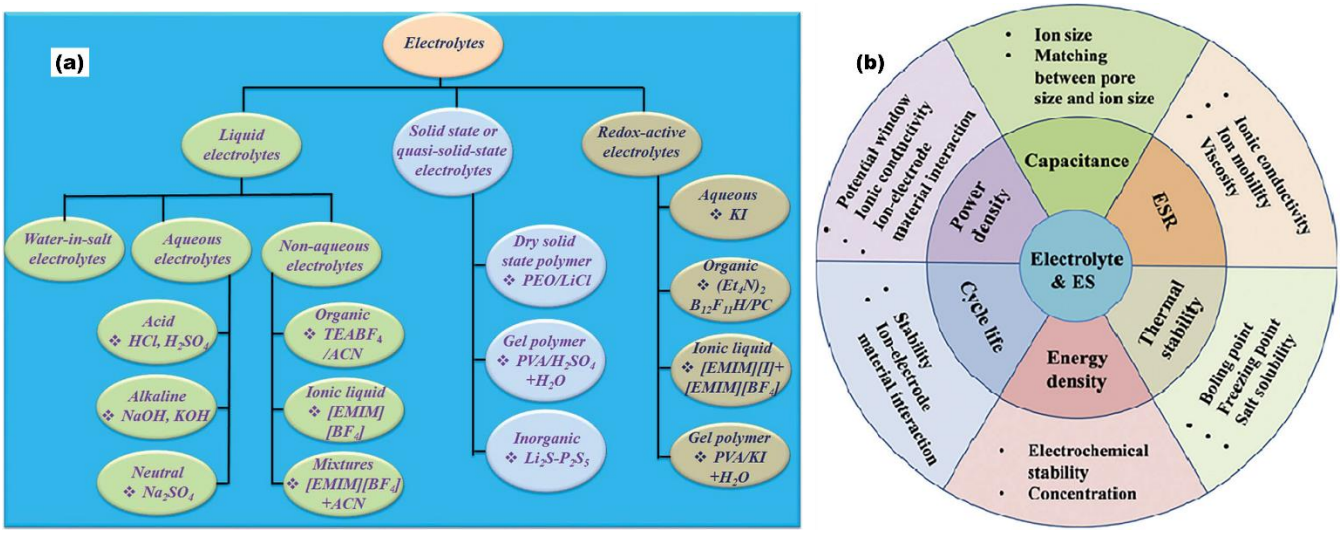

Figure 2.17: (a) Classification of electrolytes [105], (b) Effects of electrolytes on the performance of supercapacitors [77].

2.6. Conclusion

The burning of fossils for energy production results in harmful results including global warming, therefore various renewable energy sources are being developed in order to minimize or eradicate the use of fossils. Alternative energy storage mechanisms are required in order to store the produced energy for future use. Electrochemical supercapacitors are emerging as promising devices amongst the currently used energy storage devices. In this review, a detailed description of electrode materials based on metal organic frameworks, carbon materials and their composite is thoroughly given. More developments is needed for high-performance SC electrodes which can simultaneously give high capacitance, cyclic stability and excellent rate. MOFs, carbon-based materials and their composites are found to have the necessary potential for making effective electrodes for supercapacitors. Moreover, MOF-carbon hybrid composites are believed to improve the SC performances as they combine EDLC properties with those of a pseudocapacitive material. The high surface area and tunable pore sizes of MOFs allow more diffusion of the electrolyte in to the electrode structure for high performances. Generally pristine-MOFs suffer from poor conductivity and poor mechanical stability. These limitations might be overcome in near future through the hybridization of MOFs with materials with improved conductivities and stability. However, the properties of MOFs should be preserved during the process of composite formation. In summary, supercapacitor applications of MOFs and MOF-carbon based composites are still studied at a laboratory scale. Further research efforts in the enhancement of MOF properties for supercapacitors may lead to the utilisation of MOFs as electrode materials for commercial supercapacitors.

References

[1] Quartey G, Adzimah SK, (2014). Generation of electrical power by a wind turbine for charging moving electric cars. J. Energy Technol. Policy 4, 19.

[2] Goh SY, Kok SL, (2017). Electrical energy harvesting from thermal energy with converged infrared light. IOP Conf. Ser. Mater. Sci. Eng. 210.

[3] Padmanathan K, Govindarajan U, Ramachandaramurthy VK, Jeevarathinam B, (2018).Integrating solar photovoltaic energy conversion systems into industrial and commercial electrical energy utilization—a survey. J. Ind. Inf. Integr. 10, 39–54.

[4] Wang X, Han Y, Zhang J, Li Z, Li T, Zhao X, Wu Y, (2019).The design of a direct charge nuclear battery with high energy conversion efficiency. Appl. Radiat. Isot. 148, 147–151.

[5] He Y, Wang L, Jia D, (2016). CoAl/PAN interconnected carbon nanofibers with excellent energy storage performance and electrical conductivity. Electrochim. Acta 194, 239–245.

[6] Vera D, Jurado F, Carpio J, Kamel S, (2018). Biomass gasification coupled to an EFGT–ORC combined system to maximize the electrical energy generation: a case applied to the olive oil industry. Energy, 144, 41–53.

[7] Somo TR, Maponya TC, Davids MW, Hato MJ, Lototskyy MV, Modibane KD, (2020). A comprehensive review on hydrogen absorption behaviour of metal alloys prepared through mechanical alloying. Metals, 10, 562.

[8] Asongu S, Agboola OM, Alola A, Bekun FV, (2020).The criticality of growth, urbanization, electricity and fossil fuel consumption to environment sustainability in Africa. Sci. Total Environ. 712, 136376.

[9] Rolison DR, Nazar LF, (2011). Electrochemical energy storage to power the 21st century. MRS Bull. 36(7), 486–493.

[10] Chen GZ, (2017). Supercapacitor and supercapattery as emerging electrochemical energy stores. Int. Mater. Rev. 62(4), 173–202.

[11] Akinwolemiwa B, Peng C, Chen GZ, (2015). Redox electrolytes in supercapacitors. J. Electrochem. Soc. 162(5), A5054.

[12] Yu L, Chen GZ, (2016). Redox electrode materials for supercapatteries. J. Power Sources 326, 604–612.

[13] Zhang S, Pan N, (2014). Supercapacitors performance evaluation. Adv. Energy Mater. 5(6), 1401401.

[14] Brousse T, Bélanger D, Long JW, (2015). To be or not to be pseudocapacitive? J. Electrochem. Soc. 162(5), 5185.

[15] Guan L, Yu L, Chen GZ, (2016). Capacitive and non-capacitive faradaic charge storage. Electrochim. Acta 206, 464–478.

[16] Conway BE, (1999). Electrochemical Capacitors Based on Pseudocapacitance. Springer, Boston. 221–257

[17] Peng C, Li Y, Yao F, Fu H, Zhou R, Feng Y, Feng W, (2019). Ultrahigh-energy-density fluorinated calcinated macadamia nut shell cathodes for lithium/fluorinated carbon batteries. Carbon 153, 783.

[18] Shi H, Zhao X, Wu ZS, Dong Y, Lu P, et al, (2019), Free-standing integrated cathode derived from 3D graphene/carbon nanotube aerogels serving as binder-free sulfur host and interlayer for ultrahigh volumetric-energy-density lithiumsulfur batteries. Nano Energy 60, 743–751.

[19] Guo M, Balamurugan J, Thanh TD, Kim NH, Lee JH, (2016).Facile fabrication of Co_2CuS_4 nanoparticle anchored N-doped graphene for high-performance asymmetric supercapacitors. J. Mater. Chem. A 4(44), 17560–17571.

[20] Dong L, Ma X, Li Y, Zhao L, Liu W, et al, (2018). Extremely safe, high-rate and ultralong-life zinc-ion hybrid supercapacitors. Energy Storage Mater. 13, 96–102.

[21] Sethi M, Bantawal H, Shenoy US, Bhat DK, (2019). Eco-friendly synthesis of porous graphene and its utilization as high performance supercapacitor electrode material. J. Alloys Compd. 799, 256–266.

[22] J. Lin, Y. Yan, H. Wang, X. Zheng, Z. Jiang et al., Hierarchical Fe2O3 and NiO nanotube arrays as advanced anode and cathode electrodes for high-performance asymmetric supercapacitors. J. Alloys Compd. 794, 255–260 (2019).

[23] Z. Lin, Y. Liu, Y. Yao, O.J. Hildreth, Z. Li et al., Superior capacitance of functionalized graphene. J. Phys. Chem. C 115(14),7120-7125.

[24] Iqbal S, Khatoon H, Hussain PA, Ahmad S, (2019). Recent development of carbon based materials for energy storage devices. Mater. Sci. Energy Technol. 2(3), 417–428.

[25] Wang Y, Song Y, Xia Y, (2016). Electrochemical capacitors: mechanism, materials, systems, characterization and applications. Chem. Soc. Rev. 45(21), 5925–5950.

[26] Varghese J, Wang H, Pilon L, (2011). Simulating electric double layer capacitance of mesoporous electrodes with cylindrical pores. J. Electrochem. Soc. 158(10), A1106.

[27] Khomenko V, Raymundo-Piñero E, Béguin F, (2006). Optimisation of an asymmetric manganese oxide/activated carbon capacitor working at 2 V in aqueous medium. J. Power Sources 153(1), 183–190.

[28] Hughes M, Chen GZ, Shaffer MSP, Fray DJ, Windle AH, (2002). Electrochemical capacitance of a nanoporous composite of carbon nanotubes and polypyrrole. Chem. Mater. 14(4), 1610–1613.

[29] Yi CQ, Zou JP, Yang HZ, Leng X, (2018). Recent advances in pseudocapacitor electrode materials: transition metal oxides and nitrides. T. Nonferrous Metals Soc. 28(10), 1980–2001.

[30] Laforgue A, Simon P, Fauvarque JF, Sarrau JF, Lailler P, (2001). Hybrid supercapacitors based on activated carbons and conducting polymers. J. Electrochem. Soc. 148(10), A1130.

[31] Choi KM, Jeong HM, Park JH, Zhang YB, Kang JK, Yaghi OM, (2014). Supercapacitors of nanocrystalline metal–organic frameworks. ACS Nano 8(7), 7451–7457.

[32] Cao X, Zheng B, Shi W, Yang J, Fan Z, et al., (2015). Reduced graphene oxide-wrapped MoO3 composites prepared by using metal–organic frameworks as precursor for all-solidstate flexible supercapacitors. Adv. Mater. 27(32), 4695–4701.

[33] Conway BE, (1999). The Double Layer at Capacitor Electrode Interfaces: Its Structure and Capacitance .Springer. 105–124.

[34] Balasubramaniam S, Mohanty A, Balasingam SK, Kim SJ, Ramadoss A. (2020). Comprehensive Insight into the Mechanism, Material Selection and Performance Evaluation of Supercapatteries. Nano-Micro Letters, 12,1-46.

[35] Candelaria SL, Shao Y, Zhou W, Li X, Xiao J, et al.,(2012). Nanostructured carbon for energy storage and conversion. Nano Energy **1**(2), 195–220.

[36] Jiang Y, Liu J, (2019). Definitions of pseudocapacitive materials: a brief review. Energy Environ. Mater. **2**(1), 30–37.

[37] Augustyn V, Simon P, Dunn B, (2014). Pseudocapacitive oxide materials for high-rate electrochemical energy storage. Energy Environ. Sci. **7**(5), 1597–1614.

[38] Djire A, Pande P, Deb A, Siegel JB, Ajenifujah OT, et al., (2019). Unveiling the pseudocapacitive charge storage mechanisms of nanostructured vanadium nitrides using in situ analyses. Nano Energy, 60, 72–81.

[39] Chae JH, Ng KC, Chen GZ, (2010). Nanostructured materials for the construction of asymmetrical supercapacitors. Proc. Inst. Mech. Eng. Part A J. Power Energy 224(4), 479–503.

[40] Hughes M, Chen GZ, Shaffer MSP, Fray DJ, Windle AH, (2002). Electrochemical capacitance of a nanoporous composite of carbon nanotubes and polypyrrole. Chem. Mater. 14(4), 1610–1613.

[41] Hu CC, Chang KH, Lin MC, Wu YT, (2006). Design and tailoring of the nanotubular arrayed architecture of hydrous RuO_2 for next generation supercapacitors. Nano Lett. 6(12), 2690–2695.

[42] Zuo W, Li R, Zhou C, Li Y, Xia J, Liu J, (2017). Carbon-based materials as supercapacitor electrodes Battery-Supercapacitor Hybrid Devices: Recent Progress and Future Prospects. Adv. Sci. 4, 1600539.

[43] Xiea J, Yang P, Wang Y, Qi T, Lei Y, Li CM, (2018). Puzzles and confusions in supercapacitor and battery: Theory and solutions. Journal of Power Sources, 401, 213–223.

[44] Mei B-A, Munteshari O, Lau J, Dunn B, Pilon L, (2018). Physical Interpretations of Nyquist Plots for EDLC Electrodes and Devices. J. Phys. Chem. C, 122, 194−206

[45] Zhang F, Yuan C, Lu X, Zhang L, Che Q, Zhang X, (2012) Facile growth of mesoporous Co3O4 nanowire arrays on Ni foam for high performance electrochemical capacitors. J. Power Sources 203, 250–256.

[46] Lin Z, Liu Y, Yao Y, Hildreth OJ, Li Z, et al., (2011). Superior capacitance of functionalized graphene. J. Phys. Chem. C 115(14), 7120–7125.

[47] Hughes M, Chen GZ, Shaffer MSP, Fray DJ, Windle AH, (2002). Electrochemical capacitance of a nanoporous composite of carbon nanotubes and polypyrrole. Chem. Mater. 14(4), 1610–1613.

[48] Tang Q, Wang W, Wang G, (2015). The perfect matching between the low-cost Fe2O3 nanowire anode and the NiO nanoflake cathode significantly enhances the energy density of asymmetric supercapacitors. J. Mater. Chem. A 3(12), 6662–6670.

[49] Lu XF, Chen XY, Zhou W, Tong YX, Li GR, (2015). α-Fe2O3@PANI core–shell nanowire arrays as negative electrodes for asymmetric supercapacitors. Appl. Mater. Interfaces. 7(27), 14843–14850.

[50] Javed MS, Shah HU, Shaheen N, Lin R, Qiu M, et al., (2018). High energy density hybrid supercapacitor based on 3D mesoporous cuboidal Mn_2O_3 and MOF-derived porous carbon polyhedrons. Electrochim. Acta 282, 1–9.

[51] Wei X, Peng H, Li Y, Yang Y, Xiao S, Peng L, Zhang Y, Xiao P, (2018). In situ growth of zeolitic imidazolate framework- 67-derived nanoporous carbon@$K0.5Mn_2O_4$ for high-performance 2.4 V aqueous asymmetric supercapacitors. Chemsuschem 11(18), 3167–3174.

[52] Díaz R, Orcajo MG, Botas JA, Calleja G, Palma J, (2012). Co8-MOF-5 as electrode for supercapacitors. Materials Letters, 68, 126–128.

[53] Du W, Bai Y, Xu J, Zhao H, Zhang L, Li X, Zhang J, (2018). Advanced metal-organic frameworks (MOFs) and their derived electrode materials for supercapacitors. Journal of Power Sources, 402, 281–295.

[54] Zhu G, Wen H, Ma M, Wang W, Yang L, Wang L, et al, (2018). A self-supported hierarchical Co-MOF as a supercapacitor electrode with ultrahigh areal capacitance and excellent rate performance. Chem.commun, 2(4), 10499–10502.

[55] Lee DY, Yoon SJ, Shrestha NK, Lee SH, Ahn H, Han SH, (2012). Unusual energy storage and charge retention in Co-based metal–organic-frameworks. Microporous and Mesoporous Materials, 153, pp.163-165.

[56] Stock N, Biswas S, (2012). Synthesis of metal-organic frameworks (MOFs): routes to various MOF topologies, morphologies, and composites. Chemical Reviews, 112, pp. 933-969

[57] Kim DS, Chang JS, Hwang JS, Park SE, Kim JM, (2004). Synthesis of zeolite beta in fluoride media under microwave irradiation. Microporous and mesoporous materials, 68(1-3), pp.77-82.

[58] Joseph L, Jun B-M, Jang M, Park CM, Muñoz-Senmache JC, Hernández-Maldonado AJ, Heyden A, Yu M, Yoon Y, (2019). Removal of contaminants of emerging concern by metal-organic framework nanoadsorbents: A review. Chemical Engineering Journal, 369, 928–946.

[59] Friščić T, Fábián L, (2009). Mechanochemical conversion of a metal oxide into coordination polymers and porous frameworks using liquid-assisted grinding (LAG). CrystEngComm, 11(5), pp.743-745.

[60] Friščić T, Reid DG, Halasz I, Stein RS, Dinnebier RE, Duer MJ, (2010). Ion-and liquid-assisted grinding: improved mechanochemical synthesis of metal–organic frameworks reveals salt inclusion and anion templating. Angewandte Chemie International Edition, 49(4), pp.712-715.

[61] Mueller U, Schubert M, Teich F, Puetter H, Schierle-Arndt K, Pastre J, (2006). Metal–organic frameworks—prospective industrial applications. Journal of Materials Chemistry, 16(7), pp.626-636.

[62] Al-Kutubi H, Gascon J, Sudhölter EJ, Rassaei L, (2015). Electrosynthesis of metal–organic frameworks: challenges and opportunities. ChemElectroChem, 2(4), pp.462-474.

[63] Tan Y, Zhang W, Gao Y, Wu J, Tang B, (2015) Facile synthesis and supercapacitive properties of Zr-metal organic frameworks (UiO-66). RSC Adv, 5,17601–17605

[64] Wang L, Han Y, Feng X, Zhou J, Qi P, Wang B, (2016). Metalorganic frameworks for energy storage: Batteries and supercapacitors. Coordin Chem Rev 307,361–381.

[65] Yang J, Xiong P, Zheng C, et al. (2014). Metal-organic frameworks: a new promising class of materials for a high performance supercapacitor electrode. J Mater Chem A, 2, 16640–16644.

[66] Liu B, Shioyama H, Akita T, Xu Q, (2008). Metal-organic framework as a template for porous carbon synthesis. J. Am. Chem. Soc. 130, 5390–5391,

[67] Meng F, Fang Z, Li Z, et al. (2013) Porous Co_3O_4 materials prepared by solid-state thermolysis of a novel Co-MOF crystal and their superior energy storage performances for supercapacitors. J Mate Chem A, 1, 7235–7241

[68] Yang J, Zheng C, Xiong P, Li Y, Wei M, (2014). Zn-doped Ni-MOF material with a high supercapacitive performance. J. Mater. Chem. A. 2,19005–19010.

[69] Xu J, Yang C, Xue Y, Wang C, Cao J, Chen Z, (2016). Facile synthesis of novel metalorganic nickel hydroxide nanorods for high performance supercapacitor, Electrochim. Acta 211, 595–602.

[70] Ramasubbu V, Omar FS, Ramesh K, Ramesh S, Shajan XS, (2020). Three-dimensional hierarchical nanostructured porous TiO2 aerogel/Cobalt

based metal-organic framework (MOF) composite as an electrode material for supercapattery. Journal of Energy Storage, 32,101750.

[71] Obreja VV, Dinescu A, Obreja AC, (2010). Activated carbon based electrodes in commercial supercapacitors and their performance. Int. Rev. Electr. Eng. 5, 272–281.

[72] Brousse T, Bélanger D, Long JW, (2015). To be or not to be pseudocapacitive? J. Electrochem. Soc. 162, A5185–A5189.

[73] Ma Y, Jia Y, Wang L, Yang M, Bi Y, Qi Y, (2016). Facile synthesis of three-dimensional flower-like MoO_2–graphene nanostructures with enhanced electrochemical performance. J. Mater. Chem. A. 4, 10414–10418.

[74] Ye C, Qin Q, Liu J, Mao W, Yan J, Wang Y, Cui J, Zhang Q, Yang L, Wu Y, (2019). Coordination derived stable Ni–Co MOFs for foldable all-solid-state supercapacitors with high specific energy. J. Mater. Chem. A 7(9), 4998–5008.

[75] Liu Y, Wang Y, Wang H, Zhao P, Hou H, Guo L, (2019). Acetylene black enhancing the electrochemical performance of NiCo-MOF nanosheets for supercapacitor electrodes. Appl. Surf. Sci. 492, 455–463.

[76] Patterson N, Xiao B, Ignaszak A, (2020). Polypyrrole decorated metal–organic frameworks for supercapacitor devices. RSC Adv., 10, 20162.

[77] Sundriyal S, Kaur H, Kumar S, Mishra S, Kim K, Deep A, (2018). Metal-organic frameworks and their composites as efficient electrodes for supercapacitor applications. Coordination Chemistry Reviews, 369, 15–38.

[78] Rahmanifar MS, Hesari H, Noori A, Yaser M, Morsali A, Mousavi MF, (2018). A dual Ni/Co-MOF-reduced graphene oxide nanocomposite as a high

performance supercapacitor electrode material. Electrochimica Acta, 275, 76–86.

[79] Zhang Y, Lin B, Sun Y, Zhang X,Yang H. (2015). RSC Advances Mn-based symmetrical supercapacitor electrodes for enhanced charge storage. RSC Advances, 5, 58100–58106.

[80] Wen P, Gong P, Sun J, Wang J, Yang S. (2015). Design and synthesis of Ni-MOF/CNT composites and rGO/carbon nitride composites for an asymmetric supercapacitor with high energy and power density, Journal of Materials Chemistry-A. 13874, 13874–13883.

[81] Zhou Y, Mao Z, Wang W, Yang Z, Liu X. (2016). In-Situ Fabrication of Graphene Oxide Hybrid Ni-Based Metal − Organic Framework (Ni−MOFs@GO) with Ultrahigh Capacitance as Electrochemical Pseudocapacitor Materials. ACS Applied Materials & Interfaces Scheme.8, 28904−28916.

[82] Srimuk P, Luanwuthi S, Krittayavathananon A. (2015). Solid-type supercapacitor of reduced graphene oxide-metal organic framework composite coated on carbon fiber paper. Electrochimica Acta, 157, 69–77.

[83] Sundriyal S, Shrivastav V, Kaur H, Mishra S, Deep A. (2018). High-Performance Symmetrical Supercapacitor with a Combination of a ZIF-67/rGO Composite Electrode and a Redox Additive Electrolyte. ACS Omega. 3, 17348−17358.

[84] Hu J, Wang H, Gao Q, Guo H. (2010). Porous carbons prepared by using metal – organic framework as the precursor for supercapacitors. Carbon, 48(12), 3599–3606.

[85] Wang X, Ma H, He X, Wang J, Han J, Wang Y. (2017). Fabrication of interconnected mesoporous carbon sheets for use in high-performance supercapacitors. Carbon, 124, 725.

[86] Jin S, Deng H, Zhan L, Qiao W, Ling L, et al. (2012). Abstracts of New Carbon Materials 2012(2). Carbon, 50(10), 3961.

[87] Elshahawy AM, Guan C, Wang J. (2017). Controllable MnCo2S4 nanostructures for high performance hybrid supercapacitors. Journal of Materials Chemistry A: Materials for Energy and Sustainability, 5, 7494–7506.

[88] Wang C, Liu C, Li J, Sun X, Shen J, Han W, Wang L, (2017). Electrospun metal-organic framework derived hierarchical carbon nanofibers with high performance for supercapacitor. ChemComm. 53,1751-1754.

[89] Salunkhe R, Tang J, Kobayashi N, Kim J, Yamauchi Y, Tominaka S, Kim H, (2016). Ultrahigh performance supercapacitors utilizing core–shell nanoarchitectures from a metal–organic framework-derived nanoporous carbon and a conducting polymer. Chem.Sci, 7, 5704–5713.

[90] Tang J, Salunkhe RR, Liu J, Torad NL, Imura M, Furukawa S. (2015). Thermal Conversion of Core – Shell Metal – Organic Frameworks : A New Method for Selectively Functionalized Nanoporous Hybrid Carbon. Journal of American Chemical Society. 137, 1572−1580.

[91] Torad NL, Salunkhe RR, Li Y, Hamoudi H, Imura M. (2014). Electric Double-Layer Capacitors Based on Highly Graphitized Nanoporous Carbons Derived from ZIF-67. Chem. Eur. J., 20, 7895 – 7900.

[92] Mao M, Sun L, Xu F. (2017). Metal-Organic Frameworks / Carboxyl Graphene Derived Porous Carbon as a Promising Supercapacitor Electrode Material, Key Engineering Materials. 727, 756–763.

[93] Yu C, Wang Y, Cui J, Yu D, zhang X, Shu X, et al.,(2018). MOF-74 derived porous hybrid metal oxides hollow nanowires for high-performance electrochemical energy storage. Journal of Materials Chemistry A. 6, 8396-84040.

[94] Li G, Cai H, Li X, Zhang J, Zhang D, Yang Y, Xiong J, (2019). Construction of Hierarchical $NiCo_2O_4$@Ni-MOF Hybrid Arrays on Carbon Cloth as Superior Battery Type Electrodes for Flexible Solid-State Hybrid Supercapacitors. ACS Appl. Mater. Interfaces, 11, 37675−37684.

[95] Li Q, Guo H, Xue R, Wang M, Xu M, (2020). Self-assembled Mo doped Ni-MOF nanosheets based electrode material for high performance battery-supercapacitor hybrid device. International Journal of hydrogen energy. 45,20820-20831.

[96] Kim J, Park S, Chung S, Kim S, (2020). Preparation and Capacitance of Ni Metal Organic Framework / Reduced Graphene Oxide Composites for Supercapacitors as Nanoarchitectonics. J Nanosci Nanotechnol, 20(5), 2750–2754.

[97] Heng I, Wah F, Wei C, Ching J, Amin N, (2019). High performance supercapattery with rGO / TiO 2 nanocomposites anode and activated carbon cathode. Journal of Alloys and Compounds, 796, 13–24.

[98] Wang Y, Nie S, Liu Y, Yan W, Lin S, Cheng G, et al, (2019). Room-Temperature Fabrication of a Nickel- Functionalized Copper Metal – Organic

Framework (Ni@Cu-MOF) as a New Pseudocapacitive Material for Asymmetric Supercapacitors. Polymers, 11, 821.

[99] Sundriyal S, Shrivastav V, Kaur H, Mishra S, Deep A, (2018). High-Performance Symmetrical Supercapacitor with a Combination of a ZIF-67/rGO Composite Electrode and a Redox Additive Electrolyte. ACS Omega, 3, 17348−17358.

[100] Wang Y, Liu Y, Wang H, Liu W, Li Y, Zhang J, et al, (2019). Ultrathin NiCo-MOF Nanosheets for High-Performance Supercapacitor Electrodes. ACS Applied Energy Mater, 2, 2063−2071.

[101] Wen P, Gonga P, Suna J, Wanga J, Yanga S, (2015). Design and Synthesis of Ni-MOF/CNTs Composites and rGO/Carbon Nitride Composites for an Asymmetric Supercapacitor with High Energy and Power Density. Journal of Materials Chemistry A. 3, 13874.

[102] Hu J, Zhao Z, Zhang J, Li G, Li P, Zhang W. (2017). Synthesis of palladium nanoparticle modified reduced graphene oxide and multi-walled carbon nanotube hybrid structures for electrochemical applications. Applied Surface Science, 396, 523–529.

[103] Gupta KV, Fakhri A, Agarwal S, Naji M. (2018). Palladium oxide nanoparticles supported on reduced graphene oxide and gold doped : Preparation, characterization and electrochemical study of supercapacitor electrode. Journal of Molecular Liquids, 249, 61–65.

[104] Dar RA, Giri L, Karna SP, Srivastava AK. (2016). Performance of palladium nanoparticle – graphene composite as an efficient electrode material

for electrochemical double layer capacitors. Electrochimica Acta, 196, 547–557.

[105] Pal B, Yang S, Ramesh S. (2019). Electrolyte selection for supercapacitive devices: a critical review. Nanoscale Advances, 1, 3807–3835.

CHAPTER THREE

ANALYTICAL TECHNIQUES FOR CHARACTERISATION OF METAL ORGANIC FRAMEWORK COMPOSITES

Summary

The excellent chemical and physical properties of metal organic framework nanocomposites resulted in researchers and industrialists to have great interest in the discovery and applications in various systems. As the sizes of MOFs are reduced to nanoscale, the MOF based nanocomposites tend to display exceptional properties differing from those of their bulk counterparts, hence, they have found applications in supercapacitor applications. In order to apply MOF nanocomposite in supercapacitor particularly in supercabattery which is a combination of high-power EDLC and high-energy density battery-type electrode, they should be studied and analysed to determine their ability to be utilised as electrode materials. Therefore, the great challenge lies in finding the state-of-the-art characterisation techniques to study the structural, morphological and electrochemical properties of MOF materials. In this regard, there is a need to review several techniques to accurately reveal the properties of the materials where in this chapter, a comprehensive overview on analytical techniques that can be used to study the chemical, physical and surface properties of materials.

Keywords: Metal organic frameworks, composites, analytical techniques

3.1. Introduction

The field of electrochemical energy storage, more specifically, supercapacitors emerged as a promising candidate in energy applications, it experienced an exponential progress. Specifically, studies on metal organic framework have gained attention owing to their tuneable pore sizes and higher surface area [1–3]. Although the number of increasing research studies on improving MOF nanocomposites for energy applications is huge, their use in practical applications is still limited. One of the key worries of reseachers for the manufacture of novel nanocomposite based on MOF is the complexity of a deep characterisation, which would enable their perfect production and application in energy storage [4]. Therefore, a wide characterisation of MOF nanocomposites is vital before their use in real practical energy applications. Nevertheless, the present technology is challenging in the sense that many characterisation techniques have been used directly from those approaches used for bulk materials not at a nanoscale [5]. Therefore, there has been variours efforts that have been used for the improvement of the performance of current techniques. Nanocomposite characterisation can be divided into three categories: first, an analytical characterisation, useful for characterising the materials they are composed of as well as to find out the structural properties present; second, a morphological characterisation of the main parameters that will define the performance of nanomaterials; and third, the study of electrochemical characterisation of MOF nanocomposites to reveal their suitable electrochemical energy storage applications. Although numerous reviews for the characterisation of MOFs and their nanocomposites exist, most of them give a particular point of view, signalling only some techniques [6]. Hence, reserchers studying the development of novel nanocomposites find themselves lost in the huge but dispersed existent bibliography. Therefore, this encouraged other authors to write a series of these reviews with a scholastic character, to allow new scientists studying towards the nanoworld to have more knowledge for the precise characterisation methods of MOF nanocomposites. Hence, the purpose of the current review is to give a comprehensive overview of characterisations of nanocomposites. In this review, the authours did not give a deep

description of each specific characterisation method but rather designate concisely each technique to give a background to select the most appropriate characterisation technique for their study and look for relevent information in the various references assumed for each method. These techniques have been categorised as a function of the technique rather than what is being characterised: microscopic, spectroscopic, calorimetric, and electrochemical techniques for qualitative and quantitative analysis, determination of purity and confirmation of composite formation.

3.2. Structural characterisation techniques

3.2.1. Fourier transform infrared spectroscopy

Fourier transform infrared spectroscopy (FTIR) is an analytical technique focusing on the atomic vibrations of molecules by applying middle infrared light (4000 cm^{-1} to 300 cm^{-1}) through a sample. Some of the energy from the light is absorbed causing the molecules in the sample to vibrate at a specific frequency and the frequencies are determined in terms of wavenumbers. A background spectrum is usually run before running the sample to give a correct spectrum of the analyte [7]. The various vibrations observed in the sample spectrum produces a number of absorptions which uniquely corresponds to their characteristic functional groups of the molecules in the sample. FTIR is mostly used for qualitative analysis of samples where by different functional groups are determined from the sample that is being characterised [8]. For example, The FTIR spectrum of copper-based MOF is observed in Figure 3.1(a) and its corresponding peaks are tabulated. The wide peak at 3400 wavenumbers may be attributed to the water molecules absorbed in the MOF pores [9]. This shows that FTIR may also be important for the determination of impurities in the desired materials. In Figure 3.1(a) for pristine HKUST-1, the characteristic peak at 728 cm^{-1} is due to Cu-O bond, confirming metal linker coordination [10]. Therefore, in MOF nanocomposite, FTIR is used for the determination and confirmation of functional groups present and also to reveal the type of interaction between MOF and its component to form a nanocomposite. Figure 3.1(b) also displays the FTIR spectrum of Ag_3PO_4/HKUST-1 (silver phosphate/MOF) and Ag/Ag_3PO_4/HKUST-1 composites respectively. Compared with pristine HKUST-1, both Ag_3PO_4/HKUST-1 and Ag/Ag_3PO_4/HKUST-1 shows two extra prominent peaks around 550 and 830 cm^{-1} ascribed to O=P–O

bending vibration mode of Ag_3PO_4, and asymmetric stretching vibrations respectively [11]. Hence, FTIR spectroscopy is a powerful tool to study interaction of components in the nanocomposites that show to be potential candidate electrode materials in supercapacitors.

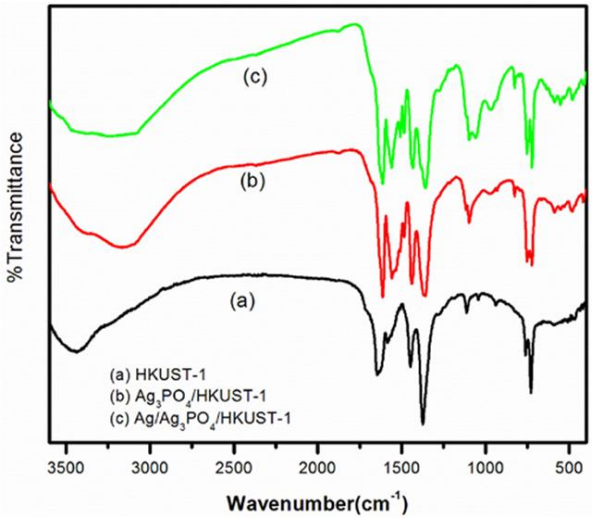

Wavenumber (CM^{-1})	Corresponding peak
3000-3500	-OH
728	Cu-O
1371	C=C
1643	C=O

Figure 3.1: FTIR spectrum of copper based MOF [11].

3.2.2. Scanning electron microscopy

Scanning electron microscopy (SEM) is one of the characterisation techniques that utilises focused beam of electrons for high-resolution imaging of surfaces of the materials and it allows analysis of inorganic, organic and nanomaterial at a very small scale. In SEM analysis, a beam of electrons is focused on the surface of a sample, as a result of the interaction of the electrons with the sample, secondary electrons, Auger electrons, back scatter electrons and others photons of different energies may occur. The images in SEM analysis come from the low energy secondary electrons and the backscattered electrons since they differ because of topographical changes [12]. The two detectors that are used for topographical imaging are: (i) through the lens detector (TLD) and (ii) Everhart-Thonely detector (ETD), these detectors can sense both backscatter and secondary electrons [13]. Through SEM analysis, the beam of electrons penetrates the sample across its surface.The contact between the electron bean and the sample gives an emission of various signals which are collected and processed by detector (Figure 3.2.). SEM technique comprises three electron signals

(Figure 10) which include secondary electrons (SEs) for specimen classification, backscattered electrons (BEs) for the determination of the atomic number and lastly the Auger electrons which determine for luminescence property of sample. The interaction of sample with electron signals is demonstrated in Figure 3.2.

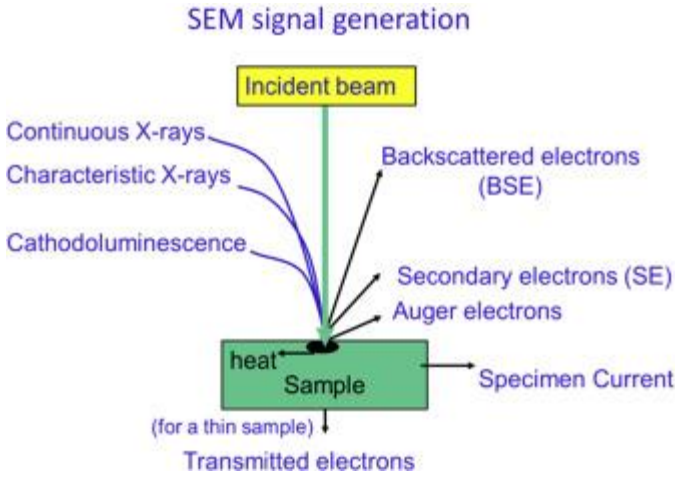

Figure 3.2: Illustration of sample-SEM signal interaction during analysis [14].

Representative SEM micrographs of MOF nanostructures obtained from a simple hydrothermal method reported by Monama et al. [15] are shown in Figure 3.3 (a). These MOF crystals are very clearly possessing an octahedral shape [15]. In addition, the inset image of Figure 3.3 (a) shows that MOF crystal has smooth surfaces with a particle size of 10-15 µm. Makhafola et al. [16] reported SEM images of GO and GO/MOF nanocomposite as shown in Figure 3.3(c) and (e), respectively, depict some dense flakes of graphene sheets and observation of rough surface. In addition, magnification of the octahedral crystals of GO/MOF composite as depicted in Figure 3.3(e) (inset) showed that the integration of GO into the composite resulted in coarse and rough morphological characteristics on the surface of MOF suggesting a possible interaction between MOF and GO through oxygen groups on GO and Cu of MOF [16].

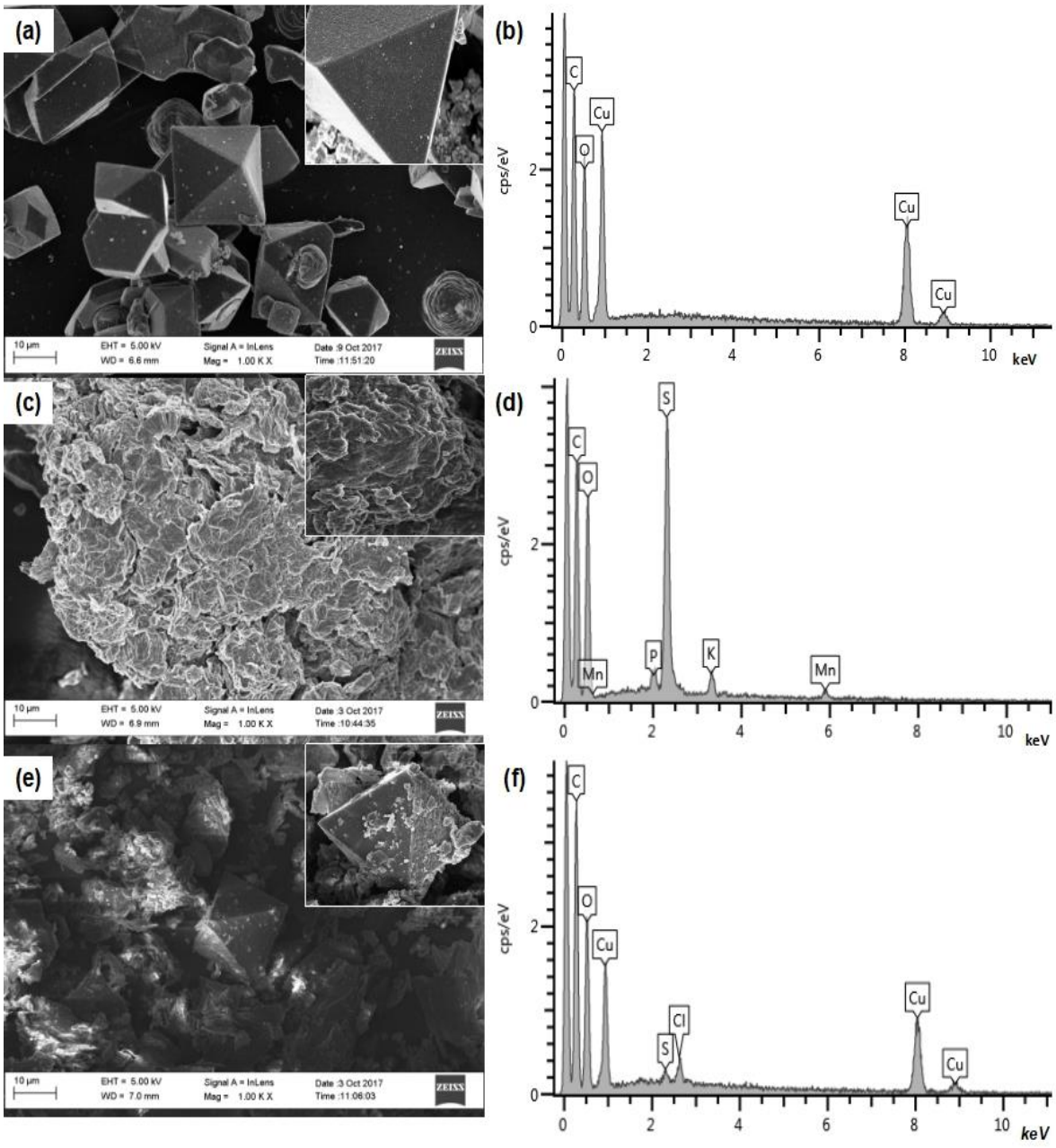

Figure 3.3: SEM images of (a) Cu-MOF, (c) GO (e) GO/Cu-MOF composite (inset: High resolution magnification) and EDS spectrum of (b) Cu-MOF, (d) GO, (f) GO/Cu-MOF composite [16].

3.2.3. Transmission electron microscopy

Transmission electron microscopy (TEM) is a technique used in material science for sample analysis. Like in SEM, a beam of electrons is directed and shone through a thin layer of a sample to create an image. The interactions between the electrons and the atoms can be used to determine features such as the crystal structure, composite formations and layer growth. In a basic TEM instrument (Figure 3.4), high energy electrons are ejected from a tungsten electron gun then the electron beam is focused on the sample using the two condensers and the condenser aperture. Part of the electron beam is transmitted through the thin specimen and the image produced is focused and enlarged using the objective lens [17]. Other techniques that are being employed within TEM that use various signals arising from the interaction of the electron beam with the sample include higher resolution-TEM (HRTEM) and selected area electron diffraction (SAED). HRTEM resolution can be used to analyse the quality, shape, size and density of quantum wells, wires and dots in a sample being studied. These technique allows direct imaging of the atomic structure of a sample. SAED is used as a method to obtain information on the crystallinity from diffraction lines, acquired by the electron-beam illumination on a specimen [18]. Application of these above techniques combined, allows researchers to obtain very detailed information about the structure, texture, morphology and composition of materials studied.

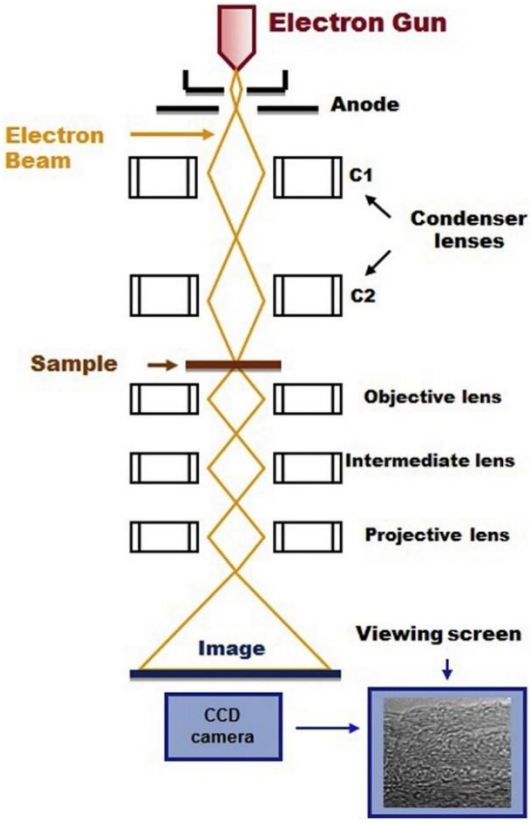

Figure 3.4: Schematic diagram of TEM principle [17].

Modibane et al. [19] reported on the use of TEM for comfirmation of poly(3-aminobenzoic acid) (PABA) incorporated cobalt zeolitic benzimidazolate framework (Co-ZIF) nanocomposite (Figure 3.5). The authors observed the wrapping of MOF by polyaniline (PANI) derivatives (PABA) as shown in Figure 3.5(b) for PABA/Co-ZIF nanocomposite compared to pure PABA depicted in Figure 3.5(a). The TEM image of nanocomposite shows a highly disordered structure confirms the fully amorphous nature due to the presence of polymer with appearance of some spherical shape due to the presence of MOF [20]. In addition, the corresponding SAED patterns (shown in the inset image) show no clear rings as an indicative of an amorphous state [20]

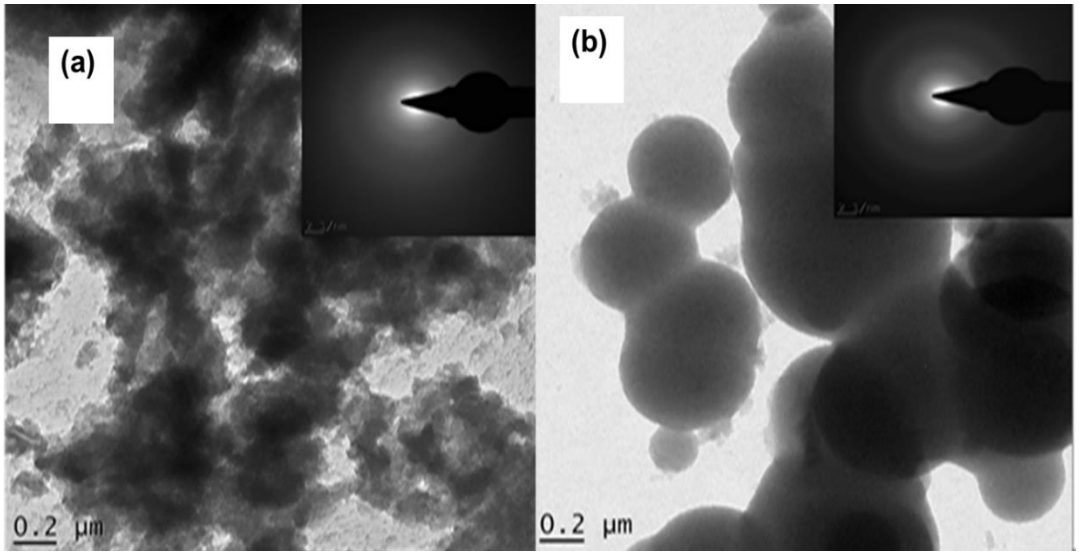

Figure 3.5: TEM images of (a) of poly (3-aminobenzoic acid) and (b) of poly (3-aminobenzoic acid)/cobalt zeolitic benzimidazolate framework nanocomposite, inset: SAED images [19].

3.2.4. Energy dispersive X-ray spectroscopy

Energy dispersive X-ray spectroscopy (EDX) is an analytical technique used to determine the elemental or chemical composition of a sample. This technique uses SEM and TEM to detect elements with atomic number that is higher than that of boron, these elements can be observed at a concentration as low as 0.1%. The use of EDX can be for determination of contaminants, evaluation and identification of materials in a sample. When the electrons interact with the sample, X-rays that are characteristic of each element in the sample are produced and therefore they can be separated and characterised due to their concentrations in the sample [21]. This technique determines the weight percentage and atomic composition of elements in a compound. For example, the elemental structure of MOF and its composites was obtained using EDS technique (see spectrum in Figure 2(b)) and the spectrum has shown the presence of carbon, copper and oxygen elements. The EDS spectra (Figure 3.3(d) and (f)) show the elemental spectrum of GO and composite, respectively. The GO comprises of oxygen and carbon, and these elements are clearly witnessed in Figure 3.3(d). Since the same elements in GO are also existing in MOF, the composite GO/MOF shows an increament in the elemental composition of carbon (Figure 3.3(f)). The EDS validate the presence of small peaks of manganese, potassium, chlorine and

phosphorus, which may be ascribed to impurities formed from precursors during the synthesis process of GO and GO/MOF composite [16].

3.2.5. X-ray diffraction

X-ray diffraction (XRD) is a powerful analytical technique that is used to characterize crystalline materials. It provides information on the unit cell dimensions, structures, phases, texture, and other structural parameters, such as average grain size, crystallinity, strain, and crystal defects. The instrumentation of this technique is made up of three main components which include the x-ray source, sample holder and the detector. When x-rays interact with matter, different absorptions and scattering are observed, and a constructive interference of monochromatic x-ray diffraction is observed in a material when Bragg's law is followed.

Bragg's law is given by:

$$n\lambda=2d\sin\theta \quad (3.1)$$

Where n is an integer (n=1, 2, 3), λ designates the wavelength of the radiation beam, d is the interplanar spacing between two diffracting lines and θ is the diffraction angle [22].

Bragg's law relates the wavelength of electromagnetic radiation as a function of the diffraction angle and the lattice spacing in a crystalline sample. The diffracted X-rays are detected, filtered, and counted. Conversion of the diffraction peaks to d-spacings allows identification of the compound because each compound has a set of unique d-spacings [23]. Typically, this is achieved by comparison of d-spacings with standard reference patterns. The crystallinity and purity of crystalline materials such as MOFs and amophours materials such as graphene oxide (GO) and carbon-nanotubes (CNTs) can be determined using this technique. For example, Figure 3.6 (d) shows very sharp peaks which are indicative highly crystalline structures of the Cu-MOF. Figure 3.6 (a-c) shows carbon materials which do not show any sharp peaks and these materials are characterized as amorphous [24]. In this study, XRD was used to determine the crystallinity of the materials using the known reference spectra and also to monitor the composite formation.

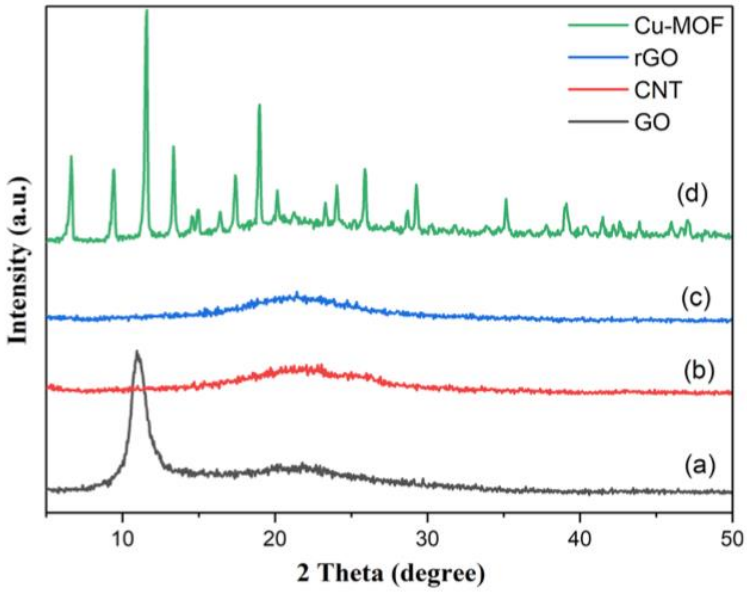

Figure 3.6: XRD of (a) MOF, (b) rGO, (c) CNT and (d) GO [24].

3.2.6. Thermogravimetric analysis

Differential scanning calorimetry (DSC) and thermogravimetric analysis (TGA) are common and widely used thermal analytical techniques for the description of crystalline and amorphous structures. These two techniques are usually performed simultaneously to determine the types of changes that occur as temperature of a sample is increased and they are performed either in the presence of nitrogen or compressed air. Thermal gravimetric analysis is mostly used to study the thermal stability of materials and thus different degradation steps can be observed in different environment. The change in weight of a material is plotted as a function of increasing temperature and various weight losses and degradations are observed. The degradations may be due to evaporations of volatiles and decomposition of the materials in the sample. DSC measures various thermal transitions associated with a material when it is heated or cooled in a controlled manner. DSC monitors the change of heat flow as the sample is heated or cooled and reveals any change in heat capacity that occurs during any solid-state transition, and is, therefore generally useful for determining the glass transition temperature of amorphous materials. This change of enthalpy is detected as a heat-absorbed (endothermic) or heat-released (exothermic)

event in DSC [25]. For example, Ramohlola et al. [26] reported the TGA thermograms of MOF, PANI and PANI/MOF nanocomposite at a heating rate of 10 °C/min (Figure 3.7). It can be seen that MOF exhibits two thermal degradation steps throughout the experimental temperature range which were attributed to water and ethanol physiosorbed in the framework of MOF, as well as the degradation of the organic linker and producing copper oxide. In the PANI/MOF nanocomposite, the lower rate of mass loss with increasing temperature may be due to the internal change in this material that is not accompanied by mass loss at elevated temperature [26].

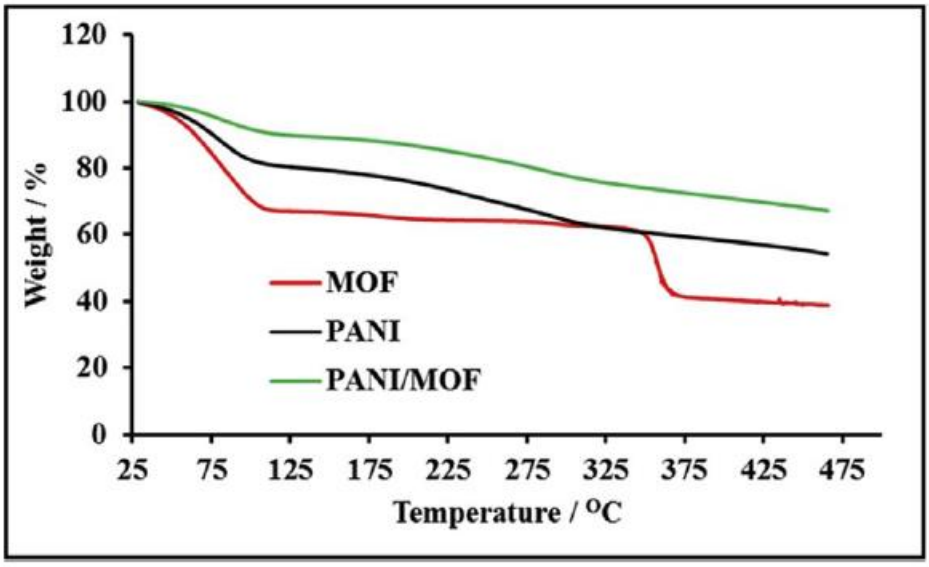

Figure 3.7: TGA curves of MOF, PANI and PANI/MOF composite [26].

3.3. Electrochemical characterisation techniques

Electrochemistry is a powerful tool to probe reactions involving electron transfers. To perform electrochemical experiments, a potentiostat comprising of three electrodes or two electrodes (which is usually for application) is required to acquire electrochemical information of a certain cell. A three electrode cell contains three principle electrodes which are working electrode (WE), counter electrode (CE) which is also known as the auxiliary electrode and a reference electrode (RE) as shown in Figure 3.8(a). The WE is the electrode at which the electrochemical phenomena (reduction or oxidation) being investigated are taking place and this is where the potential is applied and the responding current is measured. The investigated material is usually the WE. The CE is employed to complete the circuit and allow electrons to flow so that current can be

passed from the external circuit through the cell. In simple terms. The current that flows into the solution through the WE leaves the solution via the counter electrode. Examples of CE include platinum wire or carbon, this is due to their non-reactivity and high surface area. The RE is used to monitor the working electrode potential. It contains a constant electrochemical potential as long as no current flows through it. Commonly used RE is the silver-silver chloride electrode (Ag/AgCl). The two electrode system contains of a positive electrode (cathode) and a negative electrode (anode) and it is usually used for application of electrochemical systems such as supercapacitors and batteries [27]. The electrochemical studies of supercapacitors include techniques such as cyclic voltammetry (CV), galvanostatic charge-discharge (GCD) and electrochemical impedance spectroscopy (EIS).

3.3.1. Cyclic voltammetry

Cyclic voltammetry is a technique used to provide qualitative information about the kinetics and the electrochemical behaviour of a sample. This information is a result of the electrode/electrolyte interaction in an electrochemical cell. In this technique the relationship between the current and the applied potential is observed and the presence of peaks indicated the electrochemical activity of the material. CV is a vital electrochemical technique for assessing the type energy storage mechanism in devices because it can show the electrochemical behaviour of species in a forward scan and the reverse scan, within a short period of time. CV is a technique that is usually applied on the principle of three electrodes (working, reference, and counter). However, in some instances it can be applied in a cell that comprices of only two electrodes. The electrochemical behaviour of supercapacitors can be evaluated by applying voltage and reading the current response.

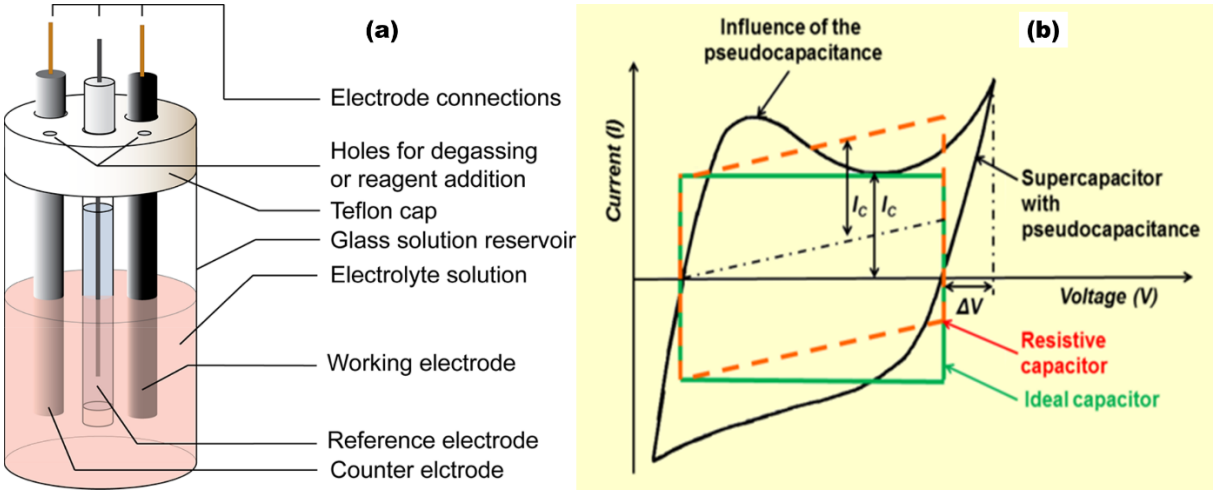

Figure 3.8: Schematic representation of (a) an electrochemical cell for CV experiments [27]. (b) CV curves of a EDLC and pseudocapacitor [27].

Theoretically, a rectangular CV curve (Figure 3.8(b), resembles an ideal capacitor; however, EDLC materials do not behave ideally, resulting in a deformed rectangular shape as displayed in the figure above. Faradaic reactions from pseudocapacitors output redox peaks. From these curves, capacitance (C) can be calculated using the formula:

$$C = \frac{Qtotal}{2Vs * \Delta V} \tag{3.2}$$

where $Qtotal$ is the CV curve integral area, which represents the total charge in coulombs, and ΔV is the change in voltage between the terminals of the device and Vs is the scan rate [27-29].

3.3.2. Gravimetric Charge-Discharge

Galvanostatic charge/discharge (GCD) is an electrochemical technique used for the evaluation of electrochemical supercapactor performance parameters, including specific capacitance and cyclic stability. In GCD technique, the current is kept constant while the potential is monitored with time at the WE relative to the RE. A potential range/limit is set for the working electrode and then it is simple to determine how a certain material charges and discharges. In this technique, a supercapacitor is charged (between E_1 and E_2) and then discharged (between E_2 and E_3) at constant

galvanostatic conditions.as demonstrated in (Figure 3.9(a)). A resistive part (Figure 3.9(b)) representing the voltage drop is usually observed when the cell is discharging and this results from the equivalent series resistance (ESR) of the supercapacitor [30]. The specific capacitance or specific capacity can be determined using both three or two electrode system. Makgopa et al. [31] determined the specific capacitances of carbon/metal oxide composite using a three electrode system and the OLC/Mn_3O_4 composite exhibited much better pseudocapacitive performance with higher discharge time as compared to other nanohybrid electrode materials [31]. In this work the charge discharge is used to determine the supercapacitor performance for the synthesised materials at various current densities. The specific capacitance, power density, energy density, cycling stability are also determined from the results of this technique.

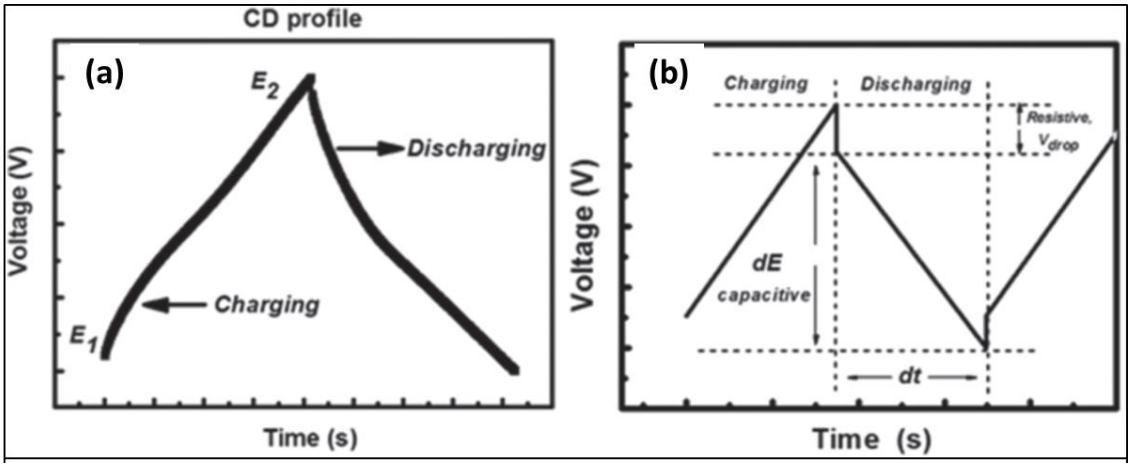

Figure 3.9: (a) and (b) Schematic diagrams showing charge-discharge curves [29].

3.3.3 Electrochemical impedance spectroscopy

Electrochemical Impedance spectroscopy (EIS) consists of a Nyquist plot which is imaginary versus the real time resistance. This technique is mostly used for a range of application including SC, corrosion monitoring, batteries and fuel cells. This technique is important and provides information such as the capacitance variation determined at a particular frequency range, the equivalent resistance of the electrode material and any potential-dependant faradaic resistance [32]. To measure the Impedance (Figure 3.10), the excitation signally is very small and the electrochemical system is subjected to a sinusoidal voltage at similar frequencies but different phases.

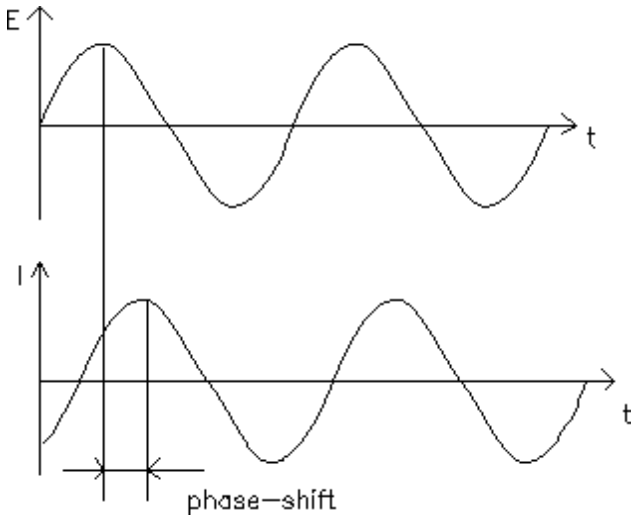

Figure 3.10: Sinusoidal voltage and its current response at the same frequency [33].

The excitation signal, expressed as a function of time, has the form

$$E_t = E_0 \sin \omega t \tag{3.3}$$

where E_t is the potential at time t, E_0 is the amplitude of the signal, and ω is the radial frequency. The relationship between radial frequency ω (expressed in radians/second) and frequency f (expressed in hertz) is:

$$\omega = 2\pi f \tag{3.4}$$

In a linear system, the response signal, I_t, is shifted in phase (Φ) and has a different amplitude than I_0.

$$I_0 = I_0 \sin(\omega t + \Phi) \tag{3.5}$$

An expression analogous to Ohm's Law allows us to calculate the impedance of the system as:

$$Z = Z_0 \frac{\sin(\omega t)}{\sin(\omega t + \Phi)} \tag{3.6}$$

The impedance is therefore expressed in terms of a magnitude, Z_o, and a phase shift, Φ.

The impedance can also be expressed as a complex function as a result of the oval produced in the Lissajous Figure,

$$Z(\omega) = \frac{E}{I} = Z_0(\cos \Phi + \mathrm{j} \sin \Phi) \quad (3.7)$$

The impedance (Z (ω)) comprises of the real impedance and the imaginary expressions [33].

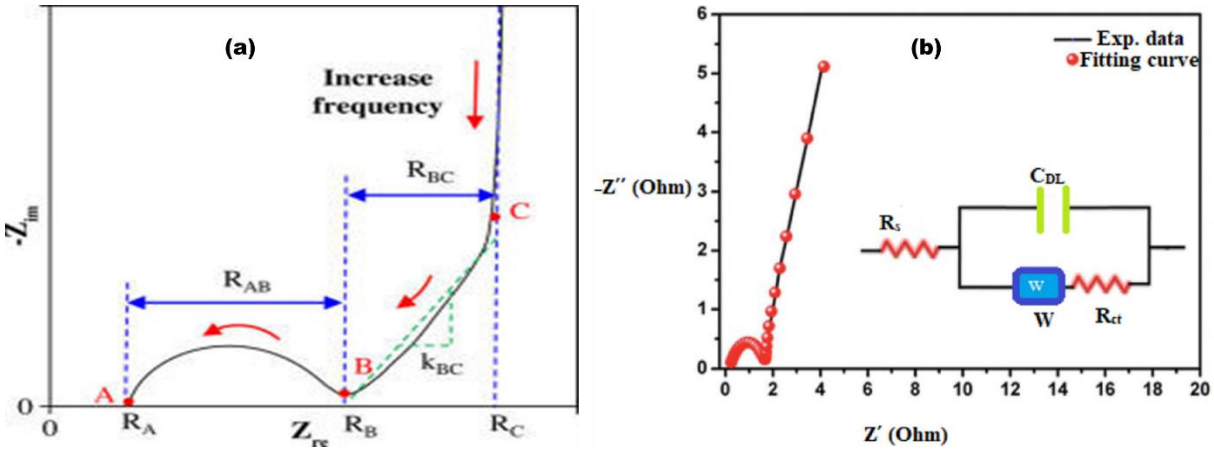

Figure 3.11: (a) Schematic Nyquist plot of a typical EDLC electrode material [34]. (b) Experimental and fitted EIS data [35].

The Figure 3.11(a) shows a typical Nyquist plot for EDLC where a semicircle at high frequencies between points A and B, a non-vertical line at intermediate frequencies between points B and C, and a nearly vertical line at low frequencies beyond point C. In this figure resistance at A (R_A) has been attributed to the equivalent series resistance (ESR) which is the total of the resistances of the electrolyte used, the electrode material and the resistance on the contact between current collector and electrode. The resistance (R_{AB}) is attributed to (i) the electrolyte resistance in the pores of the electrodes (ii) the contact resistance between electrode and current collector and (iii) the sum of the electrode resistance. R_B is regarded as the internal resistance of the electrochemical system. R_{BC} is regarded as the equivalent distribution resistance and the low frequency region below represents the capacitive behavior of the electrode material [34].

A Nyquist Plot is thus obtained when the imaginary part is plotted against the real part as shown in the Figure 3.11(b). Each Nyquist plot has a corresponding circuit that is fitted in and the capacitance can therefore be estimated using Equation 3.8.

$$C = \frac{1}{2\pi f Z} \quad (3.8)$$

where *C* represents capacitance, *f* represents frequency and *Z* represents impedance [35].

3.4. Conclusions

This work dealt to look at the role of various techniques for the characterisation of MOF nanocomposites. Several conventional analytical methods can be used for the characterisation of some features of nanocomposites. Hence in this comprehensive review, we demonstrated the use of different analytical techniques (spectroscopic, microscopic, thermal and electrochemical), emphasising on their principles as well as the mini-discussion on the corresponding results obtained from characterisation of MOF nanocomposites. Therefore, this work will help to identify suitable techniques to be used in supercapacitors. FTIR technique probes the properties of nanocomposite by absorbing the light of a certain wavelengths can be used to reveal the functional groups which are useful to confirm formation and interaction. The other important analytical methods which can reveal the phase properties of nanocomposite is the XRD, is useful to calculate the crystalline sizes of the nanocomposite from the Debye-Sherrer equations. SEM and TEM techniques scan on the surface or transmit through the nanocomposite, are valuable for revealing the external and internal morphologies of the MOF and its compounds. These microscopic techniques can be coupled with EDX detectors to reveal the elemental composition on the MOF materials. Thermal analyses can be beneficial to probe the thermal properties of MOF materials to understand their thermal stabilities and phase transitions. Finally, electrochemical methods have gained an interest in revealing the redox properties of the MOF nanocomposites and to study electrochemical energy storage in supercapacitors. It can be seen that there is still a need to understand the structural, morphological and electrochemical properties of the MOF based nanocomposites to be used in electrochemical energy storage such as solar cells, batteries or supercapacitors.

References

[1] Du W, Bai Y, Xu J, Zhao H, Zhang L, Li X, Zhang J, (2018). Advanced metal-organic frameworks (MOFs) and their derived electrode materials for supercapacitors. Journal of Power Sources, 402, 281–295.

[2] Yap MH, Fow KL, Chen GZ, (2017). Synthesis and applications of MOF-derived porous nanostructures. Green Energy & Environment, 2(3), 218–245.

[3] Zhu G, Wen H, Ma M, Wang W, Yang L, Wang L, et al., (2018). A self-supported hierarchical Co-MOF as a supercapacitor electrode with ultrahigh areal capacitance and excellent rate performance, 2(4), 10499–10502.

[4] Sundriyal S, Kaur H, Kumar S, Mishra S, Kim K, Deep A, (2018). Metal-organic frameworks and their composites as efficient electrodes for supercapacitor applications. Coordination Chemistry Reviews, 369, 15–38.

[5] Wei F, Chen D, (2017). Synthesis and characterization of metal–organic frameworks fabricated by microwave-assisted ball milling for adsorptive removal of Congo red from aqueous solutions. RSC Adv, 7, 46520–46528.

[6] Liang Z, Qu C, Guo W, (2017). Pristine Metal – Organic Frameworks and their Composites for Energy Storage and Conversion. Advanced Materials, 30(37), 1702891-1702930.

[7] Mohamed MA, Jaafar J, Ismail AF, Othman MH, Rahman MA, (2017). Fourier Transform Infrared (FTIR) Spectroscopy. In Membrane Characterization, pp. 3-29.

[8] Gaffney, J. S., Marley, N. A., & Jones, D. E. (2012). Fourier Transform Infrared (FTIR) Spectroscopy. Characterization of Materials.

[9] Ke F, Qiu LG, Yua YP, Peng FM, Jiang X, Xie AJ, et al., (2011). Thiol-functionalization of metal-organic framework by a facile coordination-based

postsynthetic strategy and enhanced removal of Hg^{2+} from water. Journal of Hazardous Materials, 196, 36–43.

[10] Gascon J, Aguado S, Kapteijn F, (2008). Manufacture of dense coatings of $Cu_3(BTC)_2$ (HKUST-1) on α-alumina, *113*, 132–138.

[11] Sofi FA, Majid K, Mehraj O, (2018). The visible light driven copper based metal-organic-framework heterojunction:HKUST-1@Ag-Ag_3PO_4 for plasmon enhanced visible light photocatalysis. Journal of Alloys and Compounds, 737, 798–808.

[12] Tai SS, Tang XM, (2001). Manipulating biological samples for environmental scanning electron microscopy observation, Scanning 23 (4), 267–272.

[13] Everhart TE, Thornley RF, Wide-band detector for micro-microampere low-energy electron currents, J. Sci. Instrum. 37 (7) (1960) 246.

[14] Thomas S, (2017). Chapter 3-Scanning Electron Microscopy under gaseous environment. Micro and Nano Technologies, 85-103.

[15] Monama GR, Modibane KD, Ramohlola KE, Molapo KM, Hato MJ, Makhafola MD, et al., (2019). ScienceDirect Copper (II) phthalocyanine / metal organic framework electrocatalyst for hydrogen evolution reaction application. International Journal of Hydrogen Energy, 44(34), 18891–18902.

[16] Makhafola MD, Ramohlola KE, Maponya TC, Somo TR, (2020). Electrocatalytic Activity of Graphene Oxide / Metal Organic Framework Hybrid Composite on Hydrogen Evolution Reaction Properties, International Journal of Electrochemical Science *15*, 4884–4899.

[17] Kumar V, Fakhri A, Agarwal S, Naji M. (2018). Palladium oxide nanoparticles supported on reduced graphene oxide and gold doped:Preparation , characterization and electrochemical study of supercapacitor electrode. Journal of Molecular Liquids, 249, 61–65.

[18] Kwiecińska B, Pusz S, Valentine BJ. (2019). Application of electron microscopy TEM and SEM for analysis of coals, organic-rich shales and carbonaceous matter. International Journal of Coal Geology, *211*, 103203.

[19] Modibane KD, Waleng NJ, Ramohlola KE, Maponya TC, Monama GR, Makgopa K, (2020). Poly (3-aminobenzoic acid) Decorated with Cobalt Zeolitic Benzimidazolate Framework for Electrochemical Production of Clean Hydrogen. Polymers, 12, 1581-1595.

[20] Monama GR, Mdluli SB, Mashao G, Makhafola MD, (2017). Polyaniline-metal organic framework nanocomposite as an efficient electrocatalyst for hydrogen evolution reaction Palladium deposition on copper (II) phthalocyanine / metal organic framework composite and electrocatalytic activity of the modified electrode towards the hydrogen evolution reaction. Renewable Energy, 119, 62–72.

[21] Su D. (2017). Advanced electron microscopy characterization of nanomaterials for catalysis. Green Energy and Environment, 2(2), 70–83.

[22] Mutalib MA, Rahman MA, Othman MH, Ismail AF, Jaafar J. (2017). Chapter 9 - Scanning Electron Microscopy; SEM; and Energy-Dispersive X-Ray;EDX; Spectroscopy. Membrane Characterization. 161^{-1}79.

[23] Bunaciu AA, Aboul-enein H, (2015). X-Ray Diffraction : Instrumentation and Applications Critical Reviews in Analytical Chemistry X-Ray Diffraction : Instrumentation and Applications,45, 289-299,

[24] Wang S, Li Q, An C, (2018).Synergistic effects between Cu metal – organic framework (Cu-MOF) and carbon nanomaterials for the catalyzation of the thermal decomposition of ammonium perchlorate (AP). Journal of Materials Science, 54(4).

[25] Khoshooei MA, Fazlollahi F, Maham Y, Hassan A, Pereira-almao P. (2019). A review on the application of differential scanning calorimetry (DSC) to petroleum

products Wax crystallization study and structural analysis. Journal of Thermal Analysis and Calorimetry, 138, 3485-3510.

[26] Ramohlola KE, Monana GR, Hato MJ, Modibane KD, Molapo KM, Masikini M, et al., (2018). Polyaniline-metal organic framework nanocomposite as an efficient electrocatalyst for hydrogen evolution reaction. Composites Part B: Engineering, 137, 129–139.

[27] Joshi PS, Sutrave DS, (2019). A Brief Study of Cyclic Voltammetry and Electrochemical Analysis. International Journal of ChemTech Research, 11(09), pp 77-88.

[28] Rountree KJ, Mccarthy BD, Rountree ES, Eisenhart TT, Dempsey JL. (2017). A Practical Beginner's Guide to Cyclic Voltammetry. Journal of Chemical Education, 95, 197−206.

[29] Kim BK, Sy S, Yu A, Zhang J, (2015). Electrochemical Supercapacitors for Energy Storage and Conversion. Handbook of Clean Energy Systems, 1–25.

[30] Raza W, Ali F, Raza N, Luo Y, Kim K, Yang J. (2018). Recent advancements in supercapacitor technology. Nano Energy, 52, 441–473.

[31] Makgopa K, Raju K, Ejikeme PM, Ozoemena KI, (2017). High-performance Mn3O4/onion-like carbon (OLC) nanohybrid pseudocapacitor: Unravelling the intrinsic properties of OLC against other carbon supports. Carbon, (117), 20-31.

[32] Zhang J, Zhao X, (2012). On the configuration of supercapacitors for maximizing electrochemical performance. ChemSusChem, 5, 818–841.

[33] Park, S. (2003). With impedance data, a complete description of an electrochemical system is possible, 455–461.

[34] Mei B, Munteshari O, Lau J, Dunn B, Pilon L, (2018). Physical Interpretations of Nyquist Plots for EDLC Electrodes and Devices. Journal for Physical chemistry, 22, 194-206.

[35] Subramani K, Sudhan N, Divya R, Sathish M, (2017). All-solid-state asymmetric supercapacitors based on cobalt hexacyanoferrate-derived CoS and activated carbon. RSC Adv. 7, 6648–6659.

CHAPTER FOUR

INTERROGATION OF ELECTROCHEMICAL PERFORMANCE OF REDUCED GRAPHENE OXIDE/METAL-ORGANIC FRAMEWORK HYBRID FOR ASYMMETRIC SUPERCABATTERY APPLICATION

Summary

Large scale energy storage system with low cost, high power, and long cycle life is crucial for addressing the energy crisis, especially when integrated with renewable energy resources. To realize grid-scale applications of the energy storage devices, there remain several key issues including the development of low-cost, high-performance materials that are environmentally friendly. This study explores the synergic contribution of the reduced graphene oxide on metal organic framework as positive electrode for asymmetric supercabattery. The structural elucidation of the synthesised hybrid material and its precursors were characterised using XRD, FTIR, TGA, SEM and TEM. The electrochemical analysis of the synthesised hybrid material and its precursors was achieved using CV, GCD and EIS. The electrochemical behaviour of NF-rGO/MOF hybrid obtained from the three-electrode system exhibited a battery-type behaviour and accomplished an improved specific capacity of 459.0 Cg^{-1} at the current density of 1.5 A/g. Furthermore, the two-electrode system fabricated in an asymmetric configuration made of NF-rGO/MOF hybrid as the positive electrode and activated carbon (AC) as the negative electrode studied in 3.0M KOH electrolyte, exhibited specific capacity of about 48.81 C/g at the current density of 0.4 A/g, the corresponding maximum energy density of 11.0 Wh/kg and the maximum power density of 640.45 W/kg. The cycling stability of the rGO/MOF hybrid asymmetric device displayed 70% capacity retention after 2000 cycles.

Keywords: Hybrid, metal organic frameworks, reduced graphene oxide, nickel foam, supercabattery.

4.1. Introduction

The exhaustion of fossil fuels and emissions of greenhouse gases has led to an intensive search for alternative natural energy sources. Various renewable and environmental pollution-free energy sources such as advanced solar cells and wind turbines are being explored but the problem becomes the storage of the energy harvested for future purposes [1-3]. Amongst the currently used energy storage devices, batteries and supercapacitors are more researched as electrochemical energy storage devices to complement the applications of the renewable energy resources [4]. Batteries are widely known for their high energy densities, with low power densities and poor cycle life, whereas supercapacitors are famously known for their high-power densities with high cycle life and poor energy densities. Supercapacitors can be classified into two categories based on their methods of storing energy, i.e. the (i) EDLC which is based on the physical adsorption of charges at the solid-liquid interface, this is where the Helmholtz double layer is observed and (ii) pseudocapacitor which stores energy by involving rapid faradaic processes such as reduction/oxidation (redox) reactions and ion insertion/extraction at the surface of the electrode [5]. The latter method displays faster kinetics as compared to the battery, and depending on the choice of the electrode material, the behaviour of this electrochemical process can lean more toward either capacitor-type or battery-type [6, 7] In the case of leaning towards a capacitor-type, the nomenclature of this process is just referred to as pseudocapacitor (capacitor-like behaviour), while in the case of the batter-type, is referred to as supercabattery. Understanding of this type of electrochemical behaviour has opened up new avenues in energy storage applications, thus, this novel energy storage device, supercabattery, which combines the advantages of supercapacitor and battery has become a hot topic in the energy storage research field [6-10]. This has been supported by the long-lasting efforts of improving the energy density of supercapacitors and power density of batteries.

As shown above that one of the important factors in supercapacitor is the materials for electrode design, which plays significant role in the performance in energy storage. Carbon materials have shown suitability as electrode materials for EDLC. Nevertheless, these materials suffer from lower energy storage capacity. Metal oxides, conducting polymers and metal organic frameworks are used as electrode materials for pseudocapacitors application with the most of these materials specifically being

tailored for supercabattery applications. Reason for the interests in these materials is due to their high energy storage capacity, even though they still suffer from poor conductivity, and expansion during the application. Hence, successful integration of these materials with carbon nanomaterials to form hybrids offer an opportunity to develop excellent energy storage device suitable for both high energy storage and high-power output applications [11, 12].

Metal organic frameworks are perfect candidates as they show strong potential as electrode materials for a well performing electrochemical energy storage device due to their tuneable pore sizes, higher surface area and abundant active sites. MOFs are made up of a metal centre coordinated to organic linkers resulting in a porous material with high surface area [13]. As reasoned above, MOFs displays relatively high capacitive performance on their own due to their high surface area and redox activities on the metal centre, but poor conductivity and stability leads to them being used as sacrificial material [14]. Díaz *et al.* [15] has shown Co-based MOF as a promising electrode material for energy storage systems due to its high surface area of 2900 m^2 g^{-1} according to Langmuir model. It has been shown that the lower conductivities and higher redox interactions of the metal organic frameworks can be counteracted by the introduction of carbon-based materials such as carbon-nanotubes [15], activated carbon [16] as well as graphene oxide materials [17].

Graphene materials are the most investigated EDLCs due to their excellent properties required for supercapacitor applications [18]. These are carbonaceous materials which can be viewed as a graphite monolayer containing various oxygen-containing functionalities. Graphene oxide materials have semiconductor or insulator characteristics, depending on the degree of oxidation, and their electronic and optical properties can be tuned in large scope [17-20]. Their insulator properties are owing to stacked portions of sp^3 hybridized carbon-oxygen bonds, which thereof lead to higher resistance [20]. Amongst all graphene-based materials, reduced graphene oxide (rGO) is currently one of the most explored material for electrochemical storage applications due to its excellent surface area, high electrical conductivity, chemical stability, and excellent mechanical properties [21]. Sykam and Rao [22] demonstrated that the specific capacitance of rGO produced at room temperature to be 112.6 C/g at a current density of 1.0 A/g in 1.0M Na_2SO_4 electrolyte in a three-electrode configuration. This lower capacitance can be due to the agglomeration of the graphene

sheets, which resulted from the strong π-π bonds between the graphene sheets leading to the graphene sheets to restack back into graphite. [23]. In addition, rGO operates at a very high charge/discharge rate with a long cycle life, but they have low energy density [24]. Hence this work, focuses on the electrochemical performance of metal-organic framework integrated on reduced graphene oxide as positive electrode for an asymmetric supercabattery. The electrochemical performance of the hybrid composite is evaluated using cyclic voltammetry, galvanostatic charge-discharge, and electrochemical impedance spectroscopy techniques.

4.2. Experimental

4.2.1. Materials and Apparatus

Copper nitrate trihydrate ($Cu(NO_3)_2.3H_2O$), trimesic acid (H_3BTC), graphite powder, hydrazine hydrate and nickel foam were purchased from Sigma-Aldrich, South Africa. Dimethylformamide (DMF), dimethyl sulfoxide (DMSO), potassium hydroxide (KOH) pellets, hydrochloric acid (HCl), sodium nitrate ($NaNO_3$) and sulphuric acid (H_2SO_4) were procured from Rochelle Chemicals, South Africa. Potassium permanganate ($KMnO_4$) was supplied by SAARCHEM and hydrogen peroxide (H_2O_2) from Moncon, South Africa. Polyvinylidene fluoride (PVDF), N-methyl pyrrolidone (NMP), activated carbon and carbon black were obtained from Sigma Aldrich.

4.2.2. Synthesis of rGO, MOF and rGO/MOF hybrid

GO was prepared from graphite according to the modified Hummers method [25]. The synthetic route for preparation of rGO is reported elsewhere [26], with our own modifications. Concisely, the prepared GO (100 mg) was loaded in a 250 mL round bottom flask and water (100 mL) was then added, yielding an inhomogeneous yellow-brown dispersion. This dispersion was ultrasonicated until it became clear with no visible particulate matter. Hydrazine hydrate (1.00 mL, 32.1 mmol) was then added and the solution heated in an oil bath at 100 ^oC under a water-cooled condenser for 24 h over which the rGO gradually precipitated out as a black solid. This product was isolated by filtration over a medium fritted glass funnel, washed four times with

deionised water (250 mL) and methanol (250 mL), and dried on the funnel under a continuous air flow.

Metal organic framework (MOF) was synthesised by following a hydrothermal procedure [27]. Briefly, 1.087 g of $Cu(NO_3)_2.3H_2O$ was dissolved in 10 ml of distilled water and then mixed with 0.525 g of H_3BTC dissolved in 10 ml of ethanol. The mixture was stirred for 30 min and then transferred to a 23 ml Teflon stainless-steel autoclave and sealed to react for 36 hours at 120 °C in thermostatic drying oven. The resulting product was washed with ethanol and deionised water and dried at 50 ^oC overnight.

The rGO/MOF hybrid was prepared through impregnation method (Scheme 1) [28]. Briefly, 0.1 g of as-synthesised MOF sample was dehydrated at 150 ^oC for 1 hour. It was then suspended in 10.00 mL DMF. In a separate beaker, 0.1 g of reduced graphene oxide was dispersed in 1.40 mL DMF, and then the two mixtures were mixed together and stirred magnetically for 24 hours at room temperature. The resulting product was recovered by filtration and washed with ethanol and then dried overnight at 50 ^oC.

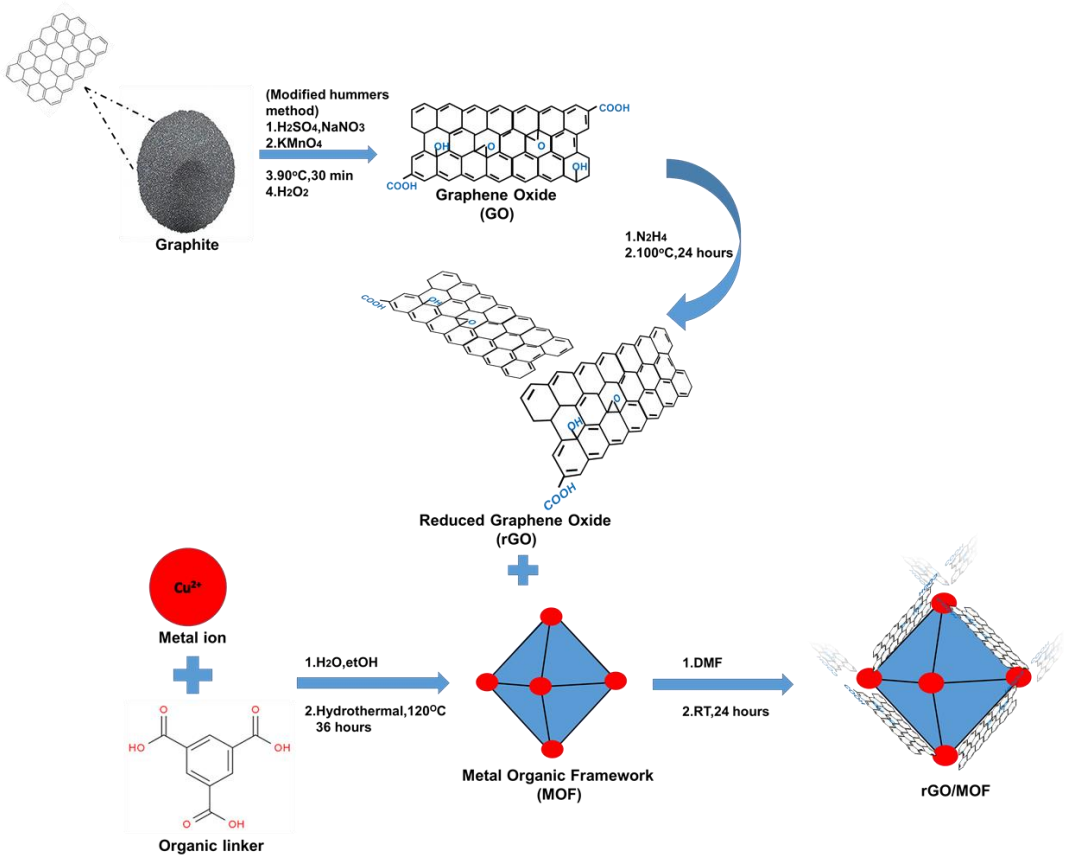

Scheme 4.1. Synthesis of rGO, MOF and rGO/MOF

4.2.3. Electrodes fabrication

The preparation of electrodes was conducted following other reported methods [29]. Nickel foam (NF) of area 0.1 cm^2 was soaked in 3M HCl and ultrasonicated for 15 min removing the nickel oxide layer, and further ultrasonicated in a mixture of deionized water and ethanol for another 15 minutes. After the pre-treatment, nickel foam was used as the current collector. The nickel foam was pressed at high pressure to close the various pores in their structure before coating the electrode materials. The working electrodes composed of three different materials which included 70% of the synthesised active materials (Cu-MOF, rGO and rGO/MOF hybrid), 10% of the binder PVDF and 20% of carbon black. The electrode materials were prepared by mixing the synthesised materials with NMP to make a paste before coated on the nickel foam. The coated electrodes were then dried overnight at 75 ^oC. The average loading of the materials on Ni foam was between 4-5 mg and only mass of MOF, rGO and rGO/MOF was included in calculating the active mass. For a two-electrode asymmetric configuration, the above electrode preparation was followed with rGO/MOF hybrid as a positive electrode and activated carbon (AC) as negative electrode.

4.2.4. Materials characterisation

Optical absorption spectra analyses were recorded at room temperature in the wavelength region 200–800 nm using a Varian Cary 300 UV-Vis-NIR spectrophotometer. The structures of GO, rGO, MOF and rGO/MOF hybrid were analysed using X-ray diffraction (XRD Phillips PW 1830, CuKα radiation, λ = 1.5406 A). The formation of the hybrid was confirmed by Cary 600 series Fourier transform infrared (FTIR) spectrometer (Agilent Technologies). The spectra were obtained at room temperature in the wave number range between 500 and 4500 cm^{-1}. A minimum of 32 scans were collected at a resolution of 4 cm^{-1}. The thermal stability was studied by a thermogravimetric analyzer (TGA Perkin-Elmer 4000). Samples ranging between 1 to 4 mg were heated from 30-500 °C at a heating rate of 20 $°C.min^{-1}$ under N_2 environment. Morphological characterisations were performed using Auriga Field Emission Scanning Electron Microscope (FESEM) coupled with EDS detector for elemental analysis. High-resolution transmission electron microscopy (HR-TEM)

observations were acquired from HR-TEM, FEI Tecnai G2 F20X-Twin MAT 200-kV, Eindhoven, Netherlands.

4.2.5. Electrochemical characterisation

All the electrochemical evaluations of the as-prepared electrode materials were carried out using a VMP-300 Biologic potentiostat operated on EC-lab software at room temperature. In order to investigate the electrochemical properties of the prepared electrodes, cyclic voltammetry (CV) tests with various scan rates, galvanostatic charge-discharge tests at various current densities, electrochemical impedance spectroscopy (EIS) and cycling stability of the fabricated cells were performed in 3.0M KOH aqueous electrolyte. For the three-electrode system, platinum wire, Ag/AgCl and the prepared electrodes coated on nickel foam were used as counter, reference and working electrodes, respectively. The electrochemical evaluation of the assembled asymmetric supercapacitor AC//rGO/MOF was done using a two-electrode system (coin cell), where rGO/MOF hybrid was used as positive electrode and activated carbon (AC) as a negative electrode, while a filter paper was used as a separator. Prior to the electrochemical evaluation of the assembled asymmetric supercabattery AC//rGO/MOF, the mass balance between the two electrodes was analysed using the mass ratio of both the positive and negative electrodes using equation 4.1:

$$\frac{m_+}{m_-} = \frac{Q_{s-}}{Q_{s+}} * \frac{\Delta V_-}{\Delta V_+} \qquad (4.1)$$

where m, Q_s and ΔV represent the mass, specific capacity, and potential window obtained from the charging/discharging process of three-electrode system of the individual positive and negative electrode, respectively.

The specific capacity (Q_s), obtained from the GCD analysis in both three-electrode and two-electrode configuration were calculated using equation 4.2:

$$Q_s = \frac{I*\Delta t}{m} \qquad (4.2)$$

where: *I* (A) is the current, Δ*t* (s) discharge time, and *m* mass of active electrode (i.e., total mass of positive and negative active materials for two electrode configuration).

The energy (*E*) and power (*P*) densities of the prepared asymmetric supercapacitor were all calculated from the gravimetric charge-discharge analysis using equation 4.3-4.4 respectively:

$$E\ (Wh/kg) = \frac{Q_s * \Delta V}{2*3.6} \quad (4.3)$$

$$P\ (W/kg) = \frac{E*3600}{\Delta t} \quad (4.4)$$

4.3. Results and Discussion

4.3.1. Spectroscopic characterisation

Figure 1(a) shows the overlaid XRD patterns of rGO, MOF, MOF CSID, and rGO/MOF hybrid. The diffraction pattern of rGO is completely different from that of GO but similar to graphite [20]. After the reduction, the sharp XRD peak of GO (d-spacing 7.94 Å at 2θ = 11º,) disappeared, but a new broad diffraction peak (d-spacing 3.7 Å at 2θ = 24.01º) appeared, which is closer to the typical (002) diffraction peak of graphite (d-spacing 3.35 Å at 2θ = 26.61º, [24]). This means that the oxygen containing groups were removed and that GO was effectively reduced to rGO by hydrazine hydrate. Furthermore, the peak also indicated that the rGO nanosheets are exfoliated into a monolayer or of few layers of rGO and resulted in a new lattice structure which is significantly different from that of GO [29]. The XRD pattern of MOF presented in Fig. 4.1 (a), is in accordance with the one reported by Ramohlola *et al*. [30], showing good crystallinity. The peaks of the MOF pattern appeared at small 2θ angles which are characteristics of microporous materials, which possess numerous tiny pores or cavities that are in accordance with typical MOF structure. One of the main intense peaks of the pattern appeared at 2θ = 12º, which accounts for the reflection (222), when calculating the lattice plane. The peaks at 35º and 43º are related to Cu_2O impurities, but their intensities are very low related to main peaks of the MOF, which confirm that the purity of the MOF was well preserved and the MOF was pure powder,

and identical to those of the simulated one (MOF CSID) [30]. It is interesting to note that the XRD pattern of the rGO/MOF hybrid is similar to that of MOF, which indicates that there was no apparent loss of crystallinity and decomposition of the framework structure after the incorporation of rGO. Furthermore, the reduction in the peak intensities of the hybrid confirmed the incorporation of rGO with MOF.

The reduction of the oxygen-containing groups in GO by hydrazine hydrate was also confirmed by FTIR spectroscopy. As shown in Fig. 4.1 (b), the intensities of the FTIR bands corresponding to oxygen functionalities such as the C=O stretching vibration band at 1726 cm^{-1}, the vibration and deformation bands of O–H groups at 3395 and 1400 cm^{-1}, respectively, the C–O (epoxy) stretching vibration peak at 1226 cm^{-1}, and the C–O (alkoxy) stretching peak at 1052 cm^{-1} decreased dramatically, and some of them disappeared entirely [29]. These observations confirmed that most oxygen functionalities in the GO were removed. In the IR spectrum of MOF, the symmetric and asymmetric stretching vibrations of carboxylate groups in BTC appear at 1645/ 1590 cm^{-1} and 1450/ 1370 cm^{-1}, respectively. The lower wavenumber region of 1300-700 cm^{-1} exhibits various bands assigned to out-of-plane vibrations of BTC [30]. The spectrum of the rGO/MOF hybrid exhibits similar bands to those of MOF but now with an enhanced band intensities, this is due to the increase in the amount of the C=O and C=C functionalities in the hybrid as compared to the parent MOF material (there is more of C=C and C=O in the hybrid, coming from both rGO and MOF). This also confirms the incorporation of MOF and rGO. In addition, there is a development of a new band appearing at around 617 cm^{-1}, attributable to the Cu-O stretching vibration. This is the result of the oxygen emanated from GO and Cu metal centres on MOF, suggesting a plausible electrostatic interaction between the two parent materials as envisaged by XRD results.

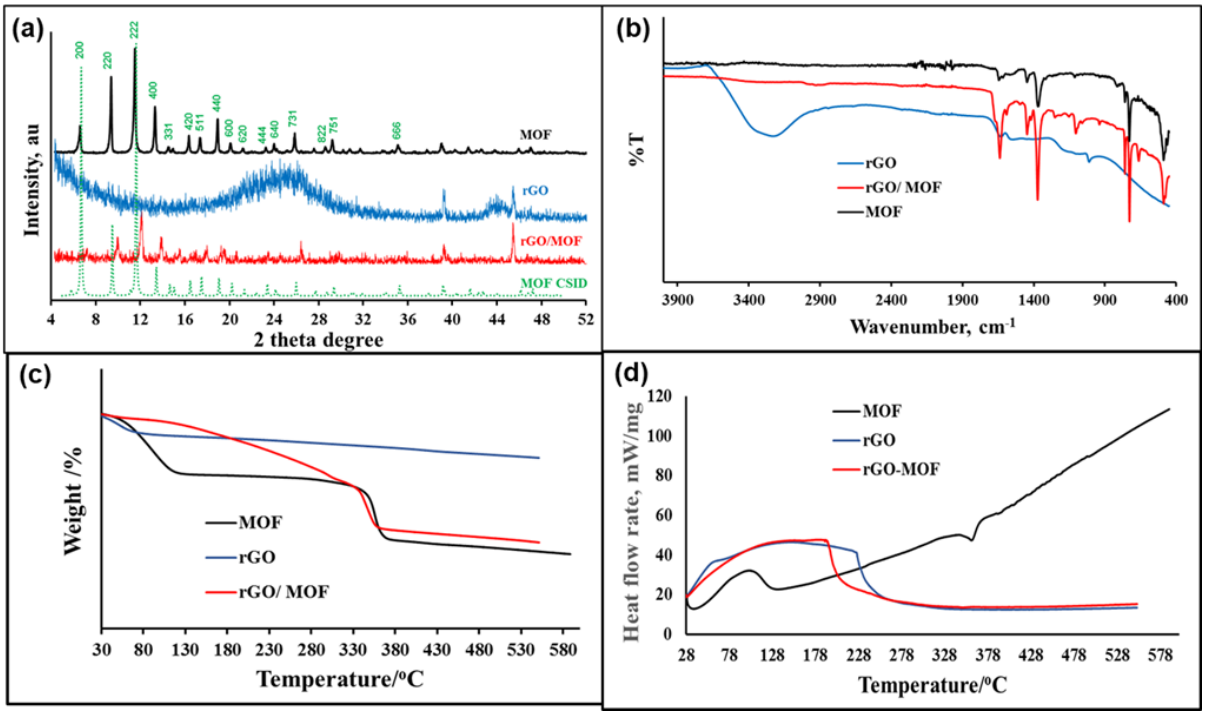

Figure 4.1: (a) XRD patterns, (b) FTIR spectra, (c) TGA and (d) DSC thermograms of MOF, rGO and rGO/MOF hybrid.

Thermogravimetric analysis (TGA) of MOF, rGO and rGO/MOF hybrid are shown in Fig. 4.1(c) below. The TGA of MOF indicated that this material was only stable up to 370 ^{o}C. Its weight loss is displayed in two degradation steps. The first step (40-150 ^{o}C) is associated with the removal of water molecules from pores, and the solvent molecules trapped in the MOF structure during synthesis [31]. At this degradation step, about 28% weight loss was observed. At the second step, degradation of OH groups and portion of organic frameworks at 280–370 ^{o}C occurred, which is responsible for a 30% weight loss. Copper oxides are the final remaining products at higher temperatures [31]. rGO was found to be thermally stable up to 550 ^{o}C with the weight loss of about 15 wt.%. The region 28 ^{o}C-100 ^{o}C shows a weight loss of about 8 wt.%, which indicates that rGO did not have a lot of water or solvents trapped in it as shown in reported analysis [24]. The rGO/MOF hybrid, however, is slightly more stable than MOF. Wherein the first stage (40-150) is now moisture stable with the weight loss of 2wt.% and the second stage has a loss of 28wt.%. DSC result correlates well to the TGA showing an exothermic peak (100–125 ^{o}C) due to the dehydration of MOF (Fig. 4.1 (d)). One endothermic peak was also discovered by DSC analysis at 375 ^{o}C. This

may be due to the absorption of heat by the sample as it undergoes the endothermic phase transition from solid to liquid [29]. The DSC curve of rGO is similar to that of rGO/MOF hybrid, indicating a broad endothermic peak from 100 ^{o}C. This peak is due to absorption of heat as rGO decomposes [30].

4.3.2 Morphological characterisations

Figure 4.2(a), (c) and (e) show SEM images of MOF, rGO and rGO/MOF hybrid respectively whereas Fig. 4.2: (b), (d) and (f) show EDS spectra of MOF, rGO and rGO/MOF hybrid, respectively. The SEM images of MOF materials produced by solvothermal method show phases that are highly crystalline, which is an indication of micro-porous materials characteristics as shown by other reported analysis from the literature [30]. The EDS confirms the presence of Cu, O and C in the organic linker. The rGO synthesised though the reduction of GO by hydrazine shows some partial agglomeration which is due to strong van der waals forces between the graphene sheets and the agglomeration is not ideal for supercabattery application since the electrolyte used cannot access its dense areas. The SEM image of the hybrid shows both rGO and MOF for which the small dispersed particles of MOF are seen indicating that the preparation process of the hybrid based on the direct mixing which can assist the dispersion of the components of both materials in the hybrid. EDS confirms the presence of all the elements presence of those materials in the hybrid.

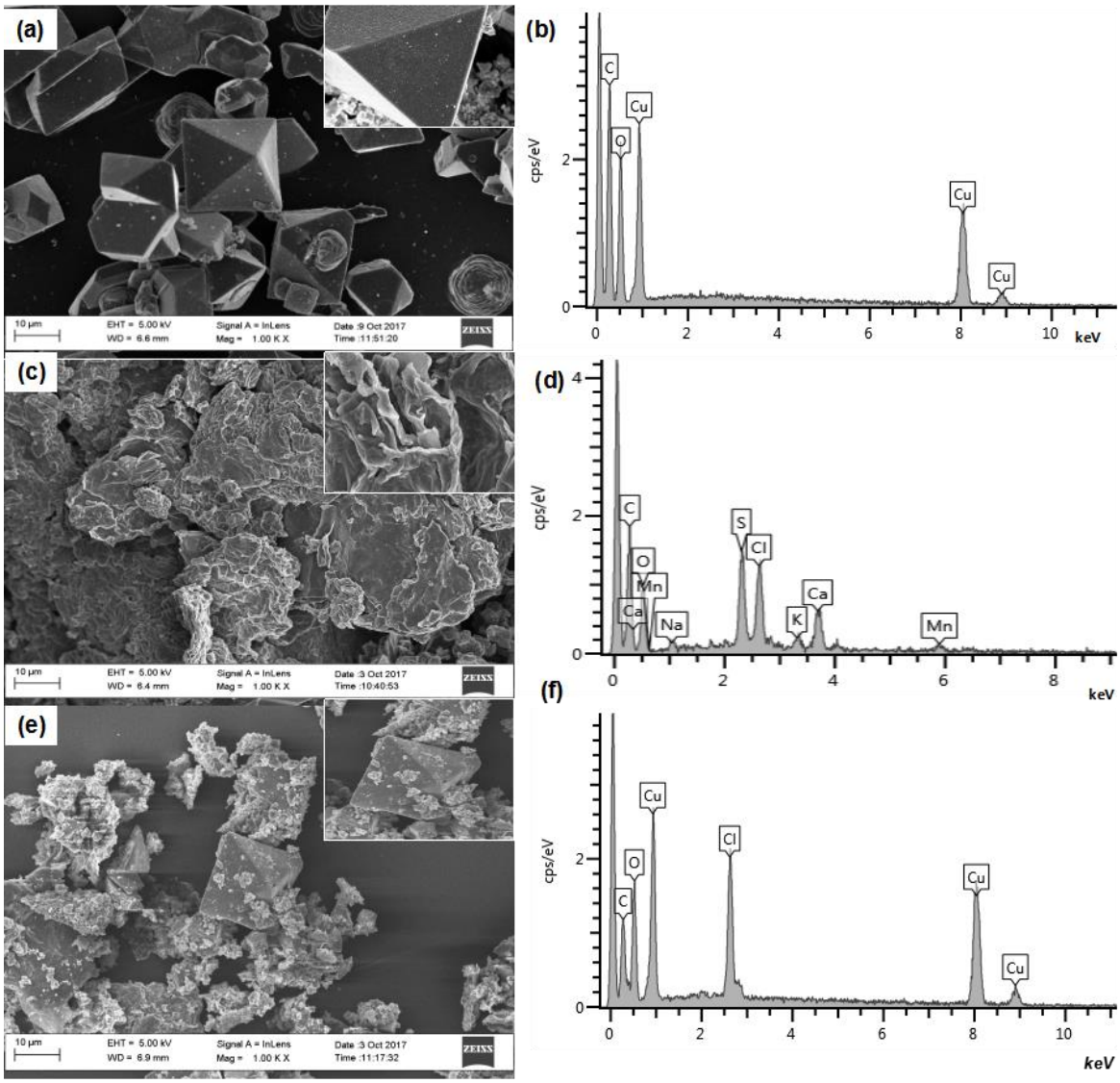

Figure 4.2: (a), (c), (e) SEM images and (b), (d), (f) EDS spectra, of MOF, rGO and rGO/MOF hybrid, respectively.

In addition, the TEM images of rGO/MOF hybrid are presented in Fig. 4.3(a) and (b). As seen in Fig. 4.3(a), the rGO layer was observed in the hybrid with a well exfoliated graphene nanosheets and wrinkled transparent sheet-like structure. The layers are due to the interaction between MOF blocks and rGO sheets. It was seen that the interaction is between the rGO benzene ring-containing functional groups and the MOF dimmers, resulting in π-π interactions upon formation of hybrids [31]. Furthermore, it was seen that upon the hybrid formation, the octahedral shape of MOF crystal structure [32] was maintained, indicating the constrain effects of the layers of

rGO subsequent in preservation of the original shapes of the MOF crystals in their carbonized phase [33]. The large aggregates can be distinguished easily between the graphene phase and the MOF phase. Moreover, the thin layers of reduced graphene seem to have wrapped some of the MOF sites. Furthermore, the SAED pattern in Fig. 4.3 (c) of rGO/MOF hybrid depicts well-defined rings suggesting that the crystalline character of the rGO has been improved. The HR-TEM results clearly suggest the successful formation of hybrid-structured rGO/MOF and these observations are in good agreement with both XRD and SEM results.

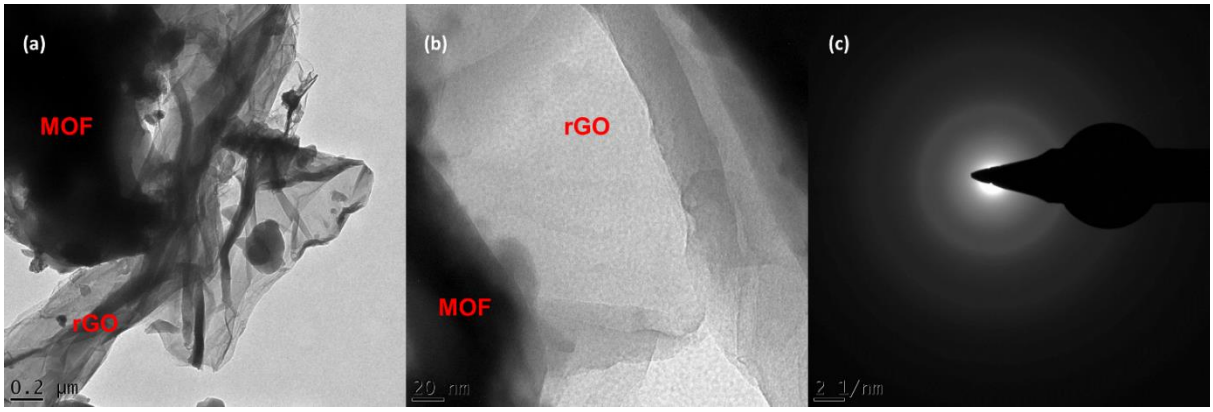

Figure 4.3: (a), (b) TEM images at different magnifications and (c) SAED, of rGO/MOF hybrid.

4.3.3. Electrochemical properties

4.3.3.1 Performance in three-electrode configuration

Figure 4.4 shows comparative electrochemical performance of NF-MOF, NF-rGO and NF-rGO/MOF hybrid in a three-electrode configuration using Ni-foam as current collector and 3.0 M KOH as an aqueous electrolyte. Fig. 4.4(a) shows the overlaid CV curves of MOF, rGO and rGO/MOF hybrid at a scan rate of 10 mV/s. The nature of the CV curves display distinction from those of an ideal electrochemical double-layer capacitance, showing two redox peaks which are responsible for the faradaic capacitive behaviour of battery-type electrode materials. The intensity current peaks observed from the NF-rGO can be attributed to the redox reaction of the nickel foam in the electrolyte. The current response and the redox curve for NF-rGO/MOF hybrid

is relatively higher than those of NF-rGO and NF-MOF, this is due to the redox interactions of Cu^{+}/Cu^{2+} and the porous nature of the MOF especially when combined with the electronic properties arising from the rGO such as an improved conductivity. These allow high diffusion of electrolyte ions on to the electrode surface thus showing better electrochemical performance for the hybrid. Thus, indicating that the hybrid is a better electrode material with energy storage capacity than its precursors [34]. The two well defined redox peaks exhibited by NF-rGO/MOF hybrid observed at around 0.4V and 0.12V on the CVs are due to the faradaic behaviour of Cu^{+}/Cu^{2+} assisted by the intercalation/de-intercalation of the OH^{-} from the electrolyte [18]. Fig. 4.4(b) show the GCD curves of NF-MOF, NF-rGO and NF-rGO/MOF hybrid at a current density of 2.5 A/g. It is observed that MOF alone displayed a lower specific capacity as compared to hybrid material. This could be attributed by the poor conductivity that resulted in lower discharging time (see Fig. 4.4(b)). After incorporation of the rGO to the framework of the MOF, a significant increase in the discharging time of the material is observed as an indication of a better electrochemical performance (i.e., energy storage capacity) than its precursors. These results correlate well with those from CV analysis in Fig. 4.4(a). The specific capacity of NF-rGO/MOF hybrid, NF-MOF, and NF-rGO at a current density of 1.5 A/g were found to be 459.0, 249.0, and 155.1 C/g, respectively. Fig. 4(c) shows the CV curves of the NF-rGO/MOF hybrid electrode at different scan rates (20 - 40 mV/s). It is observed that the current response of the hybrid increases gradually with an increase in the scan rate indicating a typical capacitive behaviour [33]. Fig. 4.4 (d) shows the charge-discharge curves of the NF-rGO/MOF hybrid at different current densities. These curves display nonlinear behaviour, demonstrating the redox process during the charge storage at a potential range of -0.2 to 0.5 V, indicative of battery-type behaviour of the electrode materials. The specific capacities increase with a decrease in current density, and these falls within the typical characteristics of electrode materials applied in hybrid supercapacitor applications.

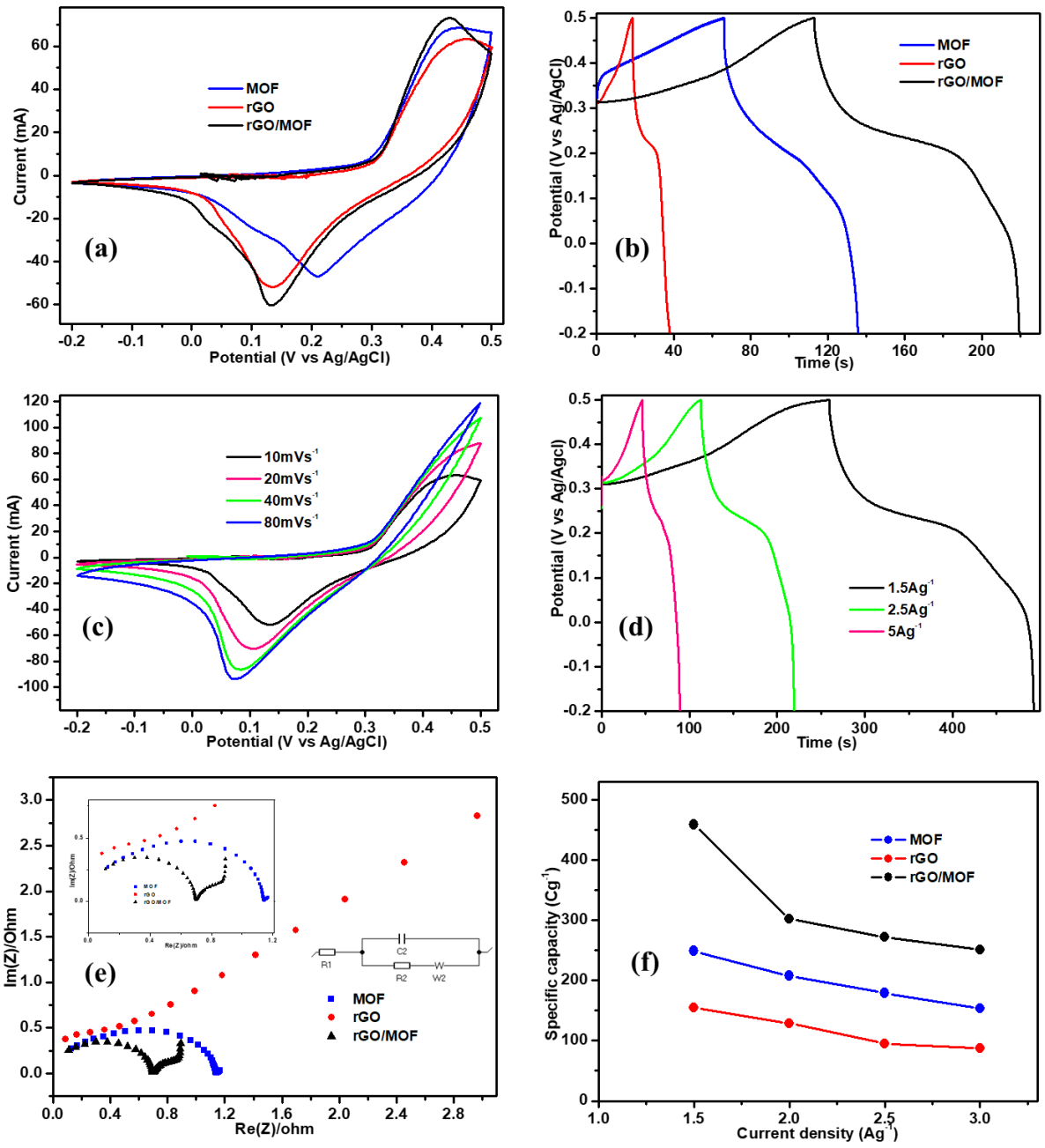

Figure 4.4: Overlaid (a) CV curves at a scan rate of 10 mV/s, (b) GCD curves at a current density of 2.5 A/g, of MOF, rGO and rGO/MOF hybrid. (c) CV curves at various scan rates, (d) GCD curves at various current densities, of rGO/MOF hybrid. Overlaid (e) EIS results, and (f) Q_s vs current density, of MOF, rGO and rGO/MOF hybrid.

In order to understand the charge mobility and electron transfer mechanism at the interface, EIS analysis was conducted in an open circuit voltage (OCV). Fig. 4.4(e)

shows the Nyquist plot of the NF-MOF, NF-rGO and NF-rGO/MOF hybrid. The plots were fitted in the circuit shown as the inset of Fig. 4.4(e) and the parameters obtained from fitting are shown in Table 4.1. The Nyquist plot of NF-MOF shows a very high resistance as compared to the NF-rGO and the NF-rGO/MOF hybrid, this is due to the insulating property of the MOF structure. However, the Nyquist plot of NF-rGO is much closer to the ideal behaviour due to the low charge transfer of the sp^2 hybridized rGO. The Nyquist plot of NF-rGO/MOF hybrid display a low charge transfer resistance as compared to MOF. This improved electrochemical performance is due to the synergistic effect between rGO and MOF (due to the conductive structure of the rGO coordinated to the MOF via π to π interaction), leading to an improved conductivity of the hybrid, resulting in a decrease in the internal resistance of the electrode. Other contributing factor for such an improvement of the hybrid electrode could be attributed to the 3D porous network structure of the nickel foam which assists in providing an easy access of ions at the electrode/electrolyte interface [39]. Fig. 4.4(f) exhibit an overlaid specific capacity vs current density curves of NF-MOF, NF-rGO and NF-rGO/MOF hybrid. The NF-rGO/MOF hybrid displayed an excellent specific capacity as the current density increases as compared to the NF-MOF and NF-rGO. All the specific capacities of the electrodes increased with a decrease in the current density, this is due to limited diffusion of electrolyte ions on the electrode surface at higher current densities. But even at higher current densities above 3 A/g the NF-rGO/MOF hybrid still showed higher specific capacity values that are above 250 C/g which indicates that the hybrid has a higher electrolyte-electrode interaction capability.

Table 4.2 shows the electrochemical properties in terms of the energy storage capacity of NF-rGO/MOF hybrid compared with the literature values obtained in a three-electrode configuration. It is observed in the Table 4.2 that upon introduction of carbon materials, MOF structures exhibits an improved specific capacity. The NF-rGO/MOF hybrid displayed much better specific capacitive properties as compared to most of the reported values.

Table 4.1: Comparative fitting parameters for the EIS data for the MOF, rGO and rGO/MOF hybrid using the Randel circuit.

Material	R1(Ω)	C2(μF)	R2(Ω)	s2(Ω/√s)
NF-MOF	0.7477	13.86	1.041	0.1719
NF-rGO	0.2071	3.085	0.8748	0.6705
NF-rGO/MOF	0.3492	1.392	0.5662	141.3

Table 4.2: Comparison of battery-type electrode materials in three-electrode configuration.

Active Material	Current Density (A /g)	Specific Capacity	Electrolyte	Potential Window (V)	Ref
SrO-Pani	0.8	258.0 C/g	1.0M KOH	0.6 V	[34]
Zn-Ni-MOF	1.0	237.0 mAh/g	3.0M KOH	0.45 V	[35]
Mo/NI-MOF	1.0	802.0 C/g	3.0M KOH	0.50 V	[36]
NiCuS	10.0	382.0 C/g	3.0 M KOH	0.40 V	[37]
rGO/TiO_2	0.2	116.70 C/g	1.0M Na_2SO_4	1.0 V	[38]
Cu-MOF/rGO	1.5	459.0 C/g	3.0M KOH	0.7 V	[this work]

Key: strontium oxide (SrO), Metal Organic Frameworks (MOF), Nickel (Ni), Titanium Oxide (TiO_2)

4.3.4. Performance in an asymmetric two-electrode configuration

Due to the leading performance of the NF-rGO/MOF hybrid in a three-electrode configuration, further investigation in an asymmetric two-electrode configuration was carried out using activated carbon (AC) and the hybrid as the negative and positive electrode, respectively, in 3.0M KOH aqueous electrolyte. The mass-balancing of the

positive and negative electrode was done using the three-electrode configuration analysis and the calculated ratio was calculated to be 0.61, according to equation (2). The CV curves of the asymmetric cell (see Fig. 4.5(a)) were run at a potential range of 0 to 1.6V and they show semi-rectangular shape indicating the combination of double layer and faradaic behaviour of the device. From the GCD analysis of AC//rGO/MOF at different current densities (Fig. 4.5(b)), the discharge time of the asymmetric supercabattery decreases with an increase in the current density. Furthermore, it is observed that the slopes of the curves are not linear, confirming the presence battery-type electrode. The calculated specific capacities of an asymmetric supercabattery are found to be 31.79 C/g and 48.81 C/g obtained at current densities of 0.8 and 0.4 A/g, respectively. All the calculated specific capacities are shown in Fig. 4.5(c). The Ragone plot in Fig. 4.5(d) shows the variation of energy density with the power density where the AC//rGO/MOF exhibited maximum energy and power densities of 11.0 Wh/kg and 640.45 W/kg, respectively. The stability of the ASC was analysed by continuous charge–discharge (2000 cycles) and the capacitance retention at a high current density of 0.85 A/g was observed.

The EIS analysis was acquired to understand the charge mobility profile of the ASC cell prior and post stability test as shown in Fig. 4.5(e). The Nyquist plots of the cell both shows a semicircle which represents Faradaic charge transfer processes at high frequency region and a linear curve in the low frequency regions. The larger Rct semicircle for the cell after 2000 charge-discharge cycles indicates an increase in the impedance [42]. The device displayed a drastic loss of the initial specific capacitance in the beginning which later stabilised. This can be due to the activation of the active materials, which led to such initial loss (30%) in the capacitance. Later, the asymmetric supercabattery displayed to be stable after 2000 cycles and retained 70% of its initial specific capacity as shown in Fig. 4.5(f). The AC//rGO/MOF cell displayed comparable capacitive performance to the ones reported in the literature (Table 4.3) suggests that the hybrid electrode material is suitable for energy storage applications in supercabattery.

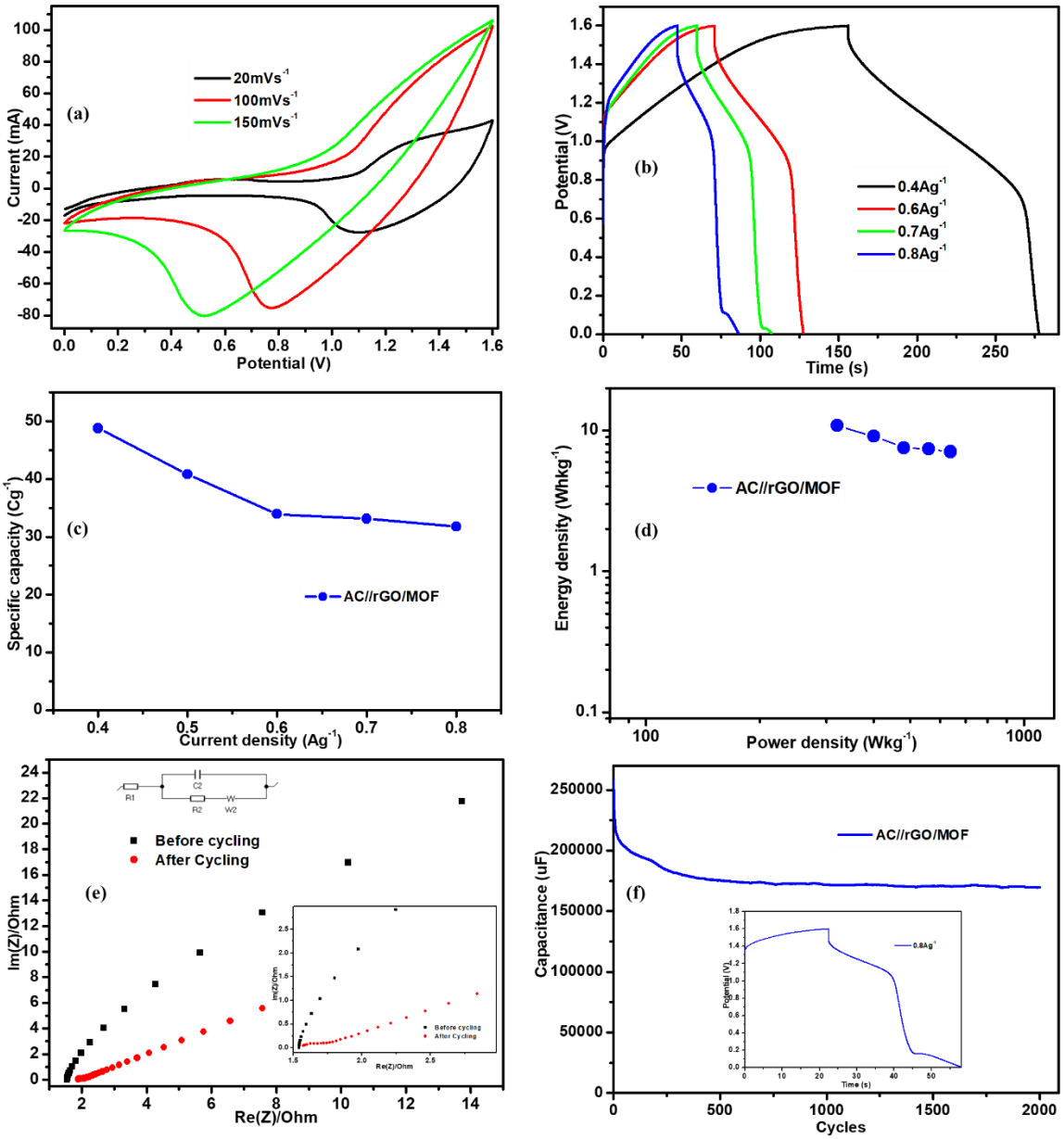

Figure 4.5: (a) CV curves at different scan rates. (b) GCD at different current densities. (c) Specific capacitance at different current densities. (d) Ragone plot (e) Nqyuist plot before and after cycling and (f) Stability test after 2000 cycles, of AC//rGO/MOF asymmetric cell.

Table 4.3: Comparison of properties for metal organic framework-carbon based

electrodes in two-electrode configuration.

Active Material	Electrolyte	Current Density (A/g)	Energy density (Wh/ Kg)	Power density (W/Kg)	Potential Window (V)	Ref
CNT/Mn-MOF//CNT/Mn-MOF	1.0 M Na_2SO_4	0.25	6.9	2240	1	[38]
AC// Ni@Cu-MOF	6.0 M KOH	1	17.3	798.5	1.6	[39]
Mn-MOF//Mn-MOF	1.0 M Na_2SO_4	0.25	4.3	171.6	1.5	[40]
ZIF-67/rGO//ZIF-67/rGO	1.0 M Na_2SO_4	3	25.5	2700	1.5	[41]
AC// NiCo-MOF	2.0 M KOH	0.5	49.4	562.5	1.5	[42]
AC// rGO/MOF	3.0 M KOH	0.8	11.0	640.45	1.6	[This work]

4.4. Conclusions

The rGO/MOF hybrid has been prepared by impregnation method. SEM and TEM analyses reveal that the rGO get wrapped around MOF. TGA analysis shows that hybrids have higher thermal stability than pure MOF. Strong interaction between rGO and MOF is evidenced by FTIR and XRD. The electrode material of the hybrid was fabricated by coating on nickel foam and it exhibited a battery-type behaviour with better capacity of 459.0 C/g at 1.5 A/g. The asymmetrical supercapacitor exhibited energy density of 11.0 Wh/Kg and power density of 640.45 W/Kg with an excellent cyclic stability after 2000 cycles and a loss of less than 30% specific capacity. rGO/MOF hybrid material is a promising electrode material for future supercabattery advances, however, compared with other asymmetrical supercapacitors there still need improvements in the developments of this type of material. This directs our future work to focus on improving the energy and power density by including more electrochemical active materials in the hybrid such as metal nanoparticles as well as to select a better performing negative electrode rather than AC.

References

[1] Xiang Z, Wang D, Xue Y, Dai L, Chen JF, Cao D, (2015). PAF-derived nitrogen-doped 3D carbon materials for efficient energy conversion and storage. Scientific Reports, *5*, 1–8.

[2] Yang Z, Ren J, Zhang Z, (2015). Recent advancement of nanostructured carbon for energy applications. Chem Rev, 115, 5159–223.

[3] Cao X, Yin Z, Zhang H (2014). Three-dimensional graphene materials: preparation, structures and application in supercapacitors. Energy Environ Sci, 7, 1850–65.

[4] Libich J, Máca J, Vondrák J, Čech O, Sedlaříková M, (2018). Supercapacitors: Properties and applications. Journal of Energy Storage, 1, 224–227.

[5] Faraji S, Ani FN, (2014). Microwave-assisted synthesis of metal oxide / hydroxide composite electrodes for high power supercapacitors; A review. Journal of Power Sources, 263, 338–360.

[6] Laheäär A, Przygocki P, Abbas Q, Béguin F, (2015). Appropriate methods for evaluating the efficiency and capacitive behaviour of different types of supercapacitors, Electrochemistry Communications, 60, 21–25.

[7] Yu S, Sankaran KJ, Korneychuk S, Verbeeck J, Haenen K, Jiang X, Yang N, (2019). High-performance supercabatteries using graphite@diamond nano-needle capacitor electrodes and redox electrolytes, Nanoscale, 11, 17939-17946.

[8] Brousse T, Belanger D, Long JW, (2015). To Be or Not To Be Pseudocapacitive?, Journal of The Electrochemical Society, 162 (5), A5185-A5189.

[9] Zhou H, Wang X, Sheridan E, Gao H, Du J, (2016). Boosting the Energy Density of 3D Dual-Manganese Oxides-Based Li-Ion Supercabattery by Controlled Mass Ratio and Charge Injection, Journal of The Electrochemical Society, 163 (13) A2618-A2622 (2016)

[10] Scharanger H, Barzegar F, Abbas Q, (2020). Hybrid electrochemical capacitors in aqueous electrolytes: Challenges and prospects, 21, 167-174.

[11] Iro ZS, Subramani C, Dash SS, (2016). A Brief Review on Electrode Materials for Supercapacitor, International journal of electrochemical science, 11, 10628–10643.

[12] Makgopa K, Ejikeme PM, Ozoemena KI, (2016). Electrochimica Acta Graphene oxide-modified nickel (II) tetra-aminophthalocyanine nanocomposites for high-power symmetric pseudocapacitor. Electrochimica Acta, 212, 876–882.

[13] Du W, Bai Y, Xu J, Zhao H, Zhang L, Li X, Zhang J, (2018). Advanced metal-organic frameworks (MOFs) and their derived electrode materials for supercapacitors. Journal of Power Sources, 402, 281–295.

[14] Deraz NM, (2018). The comparative jurisprudence of catalysts preparation methods: I . Precipitation and impregnation methods. Journal-Industrial-Environmental-chemistry, 2(1), 1–3.

[15] Díaz R, Orcajo MG, Botas JA, Calleja G, Palma J, (2012). Co8-MOF-5 as electrode for supercapacitors. Materials Letters, 68, 126–128.

[16] Zhou Y, Jin P, Zhou Y, Zhu Y, (2018). High-performance symmetric supercapacitors based on carbon nanotube/graphite nanofiber nanocomposites. Scientific Reports,8, 9005-9012.

[17] Makgopa K, Raju K, Ejikeme PM, Ozoemena KI, (2017). High-performance Mn_3O_4 / onion-like carbon (OLC) nanohybrid pseudocapacitor : Unravelling the intrinsic properties of OLC against other carbon supports. Carbon, 117, 20–32.

[18] Ates M, Caliskan S, Özten E, (2018). Supercapacitor study of reduced graphene oxide / Zn nanoparticle / polycarbazole electrode active materials and equivalent circuit models, Journal of Solid State Electrochem, 22, 3261–3271.

[19] Ibáñez-Marín F, Morales-Verdejo C, Camarada MB, (2017). Composites of electrochemically reduced graphene oxide and polythiophene and their application in supercapacitors. International Journal of Electrochemical Science, 12(12), 11546–11555.

[20] Gul H, Shah AU, Krewer U, Bilal S, (2020). Study on Direct Synthesis of Energy Efficient Multifunctional Polyaniline–Graphene Oxide Nanocomposite and Its Application in Aqueous Symmetric Supercapacitor Devices. Nanomaterials, 10(1), 118-142.

[21] Smith AT, Marie A, Zeng S, Liu B, Sun L, (2019). Nano Materials Science Synthesis, properties, and applications of graphene oxide / reduced graphene oxide and their nanocomposites. Nano Materials Science, 1(1), 31–47.

[22] Sykam, N, Rao GM, (2017). Room temperature synthesis of reduced graphene oxide nanosheets as anode material for supercapacitors. Materials Letters, 204, 169–172.

[23] Bello A, Makgopa K, Fabiane M, Dodoo-Ahrin D, Ozoemena KI, Manyala N, (2013). Chemical adsorption of NiO nanostructures on nickel foam-graphene for supercapacitor applications. Journal of Materials Science, 48(19), 6707–6712.

[24] Ladrón-de-guevara A, Boscá A, Pedrós J, Climent-pascual E, Andrés AD, Calle F, (2019). Applied Surface Science Reduced graphene oxide / polyaniline electrochemical supercapacitors fabricated by laser. Applied Surface Science, 467–468, 691–697.

[25] Johra FT, Jung W, (2017). Hydrothermally reduced graphene oxide as a supercapacitor Applied Surface Science Hydrothermally reduced graphene oxide as a supercapacitor. Applied Surface Science, 357, 1911–1914.

[26] Diode TS, Khairir NS, Mat MR, (2018). Synthesis of reduced Graphene Oxide (rGO) using different treatments of Graphene Oxide (GO) Synthesis of reduced Graphene Oxide (rGO) using different treatments of Graphene Oxide (GO). IOP Conference Series: Materials Science and Engineering, 358, 012046.

[27] Gascon J, Sonia A, Freek K, (2008). Manufacture of dense coatings of $Cu_3(BTC)_2$ (HKUST-1) on α-alumina. Microporous and Mesoporous Materials, 113, 132-138.

[28] Monama GR, Mdluli SB, Mashao G, Makhafola MD, (2017). Palladium deposition on copper (II) phthalocyanine / metal organic framework composite and electrocatalytic activity of the modified electrode towards the hydrogen evolution reaction. Renewable Energy, 119, 62–72.

[29] Xu Y, Li Y, Huang W, (2017). Porous Graphene Oxide Prepared on Nickel Foam by Electrophoretic Deposition and Thermal Reduction as High-Performance Supercapacitor Electrodes. Materials, 10, 936-954.

[30] Ramohlola KE, Monana GR, Hato MJ, Desmond KD, Mildred K, Masikini M, et al, (2018). Polyaniline-metal organic framework nanocomposite as an

efficient electrocatalyst for hydrogen evolution reaction. Composites Part B, 137, 129–139.

[31] Monama GR, Modibane KD, Ramohlola KE, Molapo KM, Hato MJ, Makhafola MD, et al, (2019). Copper (II) phthalocyanine/metal organic framework electrocatalyst for hydrogen evolution reaction application. International Journal of Hydrogen Energy, 44(34), 18891–18902.

[32] Lin K, Adhikari AK, Ku C, Chiang C, Kuo H, (2012). Synthesis and Characterisation of porous HKUST-1 metal organic frameworks for hydrogen storage. International Journal of Hydrogen Energy, 37(18), 13865–13871.

[33] Zhu G, Wen H, Ma M, Wang W, Yang L, Wang L, et al, (2018). A self-supported hierarchical Co-MOF as a supercapacitor electrode with ultrahigh areal capacitance and excellent rate performance. Chem.commun, 2(4), 10499–10502.

[34] Zahir M, Alam S, Muhammad A, Javaid M, Yaqoob K, Arshad M, et al, (2020). Binary composites of strontium oxide / polyaniline for high performance supercapattery devices. Solid State Ionics, 347, 115276.

[35] Chen Y, Ni D, Yang X, Liu C, Yin J, Cai K, (2018). Electrochimica Acta Microwave-assisted synthesis of honeycomblike hierarchical spherical Zn-doped Ni-MOF as a high-performance battery-type supercapacitor electrode material. Electrochimica Acta, 278, 114–123.

[36] Li Q, Guo H, Xue R, Wang M, Xu M, (2020). ScienceDirect Self-assembled Mo doped Ni-MOF nanosheets based electrode material for high performance battery-supercapacitor hybrid device, 5.

[37] Kang CZ, Omar FS, Gunalan S, Ramesh K, Ramesh S, (2020). Coral-like structured nickel sulfide-cobalt sulfide binder-free electrode for supercapattery, 3621–3630.

[38] Heng I, Wah F, Wei C, Ching J, Amin N, (2019). High performance supercapattery with rGO / TiO 2 nanocomposites anode and activated carbon cathode. Journal of Alloys and Compounds, 796, 13–24.

[39] Wang Y, Nie S, Liu Y, Yan W, Lin S, Cheng G, et al, (2019). Room-Temperature Fabrication of a Nickel- Functionalized Copper Metal – Organic Framework (Ni@Cu-MOF) as a New Pseudocapacitive Material for Asymmetric Supercapacitors. Polymers, 11, 821.

[40] Sundriyal S, Mishra S, Deep A, Fournier J, (2019). Study of Manganese-1,4-Benzenedicarboxylate Metal Organic Metal Organic Framework Electrodes Based Solid State Symmetrical Supercapacitor. Energy Procedia, 158, 5817–5824.

[41] Sundriyal S, Shrivastav V, Kaur H, Mishra S, Deep A, (2018). High-Performance Symmetrical Supercapacitor with a Combination of a ZIF-67/rGO Composite Electrode and a Redox Additive Electrolyte. ACS Omega, 3, 17348−17358.

[42] Wang Y, Liu Y, Wang H, Liu W, Li Y, Zhang J, et al, (2019). Ultrathin NiCo-MOF Nanosheets for High-Performance Supercapacitor Electrodes. ACS Applied Energy Mater, 2, 2063−2071.

CHAPTER FIVE

HIGH PERFORMANCE ASYMMETRIC SUPERCABATTERY BASED ON REDUCED GRAPHENE OXIDE/ METAL ORGANIC FRAMEWORK NANOCOMPOSITE DECORATED WITH PALLADIUM NANOPARTICLES

Summary

Reduced graphene oxide/metal organic framework nanocomposite decorated with palladium nanoparticles (Pd-rGO/MOF) was studied as an efficient electrode material for energy storage applications. Pd-rGO/MOF nanocomposite was prepared by electroless plating of Pd nanoparticle on rGO followed by impregnation method of Pd-rGO on to MOF. The Pd-rGO, MOF and Pd-rGO/MOF materials were characterised by X-ray diffraction, Fourier transform infrared, thermogravimetric analysis, scanning and high-resolution transmission electron microscopy. The resultant nanocomposites showed a morphology in which a thin layer of rGO coating existed over MOF with unique bright spots indicating the presence of Pd nanoparticle. The synthesised materials were analysed by cyclic voltammetry, electrochemical impedance spectrometry and galvanostatic charge-discharge for application in supercabattery. The Pd-rGO/MOF nanocomposite showed improved electron transfer kinetics and superior battery-type performance with large specific capacity of 712.0 C/g at 2.0 A/g in a three-electrode system. Furthermore, Pd-rGO/MOF nanocomposite displayed high electrochemical performance when applied as a positive electrode and activated carbon (AC) as negative electrode in an asymmetric, two-electrode system, configuration. The AC//Pd-rGO/MOF displayed excellent maximum energy density of 25.68 Wh/kg (at 0.6 A/g), power density of 1600 Wh/kg (at 2.0 A/g) and good charge-discharge stability after 3500 cycles. This highlights the impact of Pd nanoparticles on the rGO/MOF nanocomposite for energy storage applications in supercabattery.

Keywords: Nanocomposite, metal organic frameworks, palladium nanoparticles, reduced-graphene oxide, supercabattery.

5.1. Introduction

Currently, energy storage devices including batteries and supercapacitors have attracted many attentions owing to their low manufacturing cost, longer life cycles and high energy density [1-3]. However, the batteries do not have the desired efficiency in applications due to long time of charge/discharge rate [4]. On the other hand, supercapacitors are mostly applied in electronic gadgets, hybrid electric cars as power back-up to protect power disruption [5]. These are basically devices which posseses relatively high power density or fast charge-discharge rate above all types of batteries, moreover they exhibit high cycling stability, and they are environmentally friendly [6]. Supercapacitors contain two methods of storing energy, i.e. (i) electrical double layer capacitance (EDLC) which stores energy by physically adsorping charges at the electrode/electrolyte interface; and (ii) pseudocapacitance, in which charge is stored through reversible faradaic reactions at the electrode/electrolyte interface [7]. The EDLC uses carbon materials while pseudocapacitance uses metal oxides/hydroxides and conducting polymers as promising candidates for electrode materials [8]. Another emerging category of supercapacitor is supercabatteries, which is composed of a high-power EDLC electrode material on one side and high energy density battery-type electrode on the other side of the cell. Supercabatteries are also named hybrid supercapacitor or asymmetric supercapacitor or battery–supercapacitor hybrid device [9]. Recently, MOFs have received more attention as battery-type electrode materials due to their rapid redox kinetics which results relatively higher capacitance. However, their low physical stability and poor life cycle limits their application in supercapacitors [9-10]. Alternatively, carbonaceous materials especially graphene materials have high power density and long-life cycle [11, 12].

Graphene based materials including reduced graphene oxide (rGO) and graphene oxide (GO) have shown to be the most cited electrode materials used currently for EDLC supercapacitors [13-15]. These materials exhibits massive qualities for supercapacitor applications owing to their high electrical conductivity, outstanding chemical and thermal stabilities, and surface area. Therefore, in previous studies, graphene materials has resulted in supercapacitors which exhibits higher power density of about 10 kW/kg [16]. However, these materials show relatively low specific capacitances of 200 F/g or even lower [16, 17]. Hence, they do not certainly meet the preferred stipulations in terms of energy density and cycle life [17]. As a result, the

composite electrode materials based on carbon materials and metal-based materials which combine the advantages of EDLC, and high-energy density battery-type electrode can overcome these limitations leading to a hybrid supercabattery. It was also shown that the restacking of the graphene materials was improved by addition of metal organic frameworks (MOFs) which serves as a barrier between the graphene sheets [18].

MOF materials as electrodes for supercabattery applications have been reported [9-10, 19-21]. In this regard, MOFs prepared from different metals (e.g., Ni, Co, Cu, Mn, Cr, Zr, Fe, and Zn) connected to organic linkers such as BDC, amino-BDC, BTC, and imidazole have been investigated for such applications [19]. MOFs have been reported as emerging supercapacitor electrodes, however, their cyclic stability decreases with repetition of charging-discharging cycles as a result of electrode-electrolyte incompatibility and occasional material dissolution during reduction cycle [21]. Pattarrachai *et al.* [22] demonstrated a composite material based on reduced graphene oxide (rGO) and metal organic framework (rGO/MOF) which was coated on flexible carbon paper and applied as a supercapacitor electrode material. The electrode of the rGO/MOF material showed a high specific capacitance of 385 F/g at a current density of 1 A/g in the presence of 0.5 M Na_2SO_4 electrolyte for symmetry supercapacitor application. On the other hand, the introduction of metal nanoparticles to carbon materials has shown to improve the electrochemical surface area and active sites of the materials. For example, Riyadz *et al*. [23] reported palladium nanoparticle–reduced graphene nanosheet composite (Pd-rGO) showed increase in electron transfer kinetics. Their composite showed higher capacitive performance with great specific capacitance of 637 F/g, exceptional cyclic performance and extreme energy density of 56 Wh/ kg and power density of 1166 W/ kg, at a current density of 1.25 A/g. In the present work, the electrochemical performance of a novel Pd-rGO/MOF composite synthesised by electroless deposition of Pd followed by impregnation method was investigated. The electrochemical evaluation of the composite on nickel foam exhibited battery-type characteristics. Furthermore, the performance of asymmetric supercabattery containing activated carbon (AC) as the anode and Pd-rGO/MOF as the cathode materials is also reported.

5.2. Experimental

5.2.1. Materials and reagents

Copper nitrate trihydrate ($Cu(NO_3)_2.3H_2O$), trimesic acid (H_3BTC), graphite powder, hydrazine hydrate, phosphoric acid (H_3PO_4), sodium nitrate ($NaNO_3$), palladium chloride ($PdCl_2$), ammonium solution (NH_4OH), ammonium chloride (NH_4Cl) and potassium hydroxide (KOH) were purchased from Sigma Aldrich, South Africa. Dimethylformamide (DMF), dimethyl sulfoxide (DMSO), hydrogen peroxide (H_2O_2), sodium hypophosphite ($NaPO_2H_2$) and sulphuric acid (H_2SO_4) were acquired from Rochelle Chemicals, South Africa. Potassium permanganate ($KMnO_4$), and hydrochloric acid (HCl) were obtained from SAARCHEM, South Africa and hydrogen peroxide (H_2O_2) from Moncon, South Africa. Polyvinylidene fluoride (PVDF), N-methyl pyrrolidone (NMP), Nickel foam, activated carbon and carbon black were obtained from Sigma Aldrich, South Africa. The 3.0M KOH was used as a supporting electrolyte solution. All measurements were carried out at 22 $\pm$ 2 °C.

5.2.2. Synthesis of materials

MOF was synthesised as reported in the literature [24]. Briefly, 1.087g of $Cu(NO_3)_2.3H_2O$ was dissolved in 10 ml of diionised water and then mixed with 0.525 g of H_3BTC (1,3,5 tricarboxylic acid benzene/trimesic acid) dissolved in 10 ml of ethanol. The resultant mixture was then stirred for 30 min and then transferred to a 23 ml Teflon stainless-steel autoclave and sealed to react for 36 hours under 120 ^oC in thermostatic drying oven. After cooling to room temperature, the mother liquor was then decanted. The product was washed by ethanol repeatedly, and then dried at room temperature for overnight.

Graphene oxide was prepared according to the modified Hummer method [25]. Concisely, the as-prepared GO (100 mg) was loaded in a 250-mL round bottom flask and water (100 mL) was then added, yielding an inhomogeneous yellow-brown dispersion. This dispersion was sonicated until it became clear with no visible particulate matter. Hydrazine hydrate (1.00 mL, 32.1 mmol) was then added and the solution heated in an oil bath at 100 ^oC under a water-cooled condenser for 24 h over which the reduced GO (rGO) gradually precipitated out as a black solid. This rGO

product was isolated by filtration over a medium fritted glass funnel, washed copiously with water (5x100 mL) and methanol (5x100 mL), and dried on the funnel under a continuous air flow through the solid product cake [26].

Pd-rGO was prepared using electroless palladium deposition [27] through immersion of rGO in a sodium hypophosphite-based plating bath. The plating solution was prepared by firstly dissolving 2 g of $PdCl_2$ in 4 mL HCl (32%) and 20 mL of ultra-pure water, and then heated at 50 ^oC for 30 minutes with constant stirring at 300 rpm. After complete dissolution of $PdCl_2$, 160 mL of NH_4OH (28%) and 27 g of NH_4Cl were added respectively. The mixture was then transferred to 1 L volumetric flask and made up to the mark with ultra-pure water. The electroless plating bath, containing 50 mL of sodium hypophosphite (10 g/L) as a reducing agent to initiate the reaction and 5 g batch of rGO, was subjected to constant agitation (300 rpm) for 30 minutes at 50 ^oC in a separate bath to avoid decomposition during storage of the bath. Finally, the 50 mL of plating solution was added in to the bath solution and the mixture was agitated for 30 minutes to allow the plating of Pd to the surface of rGO sheets. The mixture was filtered, washed with ultra-pure water and dried for overnight at 80 ^oC.

Pd-rGO/MOF composite was synthesised by impregnation method [28] of Pd-rGO and MOF. Approximately, 0.1 g of as-synthesised MOF sample was dehydrated at 150 ^oC for 1 hour. It was then suspended in 10 mL DMF. In a separate beaker, 0. 1 g of Pd-rGO was dispersed in 1.4 mL DMF, and then the two mixtures were mixed together and stirred magnetically for 24 hours at 50 ^oC. The resulting product was recovered by filtration and washed with ethanol and then dried overnight at 50 ^oC.

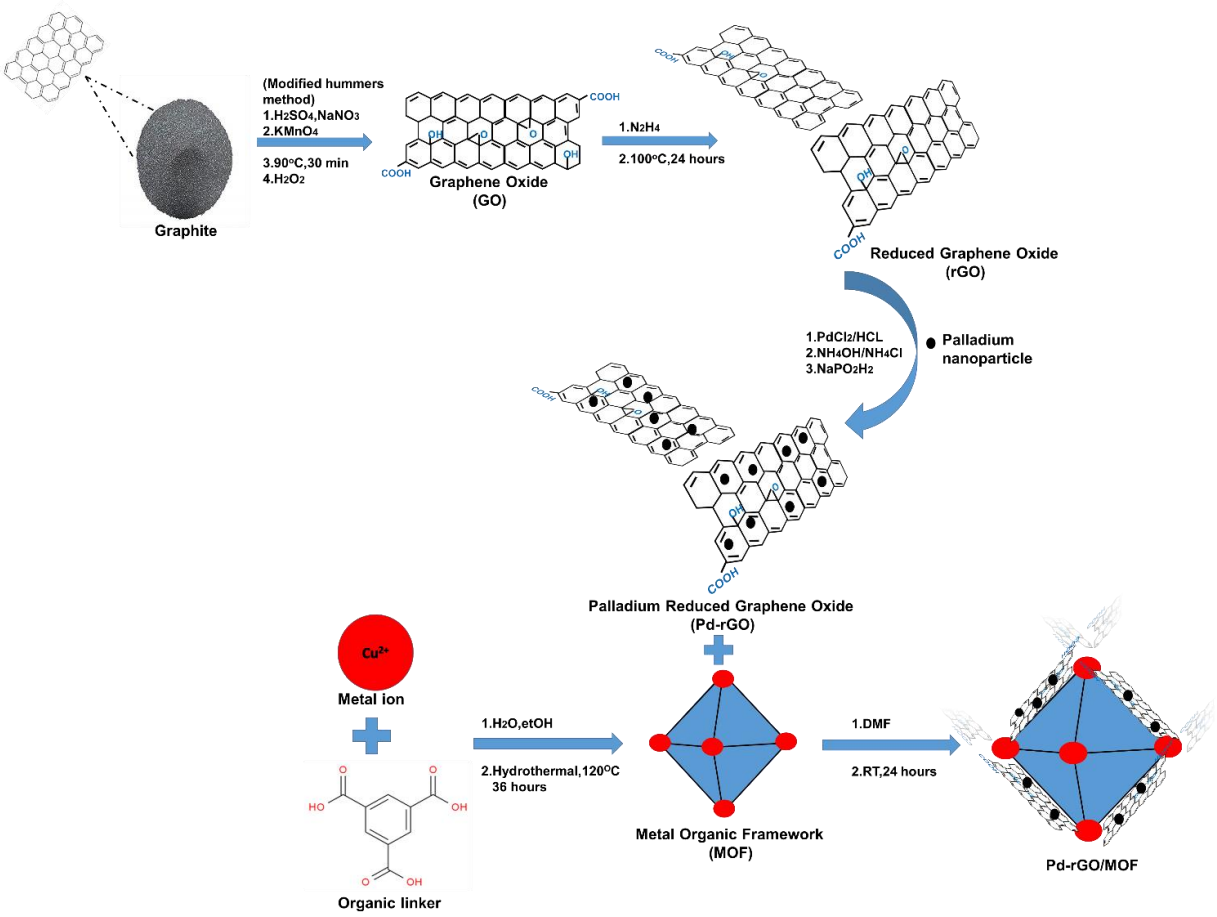

Scheme 5.1: Synthesis of the MOF, Pd-rGO and Pd-rGO/MOF composite.

5.2.3. Supercabaterry electrode fabrications

The preparation of supercabattery electrodes were conducted according to literature [29]. Nickel foam of area 0.1 cm^2 was soaked in 3M HCL and ultrasonicated for 15 min removing the nickel oxide layer, the electrodes were further ultrasonicated in a mixture of deionised water and ethanol for another 15 minutes. The nickel foam electrodes were further pressed at high pressure to close the various pores in their structure before coating. The electrodes composed of three different materials which included 70% of the synthesised materials (MOF, Pd-rGO and Pd-rGO/MOF composite), 10% of the binder (PVDF) and 20% of the solid material (carbon black).The combination of the three materials were crushed and saturated in N-methyl pyrrolidone (NMP) before coated on the nickel foam. The coated electrodes are then dried overnight at 75°C. The average loading of the materials on Ni foam was between 4-5 mg and only mass

of MOF, Pd-rGO and Pd-rGO/MOF was included in calculating the active mass. A 3M KOH electrolyte was prepared in a 500 ml volumetric flask where 84.15g KOH pellets were weighed and filled to the mark with distilled water.

5.2.4. Electrochemical assessment

The electrochemical evaluation of the materials was done using the Biologic instrument in a temperature controlled lab at 25 ^{o}C. The device uses VMP-300 Biologic potentiostat and EC lab software. For the three-electrode system platinum wire, Ag/AgCl and the prepared electrodes were used as counter, reference and working electrodes, respectively. The electrochemical evaluation of the assembled supercabattery was done using a two-electrode asymmetric system where the as-prepared electrodes were used at cathodic electrodes and activated carbon was used as an anodic electrode. Specific capacities of the battery-type composite in three electrode and two electrode systems were obtained from the galvanostatic charge-discharge curves using Equation 5.1:

$$Q_s = \frac{I*\Delta t}{m} \tag{5.1}$$

In the above equation Qs is the specific capacity, I is the average applied current, Δt is the discharging time and m is the active mass. The energy density (ED) and power density(PD) were calculated using Equations 2 and 3, respectively:

$$ED(Wh\ kg^{-1}) = \frac{1}{2*3.6} Qs\Delta V \tag{5.2}$$

$$PD(Wkg^{-1}) = \frac{ED*3600}{\Delta t} \tag{5.3}$$

where ΔV is the change in potential window.

The assembled supercabattery was prepared using AC as the negative electrode and Pd-rGO/MOF as the positive electrode (AC//Pd-rGO/MOF). The supercabattery was

tested in a 3M KOH electrolyte solution using a coin-type electrochemical cell. A filter paper was used as a separator and the mass ratio between the two electrodes were determined using Equation 4:

$$\frac{m^+}{m^-} = \frac{Q^-}{Q^+}\left(\frac{\Delta V^-}{\Delta V^+}\right) \quad (5.4)$$

where m^+, ΔV^+, and Q^+ denote the mass, potential window and specific capacity of the positive electrode, respectively; and m^-, ΔV^-, and Q^- mass, potential window and specific capacity corresponding to the negative electrode, respectively.

5.2.5. Materials characterisation

Optical absorption spectra were recorded at room temperature in the wavelength region 200 – 800 nm using a Varian Cary 300 UV-Vis-NIR spectrophotometer. The structures of Pd-rGO, MOF, and Pd-rGO/MOF composite were analysed using X-ray diffraction (XRD Phillips PW 1830, CuK_α radiation, λ = 1.5406 A). The formation of the composite was confirmed by Cary 600 series Fourier transform infrared (FTIR) spectrometer (Agilent Technologies). The spectra were obtained at room temperature in the wave number range between 500 and 4500 cm^{-1}. A minimum of 32 scans were collected at a resolution of 4 cm^{-1}. The thermal stability of the samples was performed on a Perkin-Elmer STA 6000 instrument connected to a PolyScience digital temperature controller under N_2 gas purged at a flow rate of 20 ml/min. The calibration of the instrument was performed using indium (m.p. 156.6 ºC) and aluminium (m.p. 660 ºC). Samples ranging between 1−4 mg were heated from 30-600 ºC at a constant heating rate of 10 ºC /min. The data was collected and analysed using Pyris software®. Morphological characterisations were performed using Auriga Field Emission Scanning Electron Microscope (FESEM) coupled with EDS detector for elemental analysis. High-resolution transmission electron microscopy (HR-TEM) observations

were acquired from HR-TEM, FEI Tecnai G2 F20X-Twin MAT 200-kV, Eindhoven, Netherlands.

5.3. Results and discussion

5.3.1. Structural properties

The FTIR spectra of MOF, Pd-rGO, and Pd-rGO/MOF are presented in the Figure 5.1 (a). The lattice vibrations of as-prepared MOF are in agreement with literature [30]. Since MOF consisted of benzene-1,3,5-tricarboxylicacid (BTC), bands of the spectrum essentially derived from BTC. Thus, the band at 1370 cm^{-1} was assigned to C-O of BTC and the bands at 1450 cm^{-1} as well as 1590 cm^{-1} were attributed to C=O of BTC. The band at 1645 cm^{-1} resulted from aromaticC=C and 1719 cm^{-1} from COO− of BTC [30]. The region below 1300 cm^{-1}, shows various bands assigned to out of plane vibrations of the BTC ligand. Typically, the FTIR peaks belonging to the rGO either disappear or their intensities are significantly reduced after the reduction process, which in turn confirms the formation of Pd nanoparticle on rGO. It can further be observed that the intensities of the band in Pd-rGO are very low and some disappeared with reference to rGO spectrum [31]. It implies that the incorporation of palladium on rGO is on the surface of graphene oxide sheets.

The spectrum of Pd-rGO/MOF is similar to that of MOF [27,28] with enhancement of aromatic peaks for the C=C, C-H and C-C and appearance of rGO peak at ~1000 cm^{-1} as indicative of incorporation of Pd-rGO in the nanocomposite.

The X-ray diffraction patterns of the parent materials as well as the composites are presented in Figure 5.1 (b). For MOF, the patterns obtained is in accordance with the one reported in the literature for this specific network and is supported by the MOF CSID pattern [32] with the main intense peak of the pattern appeared at $2\theta = 12^{o}$, accounting for the (222) hkl index. The peaks at 35^{o} and 43^{o} are related to Cu_2O impurities, but their intensities are very low related to main peaks of the MOF, which confirm that the purity of the MOF was well preserved and the MOF was pure powder. In the case of Pd-rGO, the characteristic peak at $2\theta = 24°$ is ascribed to the (002) planes of the chemically reduced GO stacks [33], indicating the effective reduction of GO by hydrazine hydrate. The two diffraction peaks centred at 2θ of 39^{o} and 45^{o} are corresponding to the (111) and (200) reflections of Pd nanoparticles [33], respectively.

The XRD pattern of the Pd-rGO/MOF nanocomposite is similar to that of MOF, which shows that the incorporation of Pd-rGO did not affect the crystallinity of MOF. A decrease in intensity of the diffraction peaks also confirms the formation of the Pd-rGO/MOF nanocomposite. TGA graphs (Figure 5.1 (c)) show weight profiles of powder samples as variation of temperature under N_2 flow. In the region below 250 ^oC, Pd-rGO has no weight loss, which implies that this compound does not contain water or any organic solvents. This is expected because rGO was reported to be thermally stable up to 800^oC [34]. In the case of MOF, the TGA thermogram shows the dehydration takes place with 25 wt.% mass loss, corresponding to three water molecules per copper center in the framework (fully hydrated MOF is reported to hold up to 40 wt. % water [24]). MOF was found to be thermally stable up to 370^oC before starting to gradually disintegrate at higher temperatures. The TGA curve of MOF exhibits a huge decomposition (approximately 28 wt. % mass loss) at 330-375^oC corresponding to the collapse of the structure back to its precursors, accompanied by the release of CO_2 [28]. The composite Pd-rGO/MOF show that moisture stability and overall thermal stability is now enhanced. These is supported by DSC curves of MOF, Pd-rGO and Pd-rGO/MOF nanocomposite in Figure 5.1 (d). The MOF curve exhibits an exothermic peak as an indicative of the removal of moisture from the porous structure of the MOF. The DSC curves of Pd-rGO is similar to that of Pd-rGO/MOF but the composite exhibits higher heat flow rate than Pd-rGO. The weight loss in the TGA of Pd-rGO/MOF composite is supported by the observation of the endothermic peak in the DSC results. MOF alone has a very high heat flow rate compared to Pd-rGO and the nanocomposite which indicates that MOF is highly heat sensible than the composite [34].

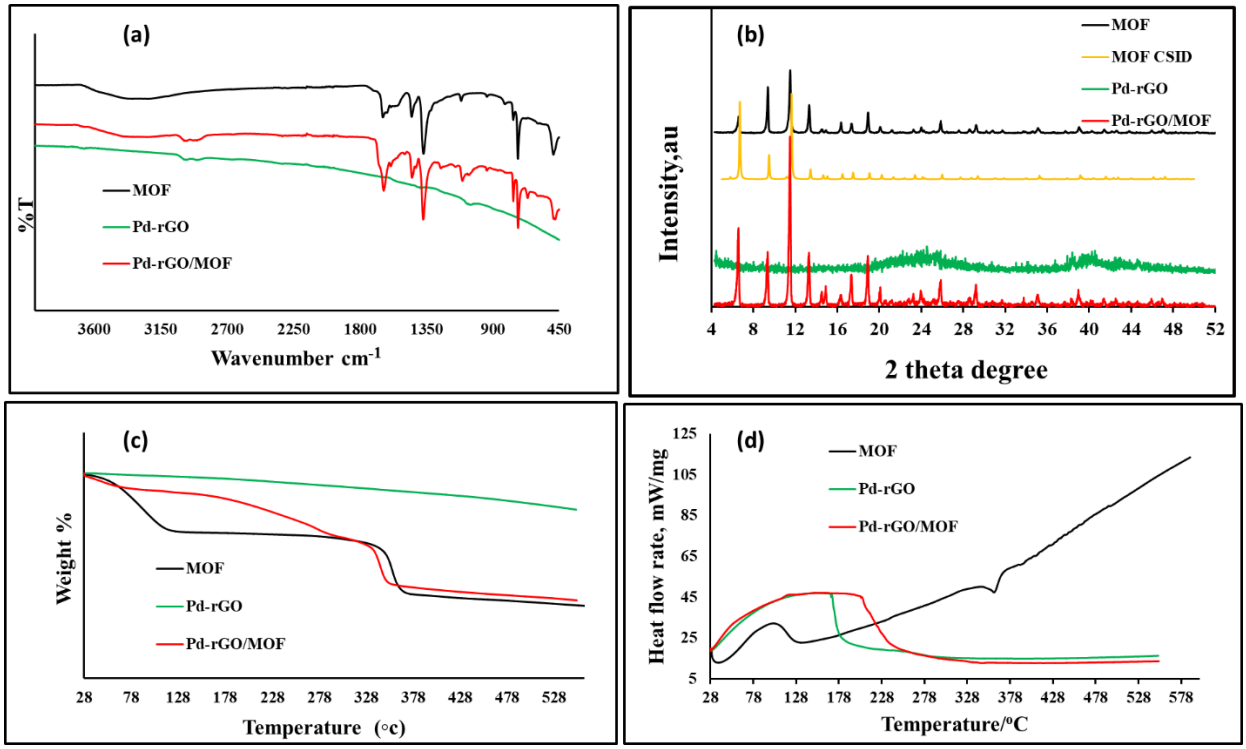

Figure 5.1: (a) FTIR spectra, (b) XRD patterns, (c) TGA and DSC curves of MOF, Pd-rGO and Pd-rGO/MOF.

5.3.2. Morphological Characterization

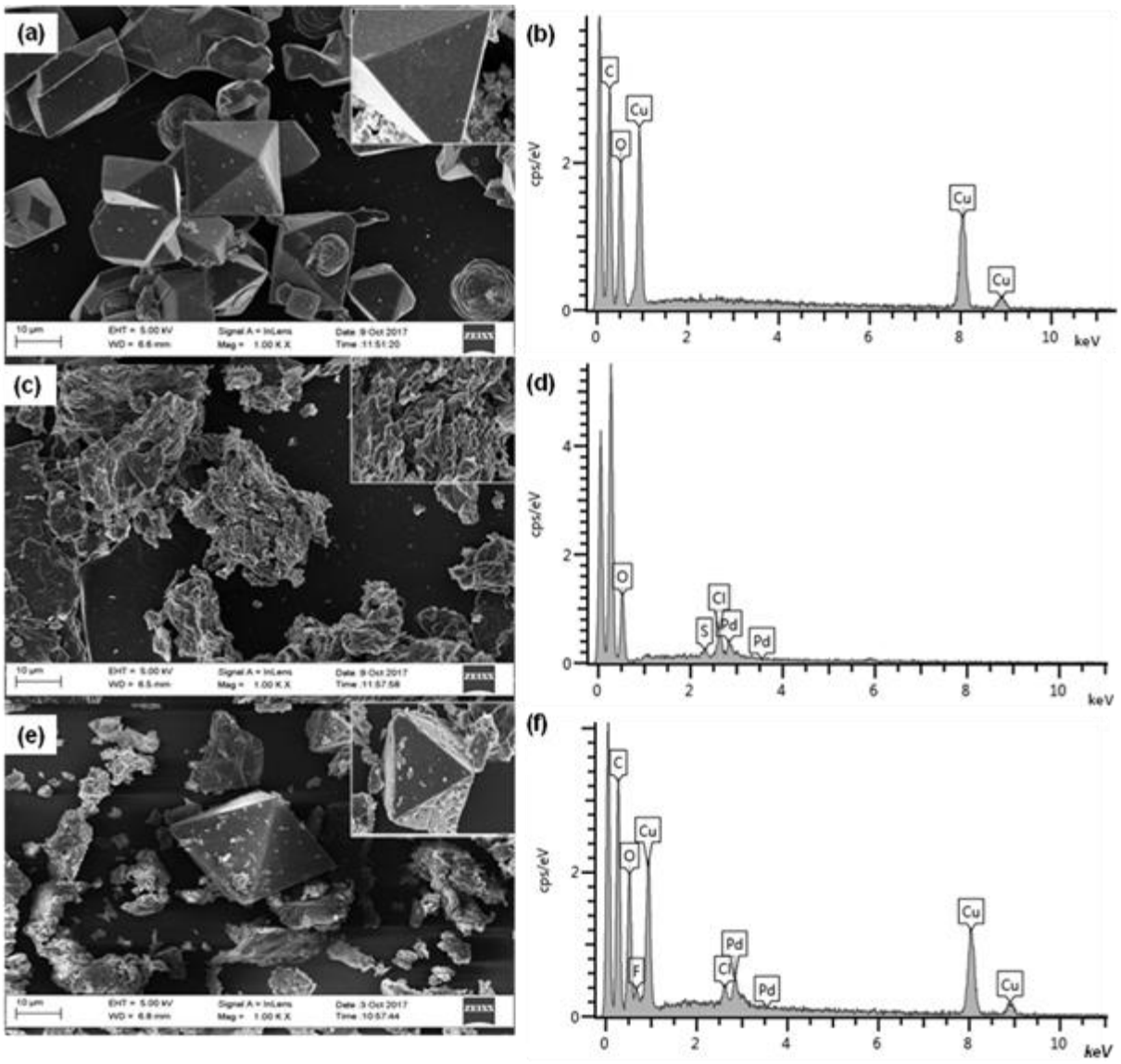

Figure 5.2: SEM image of (a) MOF, (c) Pd-rGO and (e) Pd-rGO/MOF. EDS of (b) MOF, (d) Pd-rGO and (f) Pd-rGO/MOF nanocomposite.

Figure 5.2 (a) presents SEM image of MOF. The hydrothermaly synthesized MOFexhibits only highly crystalline faces which are characteristic of micropourous octohydral materials,and this indicates indicactes the purity of our MOF [34]. The EDS spectrum of MOF (Figure 5.2 (b)) confirms the availability of Cu from the salt and O and C from the organic linker. Figure 5.2 (c) shows that the palladium nanoparticles are present in rGO as they appear as discrete bright spots while the rGO sheets shows partial agglomeration which is a result of strong van der Waals forces between the sheets [23]. The Pd nanoparticles act as spacers between the sheets reducing the restacking capacity of the graphene sheets and therefore preventing the loss of active

sites on the sheets [31]. The EDS of Pd-rGO in Figure 5.2 (d), shows the presence of Pd from the nanoparticles, C- and O-atom from the graphene material. MOF crystalline materials are observed in the SEM image of nanocomposite (Figure 5.2 (e)) and the rGO sheets with embedded bright spots are observed on the MOF surface. Its EDS spectrum (Figure 5.2 (f)) shows the presence of Pd as well as an increased in intensities of C- and O-atom from both MOF and rGO, revealing a good loading of Pd nanoparticles on rGO, which is consistent with the SEM observations. In addition, the TEM images of the Pd-rGO/MOF composite are observed in Figure 5.3(a-c)). Figure 5.3 (a) shows the low magnification TEM image where rGO sheets are clearly observed on the surfaces of MOF structures. In this image, the Pd-nanoparticles are not clearly observed. Figure 5.3 (b-c) show higher magnification TEM images of Pd-rGO/MOF. The MOF octahedral structures are still conserved in the composite (Figure 5.3 (b)) and the Pd-nanoparticles (dark spots) are observed on the surface of the graphene nanosheets and they are clearly distinguishable in Figure 5.3 (c). The electron diffraction pattern of the composite (Figure 5.3 (d)) represents a less crystalline structure, as we observe less diffraction patterns and a reduction in bright spots [23].

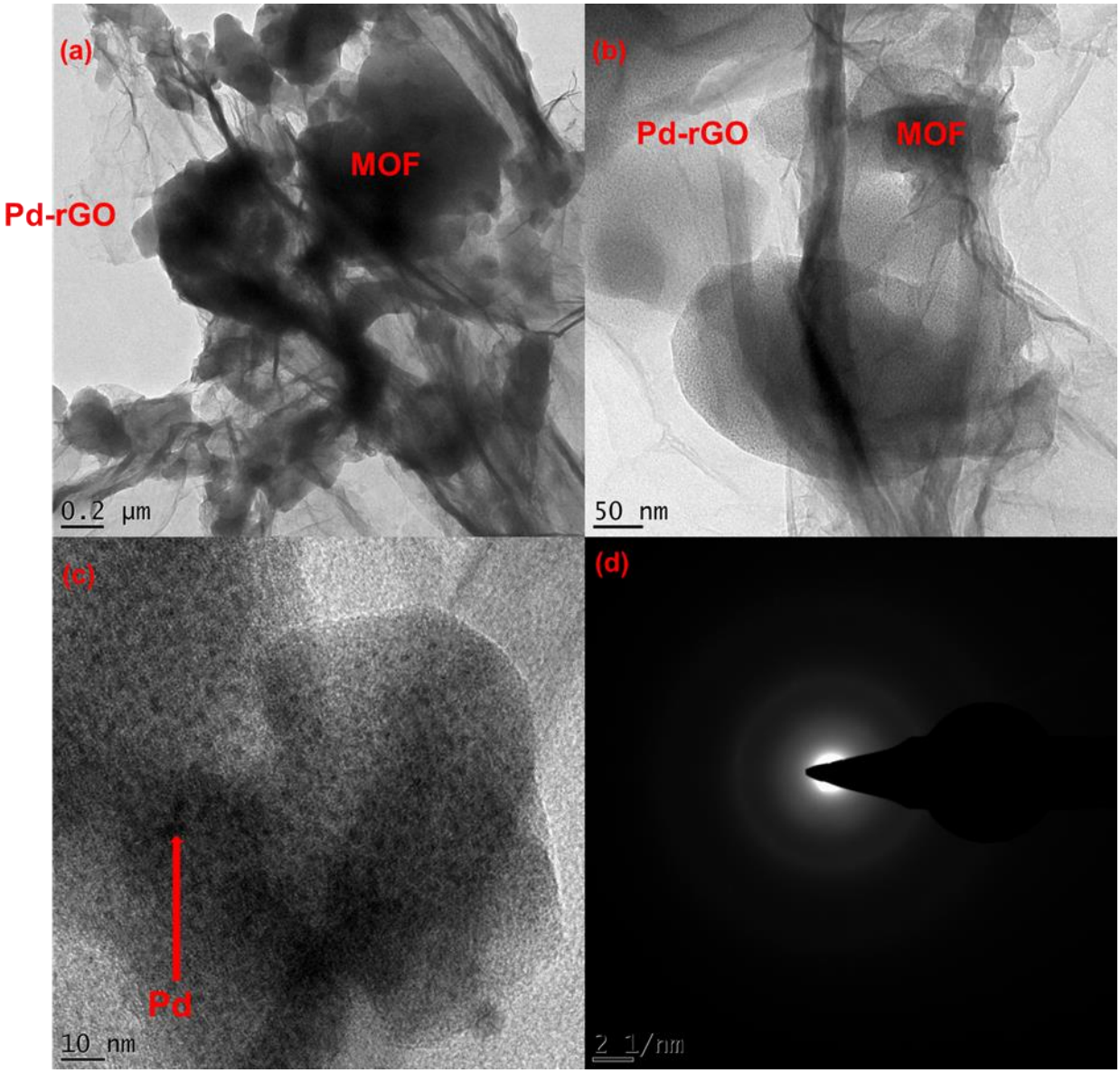

Figure 5.3: TEM images of Pd-rGO/MOF at different magnifications (a-c). (d)SAED of Pd-rGO/MOF nanocomposite.

5.3.3. Electrochemical properties

5.3.3.1. Three electrode system performance

The electrochemical testing of NF-MOF, NF-Pd-rGO and NF-Pd-rGO/MOF were performed at a potential range of -0.2 to 0.5V in a 3.0M KOH electrolyte (Figure 5.4.). Figure 5.4(a) shows an overlaid CV curves of MOF, Pd-rGO and Pd-rGO/MOF at scan rate of 10 mV/s to determine the behaviour of the electrode material. MOF, Pd-rGO and Pd-rGO/MOF shows distinct anodic and cathodic peaks observed around 0.2 and

0.4V respectively, which indicates redox activities of battery-type electrodes [35]. The current response for MOF is slightly higher due to high diffusion of the electrolytes in to MOF pores than Pd-rGO, however, the MOF is less redox active than Pd-rGO as clear redox peaks are observed on the Pd-rGO. The Pd-rGO/MOF nancomposite electrode exhibits higher current response than that of MOF and Pd-rGO with improved redox activity and high current response, this makes our final nanocomposite a good battery-type electrode material. Figure 5.4 (b) shows GCD curves of NF-MOF, NF-Pd-rGO and NF-Pd-rGO/MOF nanocomposite at current density of 2 A/g and -0.2 to 0.5V potential range. It is observed that MOF alone exhibits a short discharge time compared with Pd-rGO. The incorporation of Pd-rGO to the MOF structures resulted in a massive increase in discharge time of the material as an indication to be a suitable electrode material for supercabattery applications. The specific capacities of the individual electrodes were calculated from the GCD results and were obtained as 205.53, 173.99 and 711.99 Cg^{-1} for NF-MOF, NF-Pd-rGO and NF-Pd-rGO/MOF at current density of 2 A/g, respectively. The GCD results correspond perfectly with the CV results in Figure 5.4 (a). Figure 5.4 (c) shows CV curves of NF-Pd-rGO/MOF at different scan rates (10 to 80mV/s). A gradual increase in current response as the scan rate increases and a small shift in the redox peaks are observed indicating a low resistance of the electrode material and a good rate capability which are characteristic of a typical capacitive material [37]. In addition, the shape of the CV profile was well maintained from a lower scan rate to a higher scan rate which demonstrates that the device exhibited capacitive behavior within this range of scan rate [37]. Figure 5.4(d) demonstrates GCD curves of Pd-rGO/MOF nanocomposite at different current densities. An inverse proportionality of current density and discharge time is observed which indicates that the materials can be applied at lower current densities to obtain high discharge times and good specific capacitances. The nonlinear shape of the charge-discharge curves also provides evidence of the presence of redox reactions in the storage mechanism of the electrode [36]. The current response as a function of square root of scan rate curve in Figure 5.4(e) was used to determine the diffusion coefficient (D) employing Randles Ševćik equation shown as Equation 5.5:

$$Ip = 2.65 \times 10^5 n^{1.5} ACD^{0.5} v^{0.5} \quad (5.5)$$

where, n is the number of electrons transferred, A is the electrode area in cm^2, D is the diffusion coefficient in cm/s, C is the bulk molar concentration of the electroactive species in mol/cm^3 and v is scan rate is V/s. A high diffusion coefficient of MOF was reported by Monama *et al*. [28] to be 14.8×10^{-7} cm/s in H_2SO_4. The diffusion coefficient of Pd-rGO and Pd-rGO/MOF electrode were found to be 7.40×10^{-7} and 12.7×10^{-7} cm/s, respectively. The relationship between the specific capacity and current density of MOF, Pd-rGO and Pd-rGO/MOF nanocomposite were presented in Figure 4(f). All the materials had shown an increase in specific capacity with decrease in current density. Pd-rGO/MOF composite further demonstrated specific capacity values of more than 550 C/g at current densities above 3 A/g whereas the minimum specific capacitance was 613.79 C/g at a current density of 4 A/g. The decrease in specific capacity was due to the sluggish movement of charges. Interestingly, the Pd-rGO-MOF based electrodes displayed a specific capacity of 712 C/g at 2 A/g. This value is much greater than those obtained for NiCo-MOF as 601.0 C/g [37] and Pd-rGO as 557.6 C/g [23]. The enhanced performance is mainly because of the unique structure of the nanocomposite cause by synergic effect of Pd-rGO and MOF. The nanocomposite has a 3-D interconnected continuous network as seen in SEM and TEM, offering not only a high surface area and good pathway for charge transport but also it shortens the diffusion path and facilitates electrolyte diffusion into the pores thereby improve the electrochemical performance.

Table 5.1. Comparison of previously reported MOF-carbon electrode materials for supercapacitor applications

Active Material	**Current Density (A/g)**	**Specific Capacity (C/g)**	**Electrolyte**	**Potential Window (V)**	**Ref**
NiCo-MOF	1.00	601.0	2.0M KOH	0.5	[37]
Pd-rGO	1.25	557.6	1.0M KCl	0.8	[23]
Ni-MOF/CNT	0.50	706.0	6.0M KOH	0.4	[38]

PdO-rGO	0.50	113.6	1.0 Na_2SO_4	0.8	[39]
Pd-rGO/MOF	2.00	712.0	3.0 KOH	0.7	This work

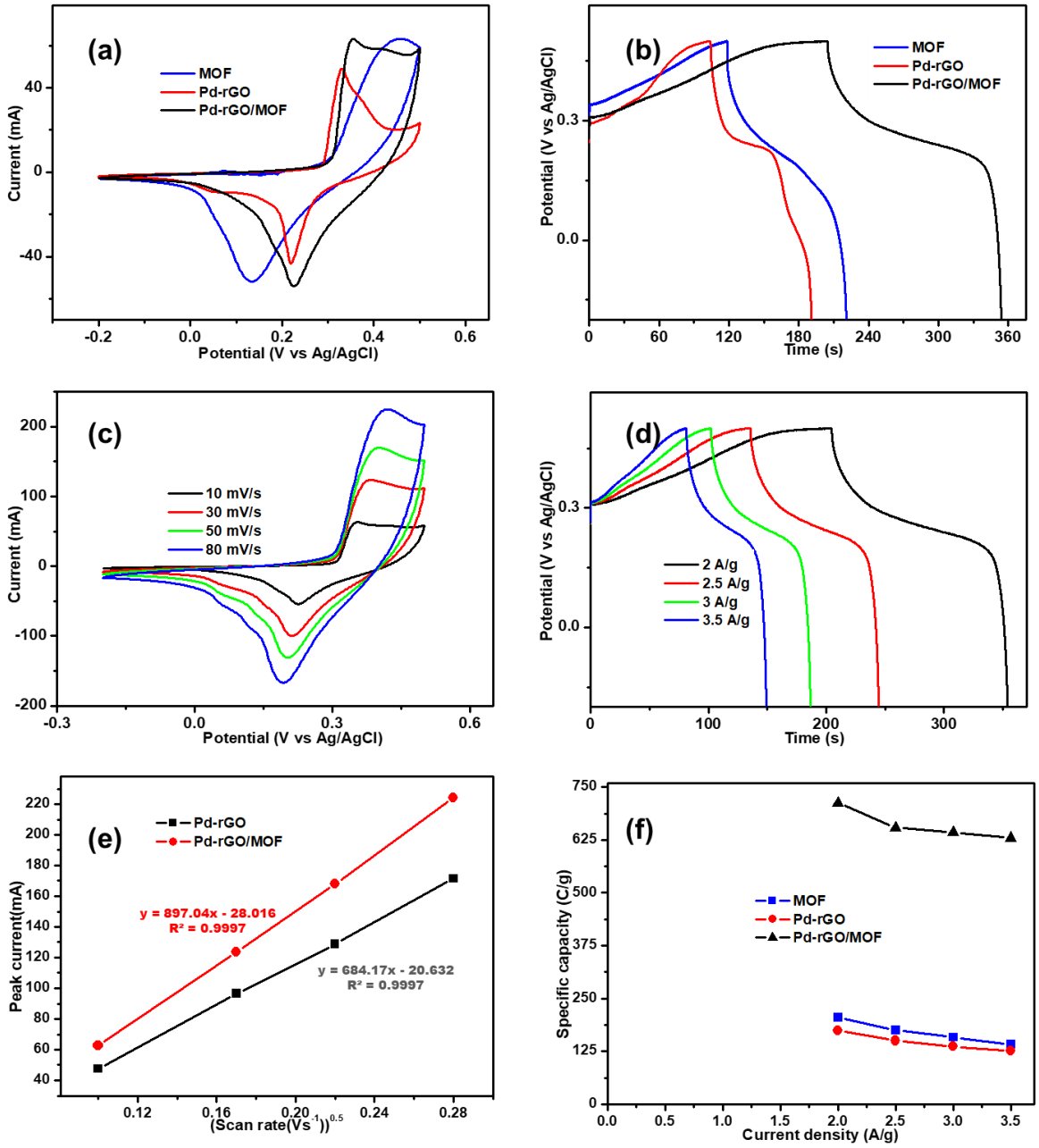

Figure 5.4: CV of (a) MOF, Pd-rGO and Pd-rGO/MOF at a scan rate of 10mV/s. (b) GCD curve of MOF, Pd-rGO and Pd-rGO/MOF at a current density of 2 A/g (c) CV

of Pd-rGO/MOF at different scan rates. (d)GCD curves of Pd-rGO/MOF at different current density. (e) Peak current as a function of square root of scan rate for Pd-rGO and Pd-rGO/MOF. (f)Specific capacity vs current density curve of MOF, Pd-rGO and Pd-rGO/MOF.

5.3.3.2. Asymmetric supercabattery evaluation

The high performance of NF-Pd-rGO/MOF composite in the three-electrode system exhibited a battery-type performance and has led to further investigation in a supercabattery system. The supercabattery comprised activated carbon (AC) as a negative electrode in 3.0M KOH electrolyte. For maximum performance of the cell, the mass ratio of the active materials on the positive and negative electrode were determined using the Equation 5.4. According to the specific capacities of AC (188.64 C/g) and Pd-rGO/MOF (653.56 C/g) at current density of 2.5 A/g and potential of 0.7 V for both electrodes; and the mass ratio was found to be 0.28. The mass of AC and Pd-rGO/MOF were determined to be 2.29 mg and 7.99 mg, respectively. In order to confirm the operational potential window of the two electrode device, Figure 5.5 (a) shows the CV curves of AC//Pd-rGO/MOF at different scan rates (50 to 150 mV/s) and they show a feeble (quasi-rectangular) redox shapes as an indicative for redox activities of the battery-type electrode and the capacitive behaviour of AC [37]. The CV curves show an increase in current response as the scan rate increases and the redox peaks are observed clearly at potentials above 1.0 V. To further evaluate the application of NF-Pd-rGO/MOF composite, the GCD experiments of the supercabattery were performed at a potential range of 0 to 1.6 V as shown in Figure 5.5 (b). The charge-discharge curve shows an increasing discharge time with a decrease in current density and a nonlinear behaviour of the curves is observed. The specific capacities of the asymmetric supercabattery were calculated to be 115.59, 114.57, 109.0, 97.5 and 89.8 C/g at current densities of 0.6, 0.7, 1.0, 1.5 and 2.0 A/g respectively as indicated in Figure 5.5 (c). The AC//Pd-rGO/MOF cell exhibited a maximum energy density of 25.68 Wh/kg and power density of 1599.99 W/kg, as shown in the ragone plot (Figure 5.5 (d)). These results are even better than other reported materials such as AC//Ni@Cu-MOF (17.3Wh/kg) and 798.5 W/kg) [40], NiS HNPs//AC(11.6 Wh/kg and 187.5 W/kg) [41], Ni-Co oxide//AC (10.8 Wh/kg and 474.4 Wk/kg) [42], MnO_2/Ni foam//AC (7.7 Whk/g at 600 W/kg) [43]. Cyclic stability of the device is one of the important factors for the realisation of the device. The cyclic

stability (Figure 5.5 (e)) of AC//Pd-rGO/MOF was evaluated by continuously charging and discharging at a current density of 0.9 A/g and potential range of 0 to 1.6 V shown in Figure 5.5 (e) insert. It is observed that the capacitance gradually decreases at higher number of cycles but more than 70% of the capacitance was retained after cycling for 3500 cycles. This shows that the specific capacity value decay only 30.0% of its initial value which manifest excellent stability of the fabricated device. To further evaluate the electrochemical behaviour of the electrodes, electrochemical impedance spectroscopy was performed before and after cycling at open circuit voltage and the Nqyuist plots are shown in Figure 5.5 (f). Depressed semicircle at the high frequency region, corresponded to the charge transfer resistance (Rct), was attributed to the redox reactions of the electrodes. The straight line at the low frequency region, corresponded to the Warburg impedance (Zw), was related to the diffusion of electrolyte along the nanostructures. The AC//Pd-rGO/MOF cell exhibits a lower charge transfer resistance (Rct) and lower internal resistance (Rb), suggesting the larger electro-active surface area, and higher electrical conductivity of the electrodes. Even after cycling more than 3000 times, the low resistance was maintained [44].

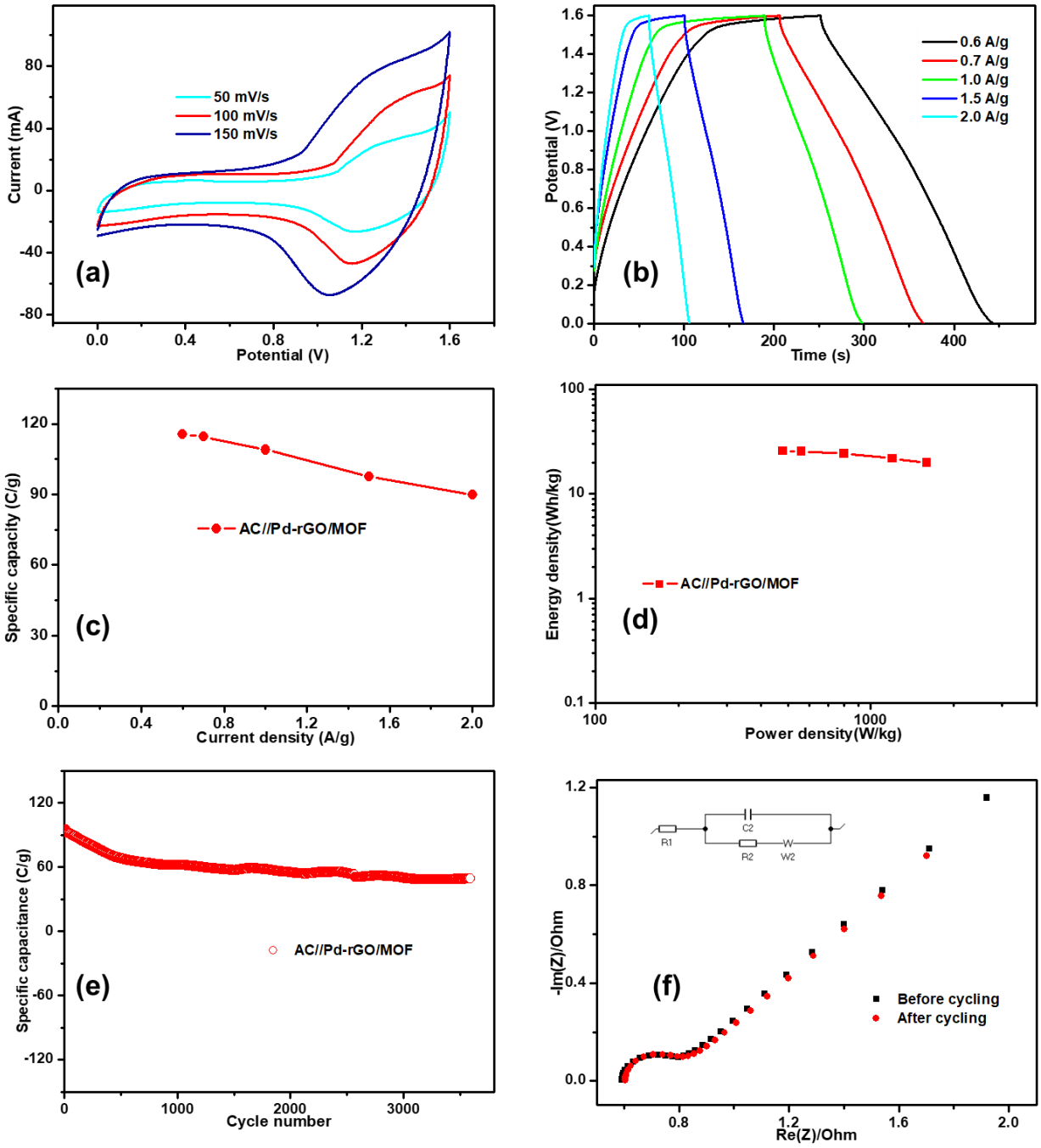

Figure 5.5: (a) CV of AC//Pd-rGO/MOF at different scan rates. (b) GCD of AC//Pd-rGO/MOF at different current densities. (c) Specific capacity vs current density curve of AC//Pd-rGO/MOF. (d) Ragone plot of AC//Pd-rGO/MOF. (e) Stability testing of AC//Pd-rGO/MOF cell at a current density of 0.9A/g. (f) Nqyuist plot of AC//Pd-rGO/MOF before and after stability cycling.

Table 5.2. EIS parameters for Pd-rGO/MOF cell before and after cycling.

Cell	R1	C2	R2	s2
Before cycling	0.5930 Ω	0.5464 mF	0.1762 Ω	2.428 $\Omega/\sqrt{s}$
After cycling	0.6036 Ω	0.7909 mF	0.1849 Ω	1.93 $\Omega/\sqrt{s}$

5.4. Conclusions

Herein, Pd-rGO/MOF nanocomposite was prepared first time by electroless deposition method followed by impregnation of Pd-rGO and MOF using 1:1 mass ratio. The successful preparation of Pd-rGO/MOF nanocomposite was confirmed by XRD, FTIR, TGA, DSC, SEM, TEM and SAED. The standard three electrode cell studies showed well defined redox behaviour of Pd-rGO/MOF nanocomposite in 3 M KOH at room temperature. This confirmed the supercabattery behaviour of Pd-rGO/MOF nanocomposite with specific capacity value of 712 C/g. The two electrode cell of AC//Pd-rGO/MOF for asymmetric supercabattery, demonstrated excellent performance in the potential range of 0 to 1.6 V. The maximum energy density was found to be of 25.68 Whk/g and power density of 1599.99 Wk/g which is considerably higher to the reported results in the literature. The enhanced performance of Pd-rGO/MOF is attributed to it unique nanostructured material which offers high electrochemical surface area and extended redox active sites as well as channels for charge transportation. Nevertheless, compared with other MOF composites the cycling stability here still needs to be improved but the specific capacitances are good but more than 30% of the capacitance was retained after 3500 cycles. Therefore, our future work will contribute to enhance the specific capacitance and cycling stability to further promote their practical applications.

References

[1] Zhao W, Zheng Y, Cui L, Jia D, Wei D, Zheng R, (2019). MOF derived Ni-Co-S nanosheets on electrochemically activated carbon cloth via an etching

/ ion exchange method for wearable hybrid supercapacitors. Chemical Engineering Journal, 371, 461–469.

[2] Inal I, Aktas, Z, (2020). Enhancing the performance of activated carbon-based scalable supercapacitors by heat treatment. Applied Surface Science, 145895-145903.

[3] Sivaraman P, Thakur AP, Shashidhara K, (2020). Poly (3-methyl thiophene) -graphene nanocomposites for asymmetric supercapacitors. Synthetic Metals, 259, 116255-116270.

[4] Libich J, Máca J, Vondrák J, Čech O, Sedlaříková M, (2018). Supercapacitors: Properties and applications. Journal of energy storage, 17, 224–227.

[5] Shagar V, Jayasinghe SG, Enshaei H, (2017). Effect of Load Changes on Hybrid Shipboard Power Systems and Energy Storage as a Potential Solution: A Review. Inventions, 2, 21-43.

[6] Yan Y, Li B, Guo W, Pang H, Xue H, (2016). Vanadium based materials as electrode materials for high performance supercapacitors. Journal of Power Sources, 329, 148–169.

[7] Faraji S, Ani FN. (2014). Microwave-assisted synthesis of metal oxide / hydroxide composite electrodes for high power supercapacitors. A review. Journal of Power Sources, 263, 338–360.

[8] Zhao Y, Zheng M, Cao J, Ke X, Liu J, Chen Y, Tao J. (2010). Easy synthesis of ordered meso / macroporous carbon monolith for use as electrode in electrochemical capacitors. Materials Letters, 62, 548–551.

[9] Li Q, Guo H, Xue R, Wang M, Xu M. (2020). Self-assembled Mo doped Ni-MOF nanosheets based electrode material for high performance battery-

supercapacitor hybrid device, International journal of hydrogen energy, 45, 20820-20831.

[10] Chen Y, Ni D, Yang X, Liu C, Yin J, Cai K. (2018). Microwave-assisted synthesis of honeycomblike hierarchical spherical Zn-doped Ni-MOF as a high-performance battery-type supercapacitor electrode material. Electrochimica Acta, 278, 114–123.

[11] Xu S, Zhang M, Zhang G, Liu J, Liu X, Zhang X, (2019). Temperature-dependent performance of carbon-based supercapacitors with water-in-salt electrolyte. Journal of Power Sources, 441, 227220-227230.

[12] Lee J, Park N, Kim B, Jung D, Im K, Hur J, Al L. (2013). Restacking-Inhibited 3D Reduced Graphene Oxide for High Performance Supercapacitor Electrodes. ACS Nano, 7, 9366–9374.

[13] Sundriyal S, Shrivastav V, Kaur H, Mishra S, Deep A. (2018). High-Performance Symmetrical Supercapacitor with a Combination of a ZIF-67/rGO Composite Electrode and a Redox Additive Electrolyte. ACS Omega, 3, 17348−17358.

[14] Meng F, Zhao L, Zhang Y, Zhai J, Li Y, Zhang W. (2019). Facile synthesis of NiCo 2 O 4 / rGO microspheres with high-performance for supercapacitor. Ceramics International, 45(17), 23701–23706.

[15] Makgopa K, Raju K, Ejikeme PM, Ozoemena KI, (2017). High-performance Mn3O4 / onion-like carbon (OLC) nanohybrid pseudocapacitor : Unravelling the intrinsic properties of OLC against other carbon supports. Carbon, 117, 20–32.

[16] Ke Q, Wang J. (2016). Graphene-based materials for supercapacitor electrodes. A review. J Materiomics, 2(1), 37–54.

[17] Jha P, Singh K, Kumar V, Rana S, Ballav N, Jha P, et al.(2017). High-Level Supercapacitive Performance of Chemically Reduced Graphene Oxide High-Level Supercapacitive Performance of Chemically Reduced Graphene Oxide. CHEMPR, 3(5), 846–860.

[18] Rahmanifar M, Hesari H, Noori A, Yaser M, Morsali A, Mousavi M. (2018). A dual Ni / Co-MOF-reduced graphene oxide nanocomposite as a high performance supercapacitor electrode material. Electrochimica Acta, 275, 76–86.

[19] Zhang X, Wang J, Ji X, Sui Y, Wei F, Qi J,et al. (2020). Nickel/cobalt bimetallic metal-organic frameworks ultrathin nanosheets with enhanced performance for supercapacitors. Journal of Alloys and Compounds, 825, 154069-15076.

[20] Maiti S, Pramanik A, Mahanty S, (2014). Extraordinarily high pseudocapacitance of metal organic framework derived nanostructured cerium oxide. Chem. Commun, 50, 11717–11720.

[21] Deng T, Zhang W, Arcelus O, Wang D, Shi X, Zhang X, et al.(2018). Vertically co-oriented two dimensional metal- organic frameworks for packaging enhanced supercapacitive performance. Communications Chemistry, 1, 6–15.

[22] Srimuk P, Luanwuthi S, Krittayavathananon A. (2015). Solid-type supercapacitor of reduced graphene oxide-metal organic framework composite coated on carbon fiber paper. Electrochimica Acta, 157, 69–77.

[23] Mofokeng T, Ipadeola A, Tetana, Z, Ozoemena, K, (2020). Defect-Engineered Nanostructured Ni/MOF-Derived Carbons for an Efficient Aqueous Battery-Type Energy Storage Device. ACS Omega, 5,

20461−20472.

[24] Dar R, Giri L, Karna S, Srivastava A, (2016). Performance of palladium nanoparticle-graphene composite as an efficient electrode material for electrochemical double layer capacitors. Electrochimica Acta, 196, 547–557.

[25] Loera-serna S, Oliver-tolentino M, López-núñez M, Santana-cruz A, Guzmán-vargas A, et al, (2012). Electrochemical behavior of [Cu3 (BTC)2] metal – organic framework : The effect of the method of synthesis. Journal of Alloys and Compounds, 540, 113–120.

[26] Jianguo S, Wang X, Chang C, (2014) Preparation and characterization of graphene oxide. Journal of Nanomaterials. Journal of Nanomaterials, 2,1-6.

[27] Gao X, Jang J, Nagase S, (2010). Hydrazine and Thermal Reduction of Graphene Oxide: Reaction Mechanisms, Product Structures, and Reaction Design. J. Phys. Chem. C, 114, 832–842.

[28] Monama G, Mdluli S, Mashao G, Makhafola M. (2017). Polyaniline-metal organic framework nanocomposite as an efficient electrocatalyst for hydrogen evolution reaction Palladium deposition on copper (II) phthalocyanine / metal organic framework composite and electrocatalytic activity of the modified electrode towards the hydrogen evolution reaction. Renewable Energy, 119, 62–72.

[29] Monama G, Modibane K, Ramohlola K, Molapo K, Hato M, Makhafola M,et al, (2019). ScienceDirect Copper (II) phthalocyanine / metal organic framework electrocatalyst for hydrogen evolution reaction application. International Journal of Hydrogen Energy, 44(34), 18891–18902.

[30] Xu Y, Li J, Huang W, (2017). Porous Graphene Oxide Prepared on Nickel Foam by Electrophoretic Deposition and Thermal Reduction as high performance supercapacitor electrode. Materials, 10, 936-954.

[31] Jorge G, Aguado S, Kapteijn F, (2008). Manufacture of dense coatings of Cu3 (BTC)2 (HKUST-1) on α-alumina. Microporous and Mesoporous Materials 113.1: 132-138.

[32] Zhao H. (2015). A Novel Synthetic Strategy for Pd3Sn Nanoparticles Loaded Reduced Graphene Oxide as Electrocatalyst for the Ethanol-Tolerant Oxygen Reduction Reaction. Int. J. Electrochem. Sci , 10, 5077-5085.

[33] Ramohlola E. Masikini M, Mdluli SB, Monama GR, Hato MJ, et al.(2017). Electrocatalytic Hydrogen Production Properties of Poly (3- aminobenzoic acid) doped with Metal Organic Frameworks. International Journal of Electrochemical Science, 12, 4392–4405.

[34] Liu J, Huiseong J, Jinzhang L, Kyungmoon L, Ji-Yong P, YeongHwan A, et al. Reduction of functionalized graphite oxides by trioctylphosphine in non-polar organic solvents. Carbon, 48(8), 2282-2289.

[35] Lopez T, Ortiz E, Alvarez M, Navarrete J, Odriozola F, Ortega E, (2010). Study of the stabilization of zinc phthalocyanine in sol-gel TiO2 for photodynamic therapy applications. Nanomed. Nanotechnol. Biol. Med, 6, 777-785.

[36] Zhou Y, Mao Z, Wang W, Yang Z, Liu X. (2016). In-Situ Fabrication of Graphene Oxide Hybrid Ni-Based Metal − Organic Framework (Ni−MOFs@GO) with Ultrahigh Capacitance as Electrochemical Pseudocapacitor Materials. ACS Appl. Mater. Interfaces, 8, 28904−28916.

[37] Li G, Cai H, Li X, Zhang J, Zhang D, Yang Y ,Xiong J. (2016). Construction of Hierarchical NiCo2O4@Ni-MOF Hybrid Arrays on Carbon Cloth as Superior Battery-Type Electrodes for Flexible Solid- State Hybrid Supercapacitors. ACS Appl. Mater. Interfaces,11,37675-37684.

[38] Wang Y, Liu Y, Wang H, Liu W, Li Y, Zhang J, et al, (2019). Ultrathin NiCo-MOF Nanosheets for High-Performance Supercapacitor Electrodes. ACS Appl. Energy Mater, 2, 2063−2071.

[39] Wen P, Gong P, Sun J, Wang J, Yang S. (2015). Design and synthesis of Ni-MOF/CNT composites and rGO/carbon nitride composites for an asymmetric supercapacitor with high energy and power density. Journal of material chemistry. 13874, 13874–13883.

[40] Kumar V, Fakhri A, Agarwal S, Naji M. (2018). Palladium oxide nanoparticles supported on reduced graphene oxide and gold doped : Preparation, characterization and electrochemical study of supercapacitor electrode. Journal of Molecular Liquids, 249, 61–65.

[41] Wang Y, Nie S, Liu Y, Yan W, Lin S, Cheng, G. (2019). Room-Temperature Fabrication of a Nickel- Functionalized Copper Metal – Organic Framework (Ni@Cu-MOF) as a New Pseudocapacitive Material for Asymmetric Supercapacitors. Polymers, 11, 821-831.

[42] Li Z, Yu X, Gu A, Tang H, Wang L, Lou Z, (2017). Anion exchange strategy to synthesis of porous NiS hexagonal nanoplates for supercapacitors. Nanotechnology, 28, 65406-65417.

[43] Tang C, Tang Z, Gong H, (2012). Hierarchically porous Ni-Co oxide for high reversibility asymmetric full-cell supercapacitors. J. Electrochem. Soc. 159, A651–A656.

[44] Tsai Y, Yang W, Lee K, Huang C, (2016). An effective electrodeposition mode for porous MnO2/Ni foam composite for asymmetric supercapacitors. Materials, 9(4), 246-259.

[45] Raj BG, Asiri AM, Wu JJ, Anandan S, (2015). Synthesis of Mn3O4 nanoparticles via chemical precipitation approach for supercapacitor application. Journal of Alloys and Compounds, 636, 234–240.

CHAPTER SIX

GENERAL CONCLUSIONS AND FUTURE RECOMMENDATIONS.

6.1. Conclusions.

This chapter focuses on the general discussions and conclusions of the results obtained in this study. The main aim was to develop a high performance electrode material for supercabattery applications. Porous materials especially MOFs have attracted extensive attention in response to an ever increasing demand for high performance supercapacitor electrodes. This is due to their porous structure which allows excessive diffusion on ions into the electrode material thus leading to better performances. On the other hand the introduction of graphene material was to improve the performance and also the mechanical and chemical stability of the MOF based electrode. Furthermore, palladium nanoparticles were introduced to improve the active sides and the electrochemical performance of the MOF/graphene composite. This study comprises of six chapters including this chapter.

Chapter one comprises of the problem statement, aims and objectives of this study. Furthermore, the solving of the problem statement is identified in the rationale whereby MOF based composites are used for supercapacitor applications. Palladium loaded MOF/rGO composite was identified as a promising electrode material for supecapacitor (supercabattery) applications. Chapter two focused on previous work done on MOF based electrode materials for supercapacitor applications and also an advanced introduction or background on supercapacitors. The analytical techniques used in this work for morphological, structural, physical and electrochemical properties were reviewed in chapter three of this work.

Chapter four of this work focused on the synthesis, characterisation and application of the rGO/MOF composite. The copper based MOF used in this work was prepared using the hydrothermal method to obtain its high crystalinity and the rGO was chemically derived from graphite powder. The composite was prepared via direct mixing in DMF where the composite has shown the preservation properties of both materials in the composite. The successful preparation of the rGO/MOF composite was confirmed using FTIR, XRD, SEM and TEM. This techniques has further shown

the high crystalinity and the rGO covering the MOF structures in the composite. The electrochemical performance of the composite was determined using CV, GCD and EIS. The composite has shown a battery-type behaviour and exhibited a more improved performance compared to MOF alone. An improved specific capacity of 459.0 Cg^{-1} was obtained at a current density of 1.5 Ag^{-1}. Furthermore, the composite in a two-electrode system using rGO/MOF hybrid as the positive electrode exhibited maximum energy density of 11.0 Wh kg^{-1} and the maximum power density of 640.45 W kg^{-1}.

In chapter five, palladium nanoparticles were loaded on rGO using electroless deposition. Furthermore the Pd-rGO/MOF composite was also prepared through direct mixing of Pd-rGO and MOF in DMF at room temperature. The main aim for the introduction of palladium nanoparticles was to improve the performance of the composite by increasing the active sites for better interaction with the electrode material. The composite was also confirmed using FTIR, XRD, SEM and TEM which has shown bright spots of the palladium between the graphene sheets. The physical properties were determined using EDX and TGA. The electrochemical performance of the composite for supercapacitor application of the composite was obtained using CV, GCD and EIS. The Pd-rGO/MOF has exhibited better performance than both MOF and rGO/MOF composite. The Pd-rGO/MOF composite showed improvement in electron transfer kinetics and superior battery-type performance with large specific capacity of 711.99 Cg^{-1}. The nanocomposite was further applied as a positive electrode in a supercabattery and possessed excellent cyclic performance, maximum energy and power densities of 3500, 25.68 Whkg^{-1} and 1599.55 Wkg^{-1}, respectively. These results has demonstrated that rGO/MOF and Pd-rGO/MOF composites can be used in supercapacitor applications for energy storage. Furthermore this works has proved that graphene materials can improve the stability of MOF materials and also improve their performance in energy storage devices. Lastly, the palladium nanoparticles have shown a massive improvement in the electrochemical performance of MOF based composites for supercapacitor applications. This work demonstrated the importance of electrochemically efficient Pd nanoparticles, reduced graphene oxide and copper based metal organic framework for energy storage applications.

6.1. Future work and recommendations.

Although this work has shown to be effective in supercapacitor applications, there are still various parts of the study that still requires to be investigated to improve the properties of the electrode materials used in this work. To improve the properties of rGO/MOF and Pd-rGO/MOF other methods such as in-situ composite preparations can be used rather than impregnation/direct mixing. For future work, higher potential window can be applied as this directly affects the energy and power densities of the supercapacitor. More studies can also be done on other electrolytes such as inorganic, organic and neutral electrolytes as this work only focused on aqueous electrolyte (KOH). It is important to explore other carbon based materials to support MOFs in energy storage. This is due to the restacking tendency of graphene sheets after long charge-discharge cycles. To get the correct stability of asymmetric supercapacitors, it is important to have more than 10 000 cycles rather than only 3500 cycles.